Azadipyrromethenes for applications in photodynamic antimicrobial chemotherapy, photodynamic therapy and optical limiting

A thesis submitted in fulfilment of the requirements for the degree of

MASTER OF SCIENCE

at

RHODES UNIVERSITY

By

Nadine Dubazana

April 2020

Acknowledgements

I would like to thank my supervisor Professor J. Mack for his patience, guidance, support throughout the research and compiling of this thesis. I would also like to thank Distinguished Prof. T. Nyokong as my co-supervisor for her support. A special thank you to Gugu Kubheka, my mentor, for her guidance and imparting knowledge, as well as Dr Balaji Babu for his patience and assistance with the PDT work. I am very grateful to Gail Cobus for all the work she does, and the attention she pays towards each individual. I thank my S22 colleagues for the support provided for this journey, the staff in the chemistry building, my family, friends and T. Ngubo for their encouragement and unwavering support, and most importantly, the Lord.

I acknowledge the financial support from DAAD-NRF for giving me an opportunity to further my studies.

Abstract

Azadipyrromethenes, azaBODIPYs and zinc azadipyrromethene complexes were prepared and characterised to examine the effect on their photophysical properties of incorporating phenyl groups at the 1,3,5,7-positions with electron-donating and withdrawing groups at the *para*-positions. To enhance their ability to generate singlet oxygen, appropriate structural modifications were made through the addition of a Zn(II) ion or halogenation at the 2,6 positions. *In vitro* photodynamic therapy (PDT) studies targeting MCF-7 human breast cancer cells were carried out. To evaluate and understand the effectiveness of the dyes as photosensitisers, cellular uptake, phototoxicity and the half-maximal inhibitory concentration (IC_{50}) values were analysed. Photodynamic antimicrobial chemotherapy (PACT) studies were also carried out to study the effectiveness of the dyes against *Staphylococcus aureus* (*S. aureus*). Dyes with donor-π-acceptor (D-π-A) properties were synthesised and tested against the second harmonic of the Nd:YAG laser in optical limiting (OL) studies. The second-order hyperpolarisability, third-order susceptibility and nonlinear absorption coefficient values were determined. The results suggest that 1,3,5,7-azaBODIPY dyes may be less suitable for use in this context than analogous D-π-A 3,5-distyrylBODIPY dyes. Molecular modelling was carried out to identify the structure-property relationships of the synthesised dyes by analysing trends in the energies of the frontier molecular orbitals (MOs) and spectroscopic properties.

Table of Contents

List of Figures

List of Schemes

List of Tables

List of Symbols

A	Absorbance
Å	Angstrom
ε	Molar extinction coefficient
F	Fluorescence
λ	Wavelength
ϕ_F	Fluorescence quantum yield
ϕ_Δ	Singlet oxygen quantum yield
$^1O_2$	Singlet oxygen
$^3O_2$	Triplet oxygen
P	Phosphorescence
S_0	Ground state
S_1	Singlet excited state
S_2	Second excited state
S_n	n^{th} electronic excited state
T_1	First triplet state
T_T	Triplet state lifetime
α	Linear absorption coefficient
β	Nonlinear absorption coefficient
γ	Second-order hyperpolarisability
I_{lim}	Optical limiting threshold
$Im[\chi^{(3)}]$	Third-order nonlinear susceptibility
η	Refractive index

List of Abbreviations

AzaBODIPY	Boron azadipyrromethene
azaPODIPY	Phosphorus dioxide azadipyrromethene
B3LYP	Becke 3-Parameter, Lee, Yang and Parr
Boc	Tert-butyloxycarbonyl
BODIPY	Boron dipyrromethene
C. Albicans	*Candida albicans*
CAM-B3LYP	Coulomb-attenuating method - Becke 3-Parameter, Lee, Yang and Parr
CFU	Colony forming units
DCM	Dichloromethane
DIPEA	N,N-Diisopropylethylamine
DMEM	Dulbecco's modified Eagle's medium
DMSO	Dimethylsulfoxide
DPBF	1,3-diphenylisobenzofuran
DPBS	Dulbecco's phosphate−buffered saline
D-π-A	Donor-π-Acceptor
E. coli	*Escherichia coli*
ESA	Excited state absorption
EtOH	Ethanol
EWG	Electron withdrawing group
FCS	Fetal calf serum
HOMO	Highest occupied molecular orbital
IC	Internal conversion
ICT	Intramolecular charge transfer

ISC	Intersystem crossing
LUMO	Lowest occupied molecular orbital
MALDI-TOF	Matrix-assisted laser desorption/ionisation time of flight
MOs	Molecular orbitals
MRSA	Methicillin-resistant *Staphylococcus aureus*
MS	Mass spectrometry
NBS	*N*-bromosuccinimide
Nd:YAG	Neodymium-doped yttrium aluminium garnet
NIR	Near-infrared region
NIS	*N*-iodosuccinimide
NLA	Nonlinear absorption
NLO	Nonlinear optics
NLS	Nonlinear light scattering
NLR	Nonlinear refraction
NMR	Nuclear magnetic resonance
OL	Optical limiting
PACT	Photodynamic antimicrobial therapy
PDT	Photodynamic therapy
PS	Photosensitiser
ROS	Reactive oxygen species
RSA	Reverse saturable absorption
RT	Room temperature
S. aureus	*Staphylococcus aureus*
TD-DFT	Time-dependent density functional theory

TEA	Triethylamine
TFA	Trifluoroacetic acid
THF	Tetrahydrofuran
TLC	Thin layer chromatography
TPA	Two-photon absorption
UV-vis	Ultraviolet-visible

1: Introduction

1.1 Introduction

Boron aza-dipyrromethene (azaBODIPY) dyes are structural analogues of boron dipyrromethenes (4,4-difluoro-4-bora-3a,4a-diaza-*s*-indacenes or BODIPYs). To gain an in depth understanding of the properties of azaBODIPY dyes, it is necessary to also explore the properties of BODIPY dyes (**Figure 1.1**). The synthesis of BODIPY dyes was first described by Treibs and Kreuzer in the 1960s, but interest surrounding these dyes was minimal prior to their application as solid-state solar concentrators in the 1980s.[1] Their use as laser dyes, fluorescent stains, and labels in fluorescent imaging and as indicator dyes in sensor applications has been reported.[1]

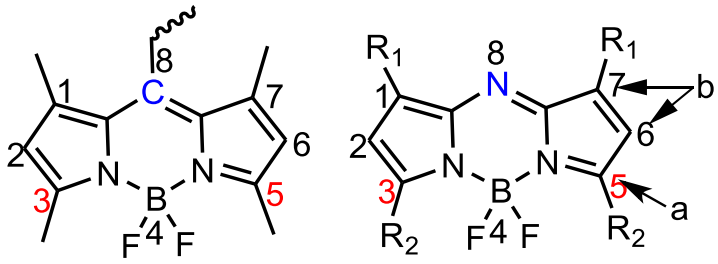

Figure 1.1: The structures of BODIPY and azaBODIPY dyes. The BODIPY and azaBODIPY core standard numbering system is depicted.

Their properties include narrow Gaussian-shaped absorption and emission bands, high molar extinction coefficients and fluorescence quantum yield values, moderate redox potentials, negligible triplet-state formation prior to heavy atom incorporation, negligible sensitivity to solvent polarity, excellent photostability and high solubility in commonly used organic solvents of varying polarities.[1–3] Since the mid-1990s, research concerned with BODIPY dyes has increased significantly and broadened in its scope.[1,2,4]

1.1.1 Molecular properties of BODIPY dyes

BODIPY dyes do not formally follow Huckel's rule describing aromaticity (4N+2). Although the pyrrole rings follow the rule, the introduction of the BF_2 moiety disrupts the aromaticity of the *s*-indacene ring structure.[1,5] The pyrrole nitrogen atoms and the cross-linking cause further disruption. As a result, the degeneracies of the π-MOs are completely lifted since the structure is characterised by the C_{2V} symmetry.[1,5] Nevertheless, the fluorophores still have properties that very closely resemble those of an aromatic system,[1] since the tetrahedral geometry of the boron centre results in the pyrrole moieties having a rigid planar dipyrromethene conformation.[1,6] The electronic structure of this class of dyes can be compared to those of an aromatic $C_{12}H_{12}^{2-}$ cyclic parameter with MOs arranged in an M_L = 0, ±1, ±2, ±3, ±4, ±5 and 6 sequence in ascending energy with regard to the magnetic quantum number (M_L).[1,7,8] The low C_{2V} symmetry,[7] results in a HOMO and LUMO that are well separated from the other MOs in the π-system,[7] and a single dominant intense absorption band in the visible region that arises primarily from the HOMO→LUMO transition.

1.1.2 History

In 1943, Rogers attempted the Leuckart reaction shown in **Scheme 1.1** and recorded an unexpected intense blue colour.[9] Leuckart had earlier described the reductive alkylation of ammonia, using formamide as the reducing agent under solventless conditions at a high temperature.[10] The Leuckart reaction would later be adapted for the synthesis of α-phenethylamines.[10] Rogers' original plan was to convert 4-nitro-1,3-diphenylbutan-1-one, to 4-(4-nitro-3-phenylbutyl)aniline using this approach. The observed blue colour resulted from reacting ketones with a nitrogen-containing source, namely nitrobutanone along with ammonium formate or formamide, which yielded a tetrarylazadipyrromethene. After

evaluating the structure, the product was likened to that of a phthalocyanine (**Scheme 1.2)**. There was some interest in this new compound due to its thermal stability.[9]

Azadipyrromethene boron difluorides (azaBODIPYs), were synthesised in 1993 by Boyer *et al.*, as structural analogues of BODIPYs that differ at the *meso*-position (also referred to as the 8-position), since a highly electron-donating nitrogen atom replaces the *meso*-carbon.[11] The recent re-emergence of azadipyrromethene research after 50 years was motivated by their tuneable properties post-synthesis. The presence of the aza-nitrogen atom is known to be partially responsible for a marked red-shift of the main absorption bands of azaBODIPYs relative to those of BODIPYs.[1] Difficulty in their preparation initially made them less likely candidates for study in the molecular dye field.

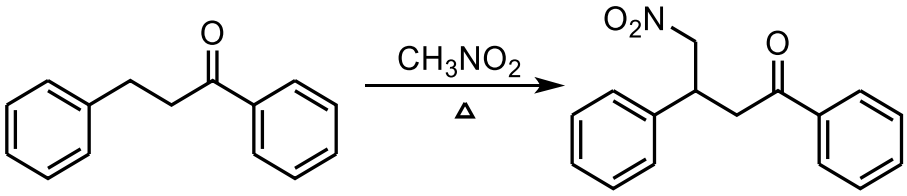

Scheme 1.1: Starting materials and intended product in the reaction studied by M. Rogers.[9]

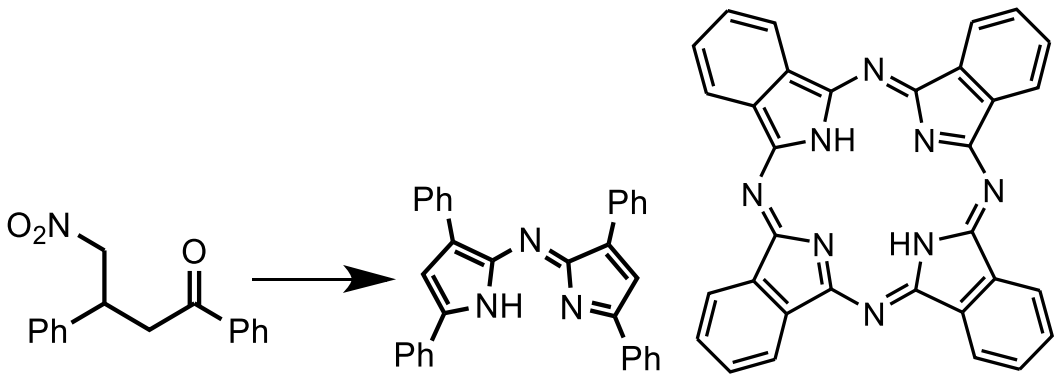

Scheme 1.2: Synthesis of the first azadipyrromethene (LEFT).[12] Structure of phthalocyanine (RIGHT).

The synthesis and characterisation of peripherally substituted azadipyrromethene complexes and chelates will be discussed in the following chapters along with an evaluation of their suitability for use as photosensitisers dyes and as optical limiters.

1.2 Synthesis

In this section, the general synthetic procedures used for the synthesis of azadipyrromethenes, zinc azadipyrromethenes, azaBODIPYs and their halogenated derivatives are described.

1.2.1 Synthesis of azadipyrromethenes

There are various synthetic routes for the synthesis of azadipyrromethenes, but the one described below is widely used. The synthetic approach to preparing the azadipyrromethene scaffold and its post-synthesis modification is described in the following section. The synthetic route developed by Rogers yielded symmetric azadipyrromethenes.[9] 4-Nitro-1,3-diphenylbutan-1-one or 4-oxo-2,4-diphenylbutanenitrile was used as the starting material under solventless high temperature conditions with ammonium formate used as the nitrogen-containing source to achieve the azadipyrromethene (**Scheme 1.3**).[9] Guided by the need to develop more efficient synthetic routes, efforts were made to optimise reaction conditions leading to the azadipyrromethene. This included testing the use of ammonium formate against ammonium acetate as the nitrogen source under solvated and solventless conditions (**Scheme 1.4**).[13] Higher yields were achieved by varying the nitrogen source and introducing a solvent to the reaction. An added advantage was the ability to carry out crystallisation of the product from the reaction followed by straightforward filtration.[13]

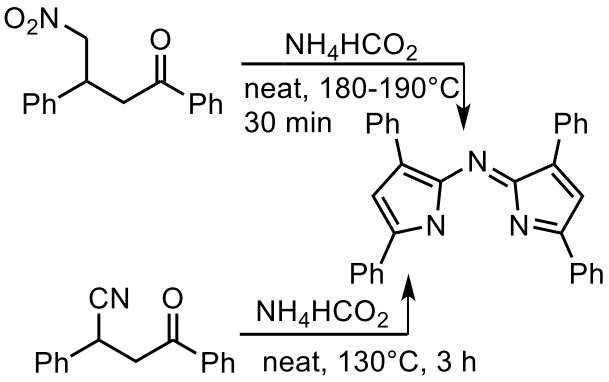

Scheme 1.3: Synthetic pathways used by Rogers.[12]

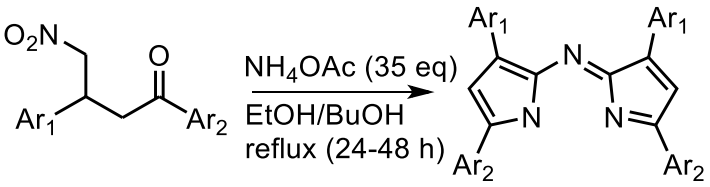

Scheme 1.4: Synthetic method used to the optimise reaction conditions.[14]

Many synthetic pathways were followed based on the initial work of Rogers. A general route for preparing azadipyrromethenes with differing aryl substituents was established. 2,4-diarylpyrrole precursors were used. To achieve this, 4-nitro-1,3-diarylbutan-1-ones were chosen as the starting material (**Scheme 1.5**).[14] The crucial step used the Nef transformation of 4-nitro-1,3-diarylbutan-1-ones into 4,4-dimethoxy-1,3-diaryl-butan-1-ones (**Scheme 1.5**). Acetal deprotection and an ammonia condensation reaction gave a diarylpyrrole. Conversion of this pyrrole into a nitrosopyrrole was accomplished with sodium nitrite in ethanolic HCl (**Scheme 1.5**).

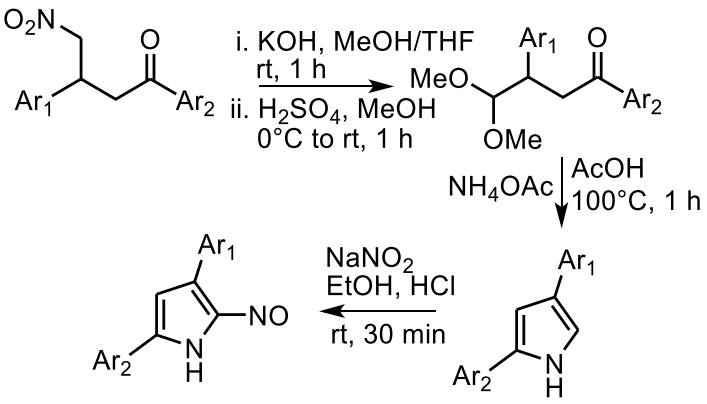

Scheme 1.5: The synthesis of nitrosopyrrole building blocks.

Condensation of nitrosopyrrole and pyrrole in acetic anhydride/acetic acid mixture at 100°C can be used to prepare asymmetrical azadipyrromethenes (**Scheme 1.6**).

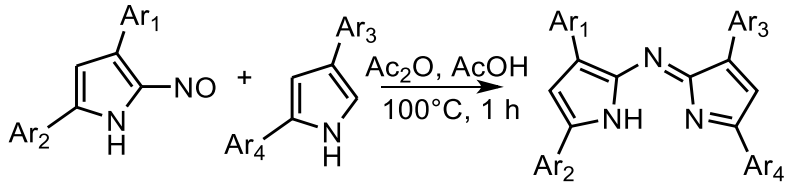

Scheme 1.6: Condensation of pyrroles to form asymmetric azadipyrromethenes.

Symmetrical azadipyrromethenes can be synthesised through a three-step reaction series (**Scheme 1.7**). The first step produces a chalcone from an aldehyde and ketone through an aldol condensation reaction. Adding nitromethane through a Michael addition reaction in the presence of a base then yields a nitromethane adduct. This then serves as a precursor for the cyclisation using ammonium acetate to form the azadipyrromethene. Originally, solventless conditions were used for the conversion of the nitromethane adduct to the azadipyrromethene. O'Shea introduced a high-boiling alcohol and varied the ammonium source from ammonium formate to ammonium acetate resulting in higher yields.[13]

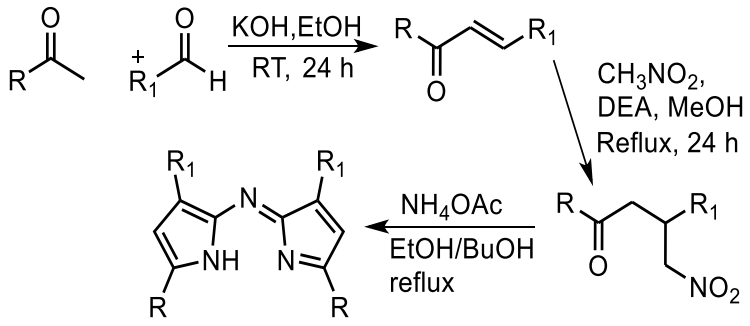

Scheme 1.7: The synthesis of azadipyrromethenes.

The postulated mechanism of the formation of azadipyrromethenes from the nitromethane adduct is provided in **Scheme 1.8**.[15] This mechanism provides insight on the high sensitivity to moisture of this step; requiring dry solvents, as well as the use of an inert atmosphere.[16] The availability of excess protons would prevent the reaction from reaching completion. The mechanism has not been fully characterised as no intermediate products have been isolated. The key step is believed to be the ring closure reaction of the ketimine moiety A to form the nitronate moiety, which is activated by protonation. Intermediate B has the ability to eliminate hyponitrous acid (to form nitrous oxide) and water giving C via the Nef reaction. D is yielded through a rearrangement of C. Pyrrole D is nitrosylated to provide nitroso-pyrrole E which condenses with D to form the azadipyrromethene.[17]

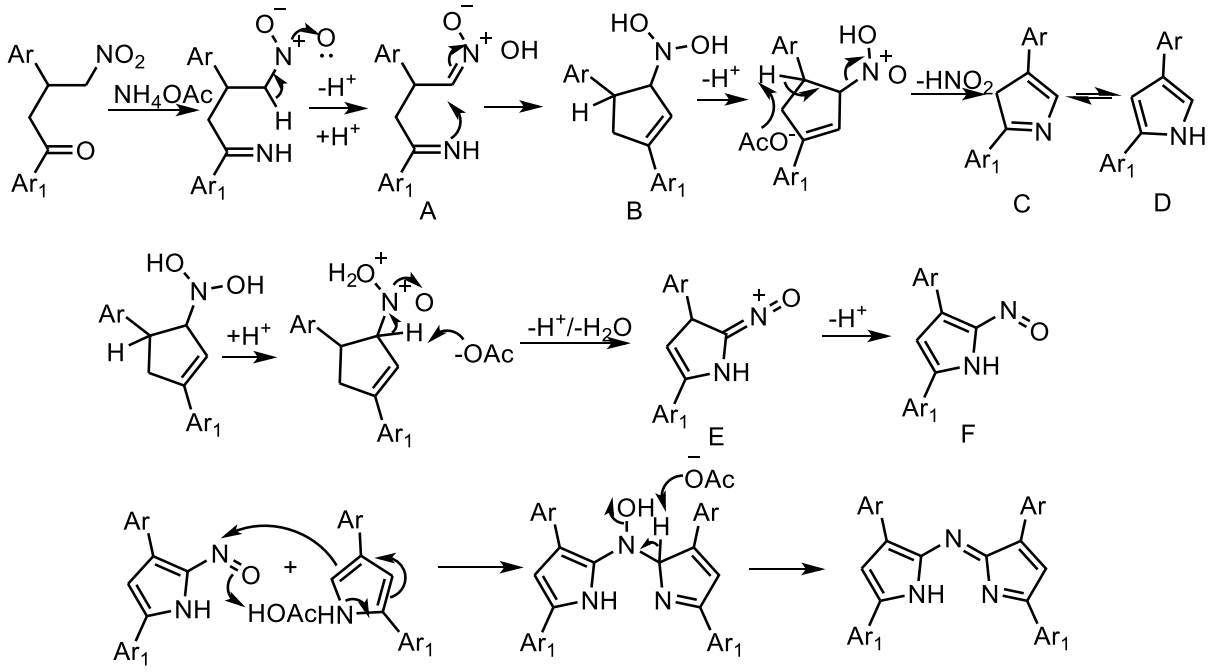

Scheme 1.8: Proposed mechanism for the synthesis of azadipyrromethenes.[18]

1.2.2 Synthesis of azaBODIPY

The two nitrogen atoms in the azadipyrromethene coordination pocket can strongly chelate with electron-deficient groups such as BF_2 and transition metal ions. BF_2 derivatives provide a rigid structure through the formation of a 5-6-5 membered fused ring system (**Scheme 1.9**). This prevents rotation at the C−N−C interpyrrole bridge. The major difference between the azadipyrromethene and its chelate is the fluorescent properties brought about by chelation. A weak organic base is required for the removal of the proton from appropriate pyrrole using a base, such as triethylamine (TEA) or N,N-diisopropylethylamine (DIPEA) at room temperature or reflux.

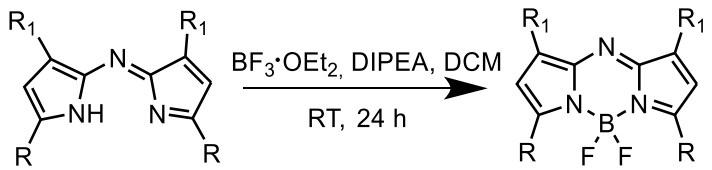

Scheme 1.9: The azaBODIPY core is made of two pyrrole rings linked by an aza-nitrogen to produce a fully conjugated system.

Other chelation reactions can be carried out with phosphorus dioxide, **Scheme 1.10**. The first example of a phosphorus dioxide-azadipyrromethene (azaPODIPY) was synthesised by reacting an azadipyrromethene with phosphorus oxychloride in the presence of triethylamine, followed by aqueous hydrolysis.[19] The success of this reaction suggests that a wide range of non-metal and metalloid chelates await synthesis in future.

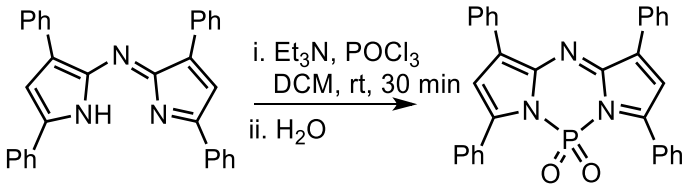

Scheme 1.10: Synthesis of azaPODIPY.

1.2.3 Synthesis of dibromoazadipyrromethenes

Electrophilic substitution of the azadipyrromethene structure can be achieved at the 2,6-positions (also referred to as the β-pyrrole positions) due to their high reactivity, **Scheme 1.11**. Incorporation of heavy atoms on the azaBODIPY core by using this approach populates enhances the rate of intersystem crossing. This change facilitates the production of singlet oxygen. Halogenation can be carried out at room temperature or under reflux. Sources of bromine include *N*-bromosuccinimide (NBS) and liquid bromine, whereas *N*-iodosuccinimide (NIS) is used for iodine.

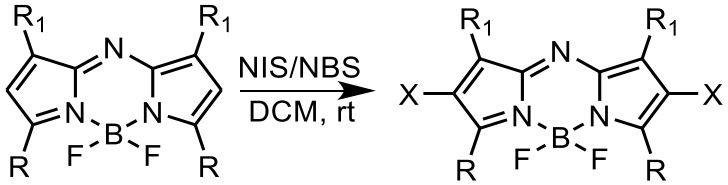

Scheme 1.11: The electrophilic substitution reaction of the azaBODIPY core.[17]

1.2.4 Modifications at the β-pyrrole positions

Formylation

Formylation reactions can be achieved by using a Vilsmeier reagent (the combination of DMF and $POCl_3$) at 70°C for 20 h via Vilsmeier-Haack formylation (**Scheme 1.12**).[20]

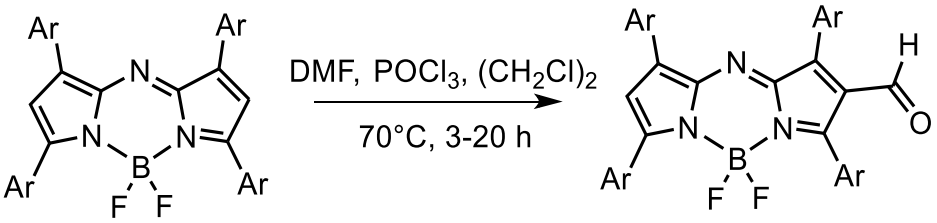

Scheme 1.12: Formylation of azaBODIPY.[20]

Sulfonation

Successful mono- and di-sulfonation of azadipyrromethenes has been achieved by using chlorosulfonic acid in CH_2Cl_2 at low temperatures (**Scheme 1.13**).[21]

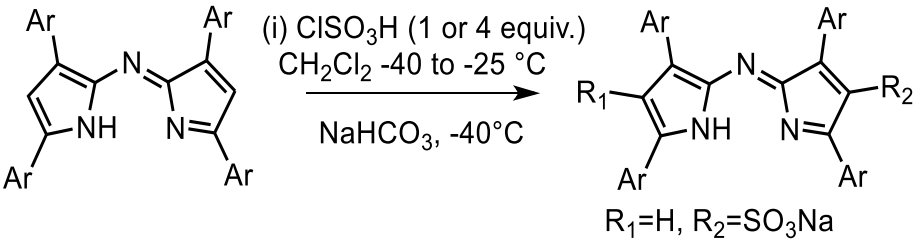

Scheme 1.13: Sulfonation of azaBODIPY.[21]

Metal-mediated coupling reactions

Azadipyrromethenes with halogen substituents at the β-pyrrole position can be used to form conjugated oligomers via Sonogashira cross-coupling reactions. For example, palladium or copper catalysed reactions of iodoazadipyrromethenes and 1,4-bis-(dodecyloxy)-2,5-diethynylbenzene followed by BF_2 chelation resulted in the formation of oligomers (**Scheme 1.14**).[22] In a similar manner, homocoupling with $FeCl_3$ affords dimerisation of azaBODIPY dyes (**Scheme 1.15**).[23]

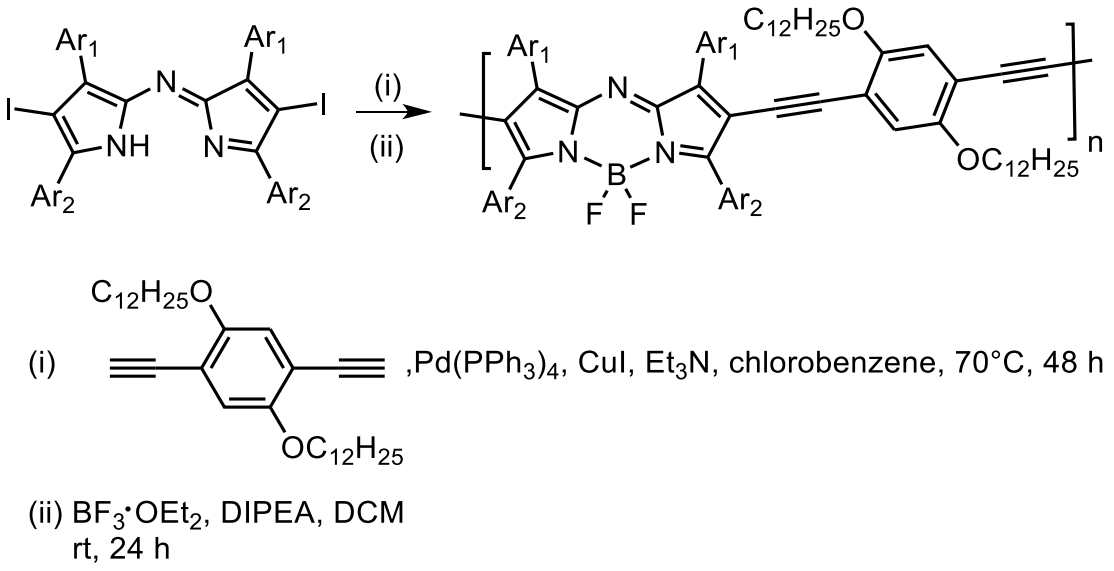

Scheme 1.14: Azadipyrromethene with conjugated oligomers.[22]

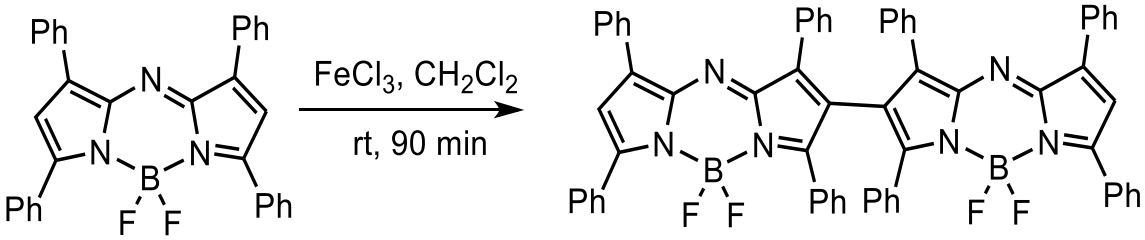

Scheme 1.15: Homocoupling of azadipyrromethenes.[23]

1.2.5 Synthesis of homoleptic metal azadipyrromethene complexes

Azadipyrromethenes readily react with transition metals in a 2:1 ratio to form a dimeric complex. Homoleptic metal complexes were reported using the acetate salts under reflux (**Scheme 1.16**).[9] By 1943, divalent metal ions, namely Co(II), Cu(II), Ni(II) and Zn(II), were explored with the bidentate azadipyrromethene ligand.[9] Full characterisation has been achieved, and the range of different ions have been expanded to include Hg(II) and Pd(II).[12,24,25] Heteroleptic complexes have also been prepared (**Scheme 1.17**).[12] Typically these metal complexes are formed under mild room temperature conditions in THF with *t*-butoxide or DIPEA as the base.

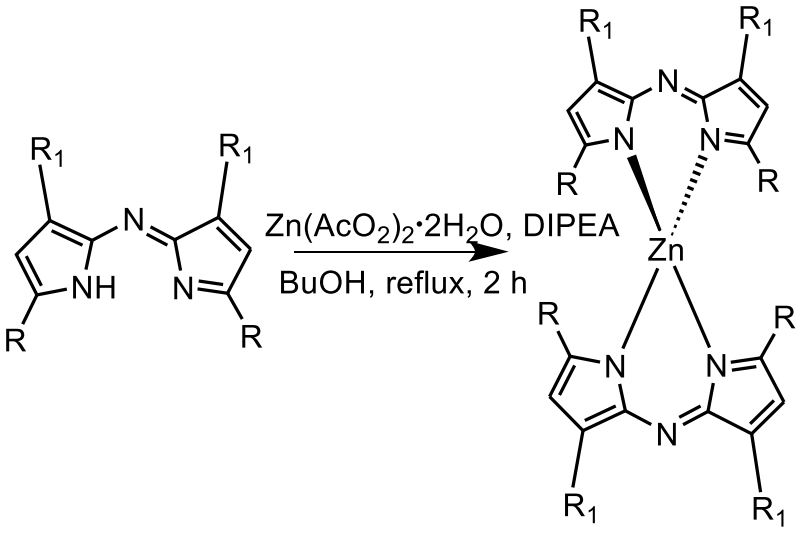

Scheme 1.16: The formation of homoleptic zinc azadipyrromethenes.

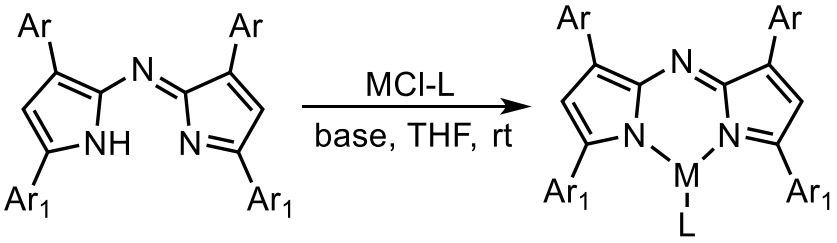

Scheme 1.17: Heteroleptic azadipyrromethene synthesis.

1.3 Photophysical properties of azadipyrromethenes

A Jablonski diagram can be used to illustrate the electronic states and processes that can occur between the electronic states after electronic excitation with electromagnetic radiation (**Figure 1.2**). When a molecular dye is excited with light of sufficient energy, the molecule is excited from the ground state (S_0) to an excited singlet state (S_n). Internal conversion (IC) takes place when a chromophore electron is excited to form a short-lived S_n excited state, typically occurring within 10^{-12} s. The S_n excited state quickly relaxes to the lowest vibrational level of the S_1 state. Relaxation from $S_1 \rightarrow S_0$ can result in the emission of a photon through fluorescence or can occur through non-radiative decay. These processes follow Kasha's rule, which states that the fluorescence emission spectra and quantum yields are independent of

the excitation wavelength since the fluorescence process occurs only from the lowest vibrational level of the S_1 excited state. Intersystem crossing from $S_1 \rightarrow T_1$ usually occurs inefficiently as this transition is spin-forbidden. At the T_1 state, the molecule can return to the S_0 state through phosphorescence or non-radiative decay.

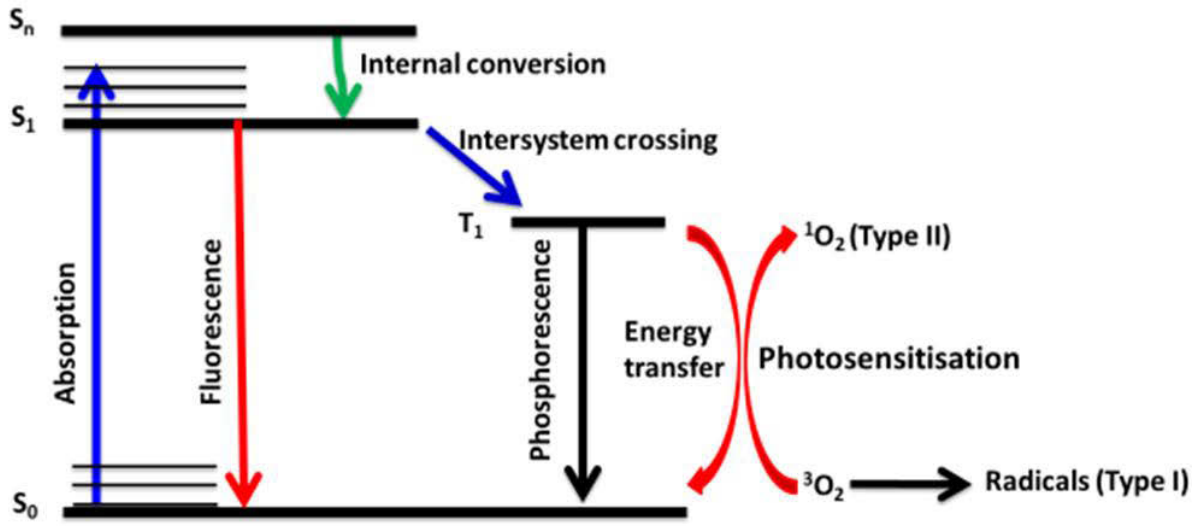

Figure 1.2: A Jablonski diagram illustrating the processes that can occur after electronic excitation.

1.3.1 Optical spectroscopy

The UV-visible absorption spectroscopy of azaBODIPY compounds, **Figure 1.3**, can be modified through changes to their structure, such as the introduction of aryl substituents.[13,18] The maximum absorbance wavelength is usually determined by the $S_0 \rightarrow S_1$ transition that is related to the excitation of an electron from the HOMO to the LUMO. Upon complexation with BF_2, there is an extension of the π-conjugation system that results in a red-shift of the main spectral band.[26] The presence of the electronegative aza-nitrogen atom stabilises the LUMO due to the large MO coefficient on the bridging nitrogen atom and this results in a further narrowing of the HOMO−LUMO gap relative to that of a conventional BODIPY dye.[5] The intense absorption band at the red end of the visible or in the near

infrared (NIR) region can be further red-shifted by extending the π-conjugated system by introducing aryl substituents at the 1,3,5,7-positions and by adding appropriate *para*-substituents to phenyl groups.[27] Strategies used to extend the absorbance to the NIR region include incorporating electron-donating and/or electron-withdrawing substituents to incorporate a "push-pull" effect.[28]

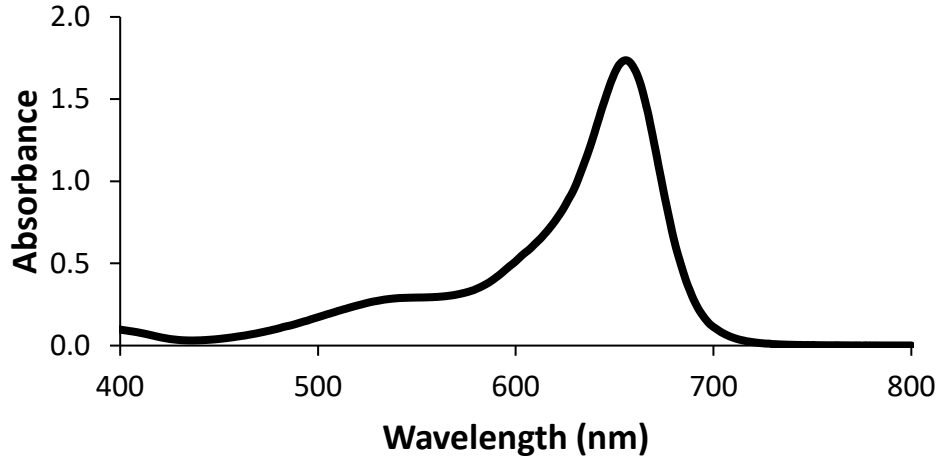

Figure 1.3: A typical visible region absorption spectrum for an azaBODIPY dye.

Zinc azadipyrromethene complexes generally have a characteristic shoulder peak, **Figure 1.4**, due to the exciton coupling between the two azadipyrromethene ligands.[29]

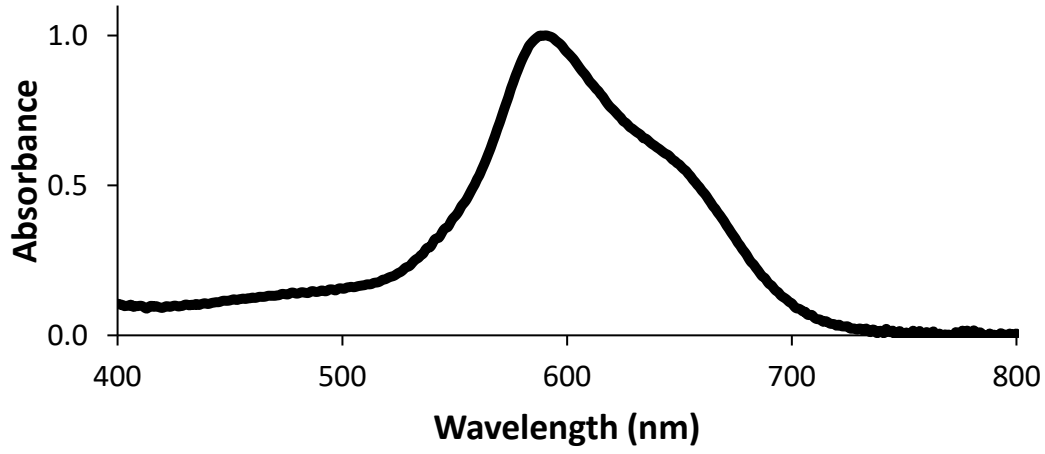

Figure 1.4: A typical visible region absorption spectrum for a zinc azadipyrromethene complex.

1.3.2 Fluorescence quantum yields

Quantum yields measure the efficiency of processes, and in the context of optical spectroscopy are defined as the number of times the process occurs per photon absorbed. Fluorescence quantum yields, therefore, measure the efficiency of photon emission given by the ratio of the number of photons emitted to the number of photons absorbed. The absorption and emission properties of azaBODIPY and BODIPY dyes can be readily tuned through further structural modifications and chelation.[30] Fluorescence quantum yields depend on the structure of the aza-dipyrromethene ligand.[31]

Equation (1) describes a comparative method used to obtain the fluorescence quantum yields using known standards:

$$\phi_F = \phi_{F\,(std)} \frac{F.A_{std}.\eta^2}{F_{std}.A.\eta^2_{std}} \qquad (1)$$

where A and A_{std} are the absorbances at the excitation wavelength, F and F_{std} are the integrated areas under the fluorescence curves of the sample and the standard, respectively; while η and η_{std} are the refractive indices of the solvents used for the sample and standard.

1.3.3 Singlet oxygen quantum yields

The singlet oxygen quantum yield provides a quantitative measure of the efficiency of photosensitiser dyes in generating this reactive oxygen species after photoexcitation. Applications such as photomicrobial antibacterial chemotherapy (PACT) and photodynamic therapy (PDT) make use of singlet oxygen for the eradication of microbes and cancerous cells. The singlet oxygen quantum yields of 1,3,5,7-tetraarylazaBODIPY compounds are enhanced by the incorporation of halogen atoms at the 2,6-positions,[32] which enhances the rate of intersystem crossing to the triplet state (T_1) through spin-orbit perturbation due to the heavy effect.[13] Efficient energy transfer between the dye and molecular dioxygen generates

singlet oxygen, ($^1O_2$) or free oxygen radicals. If there is sufficient interaction between the azaBODIPY and molecular oxygen, a high singlet oxygen quantum yield is possible.

To quantify the extent of singlet oxygen generation, a singlet oxygen scavenger, such as 1,3-diphenylisobenzofuran (DPBF), can be added to a solution of the photosensitiser dye to react with the singlet oxygen that is generated upon photoexcitation.[33] The change in intensity of the main absorption band of DPBF over time is determined by using UV-visible absorption spectroscopy. Equation (2) uses a comparative method to determine the singlet oxygen quantum yield in this context:

$$\phi_\Delta = \phi_{\Delta(std)} \frac{m_{sample}}{m_{std}} \quad (2)$$

where $\phi_{\Delta std}$ is the singlet oxygen quantum yield of the standard, and m_{sample} and m_{std} are the slopes for the absorption changes of the sample and standard solutions.

1.4 Applications

Fluorescent dyes are functional organic molecules.[34] Their photophysical properties have led to applications in a wide range of fields such as chemistry, materials science and biology, including use as optical sensors, photosensitizing agents, photoredox catalysts, and solar energy materials.[12] Intense absorption in the visible region and the NIR makes molecular dyes potentially suitable for use in PACT and PDT, following suitable structural modifications. The principles of PACT and PDT involve the use of cytotoxic singlet oxygen generated upon photoexcitation of a photosensitiser dye with light of suitable wavelength for the destruction of bacteria or cancer cells. The use of PACT avoids the problems associated with antibiotic-resistant microbes.

The study of NLO explores the interactions of electromagnetic fields in numerous media giving rise to new fields that are altered in phase, frequency, amplitude or other propagation characteristics from the incident field.[35] NLO materials can be used to manipulate optical

signals in telecommunications and other optical signal processing applications.[36] In this study, the main focus is on optical limiting (OL) applications in which the intensity of incident laser pulses is attenuated by materials that provide a strong NLO response.

1.4.1 Photodynamic antimicrobial chemotherapy

PACT is a minimally invasive antimicrobial treatment that makes use of a non-toxic photosensitizing agent, which is irradiated with light of an appropriate wavelength.[37,38] The destruction of pathogens is induced by reactive oxygen species such as singlet oxygen that accumulates and oxidises the microorganism.[37] The benefits of the treatment provided by PACT is that it avoids the problem of resistance to agents such as antibiotics and does not require the use of expensive drugs.[39] *In vitro* studies have demonstrated that there has been considerable progress in the photoinactivation of numerous bacterial strains.[40,41] Some requirements for an ideal PACT photosensitiser dye include low dark toxicity and absorbance maxima in the UV-visible or NIR regions.[39,42,43] A cationic charge is typically necessary for the photoinactivation of gram (-) bacteria, while neutral photosensitiser dyes can be effective on gram (+) microbes.

Target microorganisms

The photosensitiser dye must first interact with the bacterial cell wall. Due to the charge present in bacterial cell walls, it is beneficial for a photosensitiser dye to possess a charge opposite to the bacterial cell wall to enhance their interaction. *Staphylococcus aureus (S. aureus)* is a gram (+) bacteria with a 15−80 nm thick cell wall.[44] **Figure 1.5** shows the composition of *S. aureus,* which consists of a peptidoglycan layer, protecting the plasma membrane and has protruding lipoteichoic acids.[44]

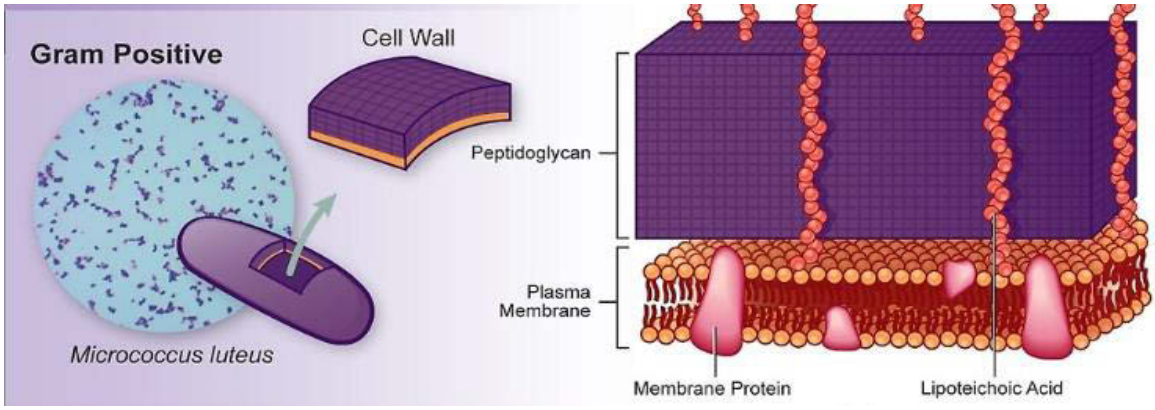

Figure 1.5: The structure of a gram (+) bacteria.[45]

AzaBODIPYs in PACT

AzaBODIPYs have only started to be studied in depth fairly recent, so although they have been studied for use in various applications, the available literature is often still quite limited. Some azaBODIPYs have been studied as photosensitisers due to having favourable singlet oxygen quantum yields, but few detailed studies have been reported. The efficacy of the azaBODIPY dyes shown in **Figure 1.6** was evaluated against *S. aureus,* Methicillin-resistant *Staphylococcus aureus (MRSA), Escherichia coli (E. Coli)* and *Candida albicans (C. albicans)*.[48] This photosensitiser dye displayed phototoxicity against all of the pathogens. Uptake studies were conducted using the non-brominated version of the dye, which displayed rapid uptake into both gram (+) and gram (−) bacteria and fungi as is necessary for an efficient photosensitiser dye.[41]

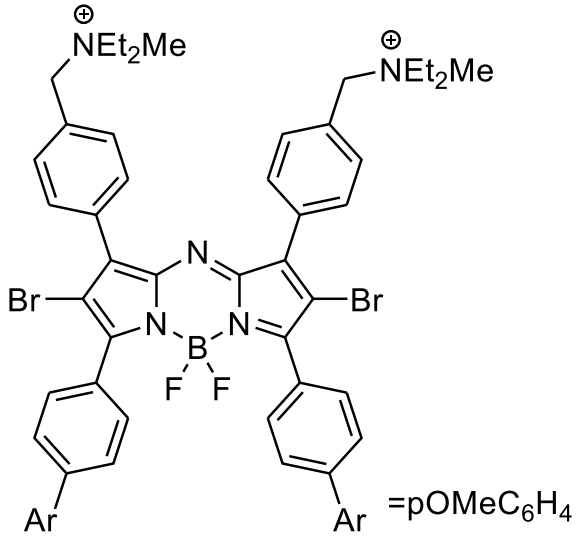

Figure 1.6: An azaBODIPY studied previously for use in PACT.[41]

1.4.2 Photodynamic Therapy

PDT is a US Food and Drug Administration approved, minimally invasive therapy for the treatment of lung, oral, oesophageal and breast cancerous cells.[46,47] PDT makes use of an appropriate photosensitiser dye that is non-toxic in its native state, but through irradiation at a suitable wavelength and fluence have the ability to interact with molecular oxygen, generating reactive oxygen species, such as singlet oxygen, to destroy cancerous cells.[48] Singlet oxygen quantum yields are generally used as a measure of the ability of a photosensitiser dye to perform in the context of PDT, but it should be noted that it is not the only available reactive oxygen species (ROS), since both Type I and Type II processes can occur through electron and energy transfer, respectively, from the T_1 state of the molecular dye to $^3O_2$, **Figure 1.2**. Significant drawbacks are encountered in the alternative treatments. Non-selectivity and toxicity towards normal cells is experienced during chemotherapy, radiography is destructive to neighbouring healthy cells and time-extensive, while surgery has a lengthy recovery time.[49–53] In contrast, PDT is cost-effective and time-efficient with treatment requiring a maximum of four days during which the patient generally is an outpatient.[54,55]

The location of a tumour determines the mode of the PDT treatment. Dermal infections are topically applied, while others are administered intravenously. For the latter, the photosensitiser dye accumulates in the target tumour cells over a period of 24−96 hours, thereafter light with an appropriate wavelength is used to irradiate the dye.[56–58] The photosensitiser dye should absorb strongly in the therapeutic window (620−1000 nm).[59] Optimal penetration in tissue requires wavelengths that minimise scattering and reflection at the tissue surface and absorption of the incident photons at shorter wavelengths. As a result, shorter wavelengths are better suited for superficial areas.[60] To penetrate deeper-seated target cells, the 800−1000 nm range is ideal.[60] At longer wavelengths, water absorbs the incident radiation making it unavailable for biological, biochemical or physiological responses.[60] The ROS generated can result in irreversible damage in the cancerous cells where the photosensitiser dye has localised and accumulated. Ideally, the photosensitiser dye should be selective to the target cells.[61] This avoids the destruction of healthy cells as the photosensitiser dye accumulates selectively in the tumour.

There have been relatively few previous studies on the PDT activity of azaBODIPY dyes, **Table 1.1**. In **Table 1.1 A**, a range of azaBODIPY dyes were synthesised and examined as catalysts for photooxygenation reactions.[62] The dyes were proposed for use in PDT due to their favourable singlet oxygen quantum yields and intense absorption in the near IR region. The dye in **Table 1.1 B** displayed potent activity towards a broad range of tumour cells, low to undeterminable dark toxicity and sustained activity under hypoxic conditions.[63] A trifunctional theranostic dye (**Table 1.1 C**) was prepared that is suitable for *in vivo* tumour imaging, efficient PDT activity and therapeutic self-monitoring.[48] The azaBODIPY is activated by pH in acidic environments. The main spectral band of this dye lies beyond 800 nm, improving the imaging sensitivity and increasing penetration depth for PDT.

Table 1.1: The azaBODIPY dyes that have been proposed and studied previously for use in PDT.

AzaBODIPY		Reference
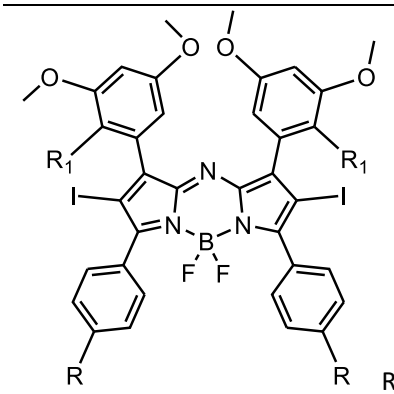 R= H, I, Br; R_1=H, I	**A**	[62]
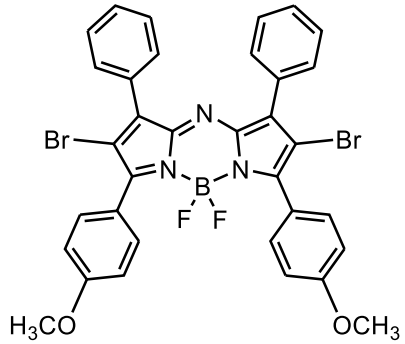	**B**	[63]
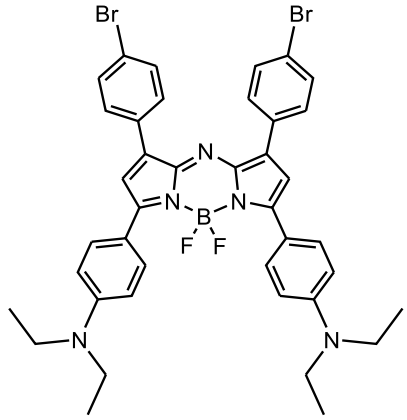	**C**	[48]

1.4.3 Nonlinear optics

Advances in technology have resulted in new laser systems that are compact, efficient and offer a variety of wavelengths. The availability of these systems has led to issues with the irresponsible use of lasers during runway approaches by aircraft in a manner that can damage the eyesight of pilots.[64] The development of modern optical technology has hence led to a need for research aimed at attenuating the intensity of light originating from optical

beams.[65] There is an ongoing search for inorganic and organic materials which control optical beams such that transmittance is drastically lowered with increasing light fluence.[15] Nonlinear optics is a field of optics that is concerned with the behaviour of materials when interacting with light of differing incident intensities. These materials are based on different processes associated with nonlinear optics such as nonlinear scattering (NLS), nonlinear refraction (NLR) and nonlinear absorption (NLA). Reverse saturable absorption (RSA), a type of NLA response in which the transmission of light decreases as incident intensity increases, is sought after in optical limiting studies. Other nonlinear optical effects include two-photon absorption (TPA), multi-photon absorption and excited state absorption (ESA).

This study focusses on the development of optical limiting materials based on the NLA properties of molecular dyes. A good optical limiter attenuates light at high intensities while remaining largely transparent under ambient light conditions. The transmitted intensity should remain unchanged, and possibly decrease to a small value above a certain threshold. The initial uniform transmittance should decrease significantly to near zero above a threshold limiting fluence (**Figure 1.7**).[66]

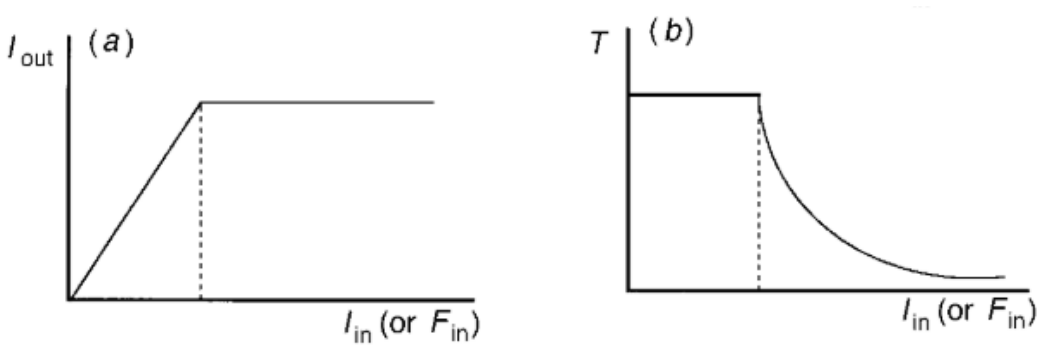

Figure 1.7: Ideal behaviour of an optical limiter. (a) transmitted intensity vs incident intensity (b) transmittance vs incident intensity.[66]

This usually involves TPA, **Figure 1.8**, which is a third-order nonlinear process of simultaneous absorption of two photons from $S_0 \rightarrow S_n$, or ESA, a fifth-order NLA process in which absorption of a photon results in excitation from a lower excited state to a higher excited state.[67]

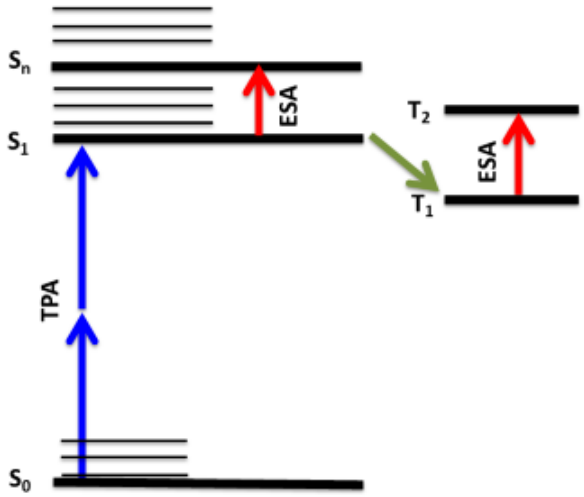

Figure 1.8: A Jablonski diagram illustrating TPA, blue arrows showing absorption of the first and second photon, red arrows illustrate photon absorbed at excited state while the green arrow highlights intersystem crossing.[67]

Organic compounds that have previously been studied in this context typically possess delocalised π-conjugation systems with high polarisabilities, and this enhances their interaction with laser light.[66,68,69] Other ideal characteristics in this context include high solubility; a high linear transmission under ambient light conditions; intense NLA with a sub-nanosecond response time over a broad spectral bandwidth providing a high threshold for damage.[70]

The Z-scan setup, **Figure 1.9**, measures intensity-dependent optical nonlinearities of materials. It is based on the self-focusing of an optical beam by a thin sample, where the sample is moved along the light propagation direction (Z-axis) of a focused beam.[71] The sample experiences a phase and intensity modulation and its transmittance is measured as a

function of the sample position.[72] Gaussian-shaped beams are primarily involved in terms of the time profile of the laser pulses, while the beam shape is typically circular.

The open-aperture (OA) Z-scan technique is well suited for NLA related measurements as it offers a direct and accurate measurement by fitting changes in normalised transmittance.[73] Closed-aperture Z-scan examines the nonlinear refractive index of a material by fitting the Sheik-Bahae formalism to the characteristic RSA curve that is obtained.[74]

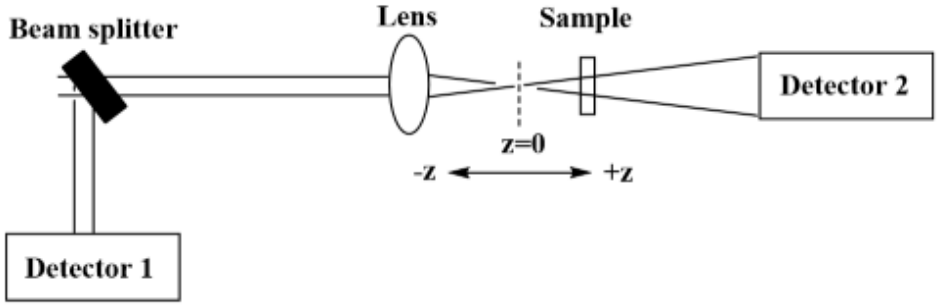

Figure 1.9: A schematic representation of the Z-scan setup.

The data are analysed using Equation (3):[15]

$$T(z) = \frac{1}{\sqrt{\pi} q_0(z)} \int_{-\infty}^{\infty} \ln\left[1 + q_0(z) e^{-\tau^2}\right] d\tau \quad (3)$$

Where $q_0(z)$ provides an indication of the magnitude of the nonlinear response. For circular-shaped beams, $q_0(z)$ is given by Equation (4):

$$q_0(z) = \frac{2\beta_{eff} P_0 I_{eff}}{\pi \omega(z)^2} \quad (4)$$

Where β_{eff} is the effective nonlinear absorption coefficient, P_0 is the peak power of the laser pulse and I_{eff} is the effective pathlength described by Equation (5):

$$I_{eff} = \frac{1 - e^{(-\alpha L)}}{\alpha} \quad (5)$$

Where α and l are the linear absorption coefficient and pathlength, respectively. The beam width as a function of the sample position $\omega(z)$ can be obtained from Equation (6):

$$\omega(z) = \omega_0\sqrt{1 + (\frac{z}{z_0})^2} \quad (6)$$

Where ω_0 is the beam waist, location of light with its minimum beam radius, z is the translation distance of the sample relative to the focus and z_0 is the Rayleigh length, which is defined by $\pi{\omega_0}^2/\lambda$ where λ is the laser wavelength.

The β_{eff} value can be extracted from the experimental transmittance using Equations (3-6). The use of nanosecond instead of femtosecond laser pulses results in RSA responses that are no longer due primarily to TPA. Since ESA occurs on a nanosecond timescale, an RSA response can be generated,[69] if the ESA is more intense than ground state absorption. This means that the intrinsic β value associated with TPA only cannot be determined, and an effective nonlinear absorption coefficient (β_{eff}) is derived instead.

Equation (3) is not suitable for directly fitting the data, so a numerical version is normally used instead to derive $q_0(z)$ from normalised transmittance:

$$T(z) = 0.363e^{(\frac{-q_0(z)}{5.60})} + 0.286e^{(\frac{-q_0(z)}{1.21})} + 0.213e^{(\frac{-q_0(z)}{24.62})} + 0.096e^{(\frac{-q_0(z)}{115.95})} + 0.038e^{(\frac{-q_0(z)}{965.08})} \quad (7)$$

On substituting Equation (6) into (4), $q_0(z)$ is given by Equation (8):

$$q_0(z) = \frac{Q_0}{1 + \frac{z^2}{{z_0}^2}}$$

Where Q_0 is:

$$Q_0 = \frac{2\beta_{eff}P_0I_{eff}}{\pi{\omega_0}^2} \quad (8)$$

A Gaussian-shaped curve with Q_0 as the maximum value at z_0 can be obtained from Equation (8). The peak and full width at half minimum values are derived from the plot giving Q_0 and z_0. β_{eff} provides a direct measure of the magnitude of the RSA response of the material for OL:

$$\beta_{eff} = \frac{\lambda z_0 Q_0}{2P_0I_{eff}} \quad (9)$$

The imaginary third-order susceptibility (Im[$\chi^{(3)}$]) is a measure of how rapid the response of the optical limiter is to the perturbation induced by the incident laser pulse. The third-order susceptibility value is directly proportional to the β_{eff} value:

$$I_m[\chi^{(3)}] = \frac{\eta^2 \varepsilon_0 c \lambda \beta_{eff}}{2\pi} \quad (10)$$

Where η is the linear refractive index, c is the speed of light, ε_0 is the permittivity of free space and λ is the wavelength of the laser.

The second-order hyperpolarisability (γ) measures the interaction of the incident photon with the permanent dipole moment of the optical limiting material. This value has a direct relationship with Im[$\chi^{(3)}$] as shown in Equation (11):

$$\gamma = \frac{I_m[\chi^{(3)}]}{f^4 C_{mol} N_A} \quad (11)$$

Where f is Lorentz field factor, $f = (\eta^2 + 2)/3$, C_{mol} is the molar concentration of the active species and N_A is Avogadro's constant.

AzaBODIPYs in Nonlinear Optics

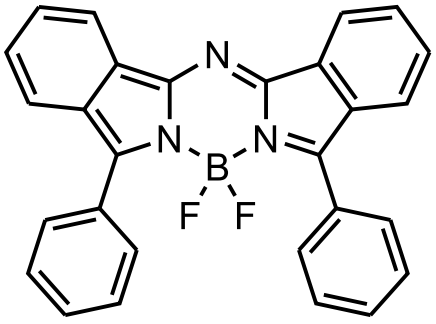

Figure 1.10: An azaBODIPY studied previously for use as an optical limiter.[70]

Kubheka, Mack and coworkers [72] recently reported a study of the optical limiting properties of a benzo-fused azaBODIPY (**Figure 1.10**) by open aperture Z-scan at 532 nm, the second harmonic of Nd:YAG lasers. In the absence of ground state absorbance (α = 0), the observed

RSA response related to a TPA-assisted ESA mechanism due to its relatively long-lived S_1 excited state. The OL properties were enhanced when the azaBODIPY dye was embedded in polymer thin films. The trends observed for the β_{eff} and γ values were consistent with the trends observed in the ϕ_F values in various solvents. The study showed a correlation between the population of the S_1 excited state and OL ability where a higher population, influenced by the choice of solvent, and this results in enhanced optical limiting properties. One of the goals of this study is to extend this earlier study to non-benzo-fused 1,3,5,7-tetraarylBODIPY dyes.

1.5 Aims

The aim of this thesis was to synthesise and characterise azadipyrromethene complexes which exhibit the following features: (i) red-shifted absorption bands and (ii) enhanced photophysical and photochemical properties with regards to applications.

The aims of the study can be summarised as follows:

1. Synthesise and characterise the photophysical properties of azaBODIPY dyes with heavy atoms for assessment in PACT studies.

2. Study the optical limiting abilities of a series of azadipyrromethene complexes.

3. Assess the effectiveness of zinc azadipyrromethene complexes and brominated 1,3,5,7-tetraarylazaBODIPY dyes for use in PDT.

4. Conduct molecular modelling of the dyes that were synthesised to identify the structure-property relationships.

2: Experimental

2.1 Materials

All reagents were used without further purification unless otherwise stated. Acetophenone, 4-bromoacetophenone, 4-nitroacetophenone, benzaldehyde, 4-methoxybenzaldehyde, 4-dimethylaminobenzaldehyde, 1,3-diphenylisobenzofuran (DBPF), boron trifluoride diethyl etherate ($BF_3 \cdot Et_2O$), N-bromosuccinimide (NBS), sodium sulfate, N,N-diisopropylethylamine (DIPEA), triethylamine (TEA), nitromethane, urea, ammonium acetate were purchased from Sigma Aldrich. Rose Bengal was purchased from Fluka. Sodium hydroxide (NaOH) and sodium chloride (NaCl) were obtained from B&M Scientific. Glacial acetic acid (99%) was purchased from Minema. Hydrochloric acid (32%), pyrrole, propionic acid, methanol, ammonia solution, 1,8-diazabicyclo[5.4.0]undec-7-ene (DBU) and the silica gel used for chromatography were purchased from Merck. Dimethylsulfoxide (DMSO), petroleum ether, ethyl acetate, glacial acetic acid and piperidine were purchased from Sigma-Aldrich. Dichloromethane (DCM) was obtained from Saarchem. Ultrapure water was obtained from a Milli-Q Water System (Millipore Corp, Bedford, MA, USA). Silica gel 60 for flash column chromatography was purchased from Merck.

Argon gas and dry solvents were used for all air and moisture sensitive reactions. Cultures of MCF-7 cells were obtained from Cellonex®. Heat-inactivated fetal calf serum (FCS) and 100 unit/mL penicillin-100 µg/mL streptomycin-amphotericin B were obtained from Biowest®. Dulbecco's phosphate-buffered saline (DPBS) and Dulbecco's modified Eagle's medium (DMEM) were obtained from Lonza®. Cell proliferation yellow reagent (MTT assay) and trypan blue were obtained from Sigma-Aldrich. *Staphylococcus aureus* (ATTCC 25923) was obtained from Davies Diagnostic. PBS solution pH 7.4 was prepared using appropriate amounts of Na_2HPO_4 and NaOH in ultrapure water. Nutrient agar and agar bacteriological BBL Muller Hinton broth were purchased from Merck.

2.2 Instrumentation

- Ground state electronic absorption spectra were measured on a Shimadzu UV−2550 spectrophotometer.
- Fluorescence emission spectra were recorded on a Varian Eclipse spectrofluorimeter.
- ^{1}H nuclear magnetic resonance (NMR) measurements were recorded on a Bruker AMX 600 MHz spectrometer.
- Mass spectral data were acquired on a Bruker Auto-FLEX III Smartbeam MALDI-TOF mass spectrometer operated in positive ion mode, using α-cyano-4-hydroxycinnamic acid as a matrix.
- Monochromatic laser light between 400–700 nm from an Ekspla NT 342B-20-AW pulsed laser (2.0 mJ/5 ns, 20 Hz) was used for quantifying the singlet oxygen quantum yields of compounds with DPBF as a $^{1}O_2$ quencher.
- The Centre for High Performance Computing in Cape Town was used to carry out the theoretical calculations. All calculations were carried out using the Gaussian 09 software package.[75] The Beck, three-parameter, Lee-Yang-Parr (B3LYP) exchange-correlation functional and SDD basis sets were used for the geometry optimisation. The time-dependent DFT (TD–DFT) method was used to calculate the electronic absorption properties with the Coulomb attenuated B3LYP (CAM-B3LYP) functional and SDD basis sets. The molecular orbitals were visualised by using the Avogadro software package.[76]
- The MCF-7 cells were cultured in 25 cm^2 vented flasks (Porvair) then subcultured in 75 cm^2 vented flasks (Porvair) in a humidified atmosphere incubator with 5% CO_2 at a physiological temperature of 37°C (Heal Force). MTT cell proliferation neutral yellow reagent was used to measure the cell viability through a Synergy 2 multi-mode

microplate reader (BioTek®). PDT studies were conducted using a Modulight® Medical Laser system (ML) 7710−680 fitted with a Thorlabs M625L3 light-emitting diode (LED).

- The optical density of bacteria culture was determined using a Ledetect 96 from Labxim Products.
- A China Medical Device RAU–530D autoclave was used to sterilise and autoclave nutrient broth and agar, PBS buffer and the apparatus used for bacterial and cancer studies.
- A Vortex mixer from Lasiec was used to mix the bacteria suspension.
- A Hermle Z233M–2 centrifuge from Lasiec was used to harvest bacteria from the suspension.
- A Scan® 500 automatic colour colony counter was used for determination of colony-forming units (CFU) / ml values for the bacteria.
- All Z-scan analyses were performed with frequency-doubled Nd:YAG lasers (Quanta-Ray, 1.5 J / 7 or 10 ns FWHM pulse duration) as the source of excitation. The laser was operated in a near Gaussian transverse mode at 532 nm (second harmonic), with a repetition rate of 10 Hz and an energy range of 0.1 μJ–0.1 mJ, limited by the use of Coherent J5-09 energy detectors. The low repetition rate of the laser prevents cumulative thermal nonlinearities. The beam was spatially filtered to remove the higher-order modes and tightly focused with a 15 cm focal length lens. No damage was detected between runs after the samples were moved or replaced. The Z-scan data were obtained using a 2 mm optical glass cuvette.

2.3 Synthesis of azadipyrromethenes

A series of azadipyrromethenes was synthesised as described below.

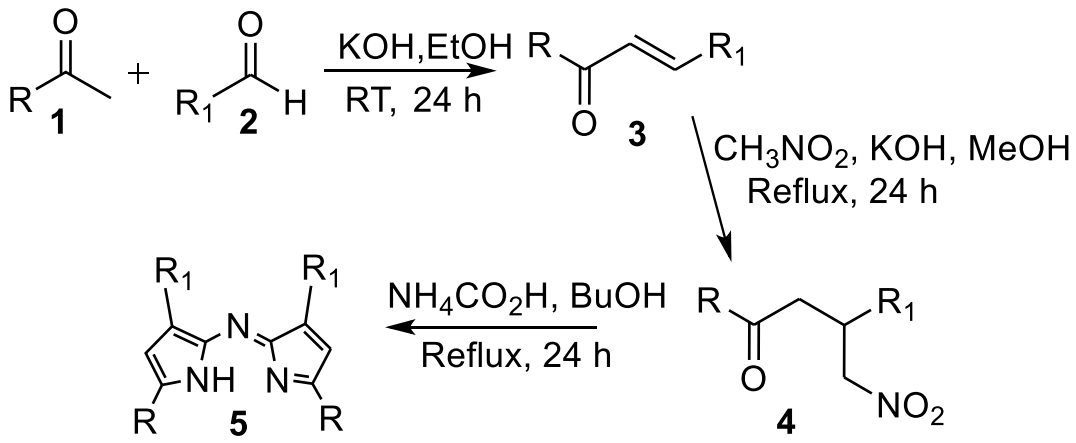

	R_1	R
N1 azadpy	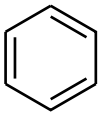	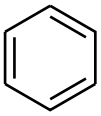
N3 azadpy	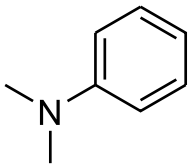	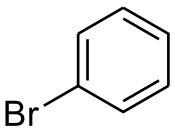
N5 azadpy	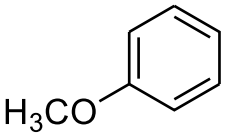	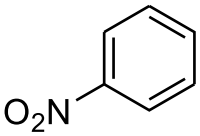
N6 azadpy	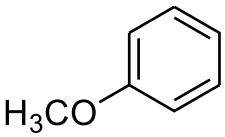	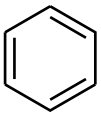

Scheme 2.1: Synthesis of azadipyrromethenes.

A general synthesis procedure was followed to prepare the azadipyrromethenes, **Scheme 2.1**. The choice of aldehyde and ketone dictates the substituents at the 1,7- and 3,5-positions, respectively. A 1:1 mol equiv. ratio of the aldehyde and ketone was dissolved in ethanol, followed by 14 mol equiv. of base (KOH or NaOH) for 24 h. The details of the choice of

aldehyde and ketone are as follows: **N1-azadpy,** acetophenone (4 mL, 34.29 mmol) and benzaldehyde (3.48 mL, 34.29 mmol); **N3-azadpy,** 4-dimethylaminobenzaldeyde (2 g, 13.4 mmol) and 4-bromoacetophenone (2.66 g, 13.4 mmol); **N5-azadpy**, 4-methoxybenzaldehyde (2.23 mL, 18.3 mmol) and 4-nitroacetophenone (3.03 g, 18.3 mmol); and **N6-azadpy**, acetophenone (4 mL, 34.29 mmol) and 4-methoxybenzaldehyde (4.16 mL, 34.29 mmol).

The chalcone was crystallised by pouring it over ice and neutralised with HCl. Thereafter, recrystallisation was achieved using MeOH or EtOH depending on the solubility of the chalcone. The recrystallised product was vacuum filtered and allowed to dry. To synthesise the nitromethane adduct, the chalcone was dissolved in degassed MeOH or EtOH. 2-4 pellets of base and 5 mol equiv. of nitromethane were added under an inert atmosphere, and the mixture was heated at reflux for 24 h. Thin-layer chromatography (TLC) was used to track the completion of the reaction. The reaction mixture was adjusted to pH ≈ 4, washed with DCM or chloroform or ethyl acetate, distilled water, brine solution and dried with sodium sulfate. Finally, a solution of the nitromethane adduct in butanol/glacial acetic acid (3:2) was purged with nitrogen or argon gas. 30 mol equiv. of ammonium acetate or urea was used for the conversion to the azadipyrromethene. TLC was used to monitor whether all the starting material was consumed, the residue is washed with DCM/chloroform/ethyl acetate and distilled water, and rotavapped. The resultant product was purified by silica gel column chromatography using ethyl acetate/pentane (1:1) for **N3-azadpy**, toluene for **N1-azadpy**, and THF for **N5-azadpy** and **N6-azadpy**.

N1-azadpy

[(3-phenyl-5-phenyl-1*H*-pyrrol-2-yl)-(3-phenyl-5-phenyl-pyrrol-2-ylidene)]amine, yield: 60%. ^{1}H NMR (600 MHz, $CDCl_3$) δ 8.07 (d, *J* = 7.2 Hz, 4H), 7.96 (d, *J* = 7.2 Hz, 4H), 7.47−7.57 (m, 6H), 7.36−7.45 (m, 6H), 7.22 (s, 2H) ppm. MALDI TOF-MS calc. 449.56 amu; Found 450.08 m/z.

N3-azadpy

[(3-(4-bromophenyl)-5-(4-dimethylaminophenyl)-1*H*-pyrrol-2-yl)-(3-(bromophenyl)-5-(4-dimethylaminophenyl)-pyrrol-2-ylidene)]amine, yield: 55%. ^{1}H NMR (600 MHz, $CDCl_3$) δ 8.02 (d, *J* = 8.4 Hz, 4H), 7.76 (d, *J* = 8.4 Hz, 4H), 7.63 (d, *J* = 8.4Hz, 4H), 7.01 (s, 2H), 6.77 (d, *J* = 7.8 Hz, 4H), 3.05 (s, 12H) ppm. MALDI TOF-MS calc. 693.49 amu; Found 694.60 m/z.

N5-azadpy

[(3-(4-methoxyphenyl)-5-(4-nitrophenyl)-1*H*-pyrrol-2-yl)-(3-(4-methoxyphenyl)-5-(4-nitrophenyl)-pyrrol-2-ylidene)]amine, yield: 46%. ^{1}H NMR (600 MHz, $CDCl_3$) δ 7.62−7.66 (m, 4H), 7.57−7.61 (m, 4H), 7.51−7.55 (m, 4H), 7.43 (s, 2H), 6.81 (d, *J* = 9.0 Hz, 4H) 3.88 (s, 6H) ppm.

N6-azadpy

[(3-(4-methoxyphenyl)-5-phenyl-1*H*-pyrrol-2-yl)-(3-(4-methoxyphenyl)-5-phenyl-pyrrol-2-ylidene)]amine, yield: 40%. ^{1}H NMR (600 MHz, $CDCl_3$) δ 8.20 (d, *J* = 7.8 Hz, 4H), 7.86 (s, 2H), 7.72 (d, *J* = 7.8 Hz, 3H), 7.49−7.55 (m, 6H), 7.43−7.47 (m, 3H), 3.90 (s, 6H) ppm.

NH_2-azadpy

[(5-(4-aminophenyl)-3-phenyl-1*H*-pyrrol-2-yl)-(5-(4-aminophenyl)-3-phenyl-pyrrol-2-ylidene)]amine, yield: 48%. ^{1}H NMR (400 MHz, $CDCl_3$) δ 8.07 (d, *J* = 7.2 Hz, 4H), 7.78 (d, *J* = 8.0 Hz, 4H), 7.35−7.43 (m, 4H), 7.30−7.34 (m, 3H), 7.10 (s, 2H), 6.80 (d, *J* = 8.4 Hz, 4H), 4.03 (s, 4H) ppm.

2.4 Synthesis of azaBODIPYs

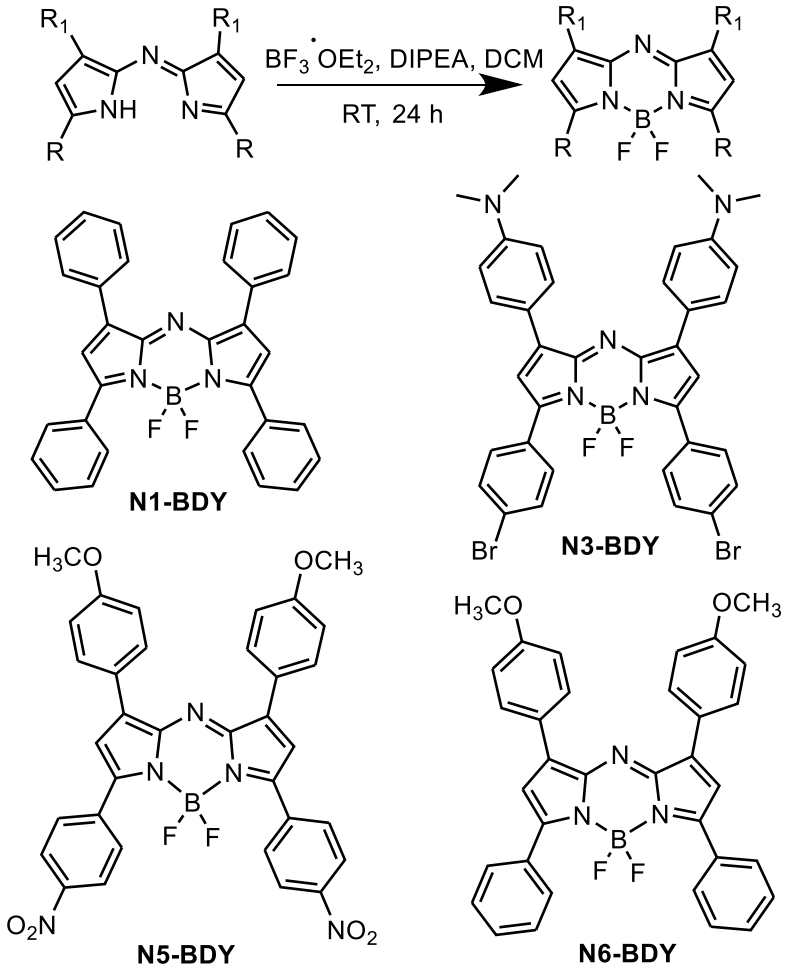

Scheme 2.2: Synthesis of azaBODIPYs.

For the chelation of the azadipyrromethene, **Scheme 2.2**, the azadipyrromethene was dissolved in DCM. 1 g of **N1-azadpy** (2.22 mmol), 1.11 g of **N3-azadpy** (1.60 mmol), 1.15 g of **N5-azadpy** (1.91 mmol) and 1.4 g (2.75 mmol) of **N6-azadpy** were used. 48 mol equiv. of $BF_3{\cdot}OEt_2$ were added and the reaction was left to stir for 24 h. Due to unsuccessful attempts at the synthesis using DIPEA and TEA as the base, DBU was used for azaBODIPYs **N5-BDY** and **N6-BDY**. The mol equiv. used were adjusted from 48 for DIPEA to 24 as DBU is a slightly stronger base. TLC and UV-Vis spectroscopy were used to track the completion of the reaction. The resultant product was purified by silica column chromatography with toluene, THF or chloroform used as the eluent.

N1-BDY

1,3,5,7-Tetraphenyl-borondifluoride azadipyrromethene, yield: 55%. ^{1}H NMR (600 MHz, $CDCl_3$) δ 8.21 (d, *J* = 7.8 Hz, 4H), 8.03−8.09 (m, 2H), 7.91 (s, 2H), 7.76 (d, *J* = 7.2 Hz, 2H), 7.43−7.58 (m, 12H) ppm. MALDI TOF-MS calc. 497.36 amu; Found 497.39 m/z.

N3-BDY

1,7-Di-(4-bromophenyl)-di-3,5-(4-dimethylaminophenyl)-borondifluoride azadipyrromethene, yield: 401 mg. ^{1}H NMR (600 MHz, $CDCl_3$) δ 8.22 (d, *J* = 9.0 Hz, 4H), 8.02 (d, *J* = 7.8 Hz, 4H), 7.70 (d, *J* = 8.4 Hz, 4H), 7.17 (s, 2H), 6.91 (d, *J* = 9.0 Hz, 4H), 3.13 (s, 12H) ppm. MALDI TOF-MS calc. 741.29 amu; Found 741.86 m/z.

N5-BDY

1,7-Di-(4-methoxyphenyl)-3,5-di-(4-nitrophenyl)-borondifluoride azadipyrromethene, yield: 44%. The compound was used to form **Br-N5** without further characterisation.

N6-BDY

1,7-Di-(4-methoxyphenyl)-3,5-diphenyl-borondifluoride azadipyrromethene, yield: 40%. ^{1}H NMR (600 MHz, $CDCl_3$) δ 8.20 (d, *J* = 7.2 Hz, 4H), 8.06 (d, *J* = 9.0 Hz, 4H), 7.86 (s, 2H), 7.70−7.73 (m, 4H), 7.49−7.54 (m, 6H), 3.90 (s, 6H) ppm. MALDI TOF-MS calc. 557.41 amu; Found 557.66 m/z.

2.5 Synthesis of 2,6 halogenated azaBODIPYs

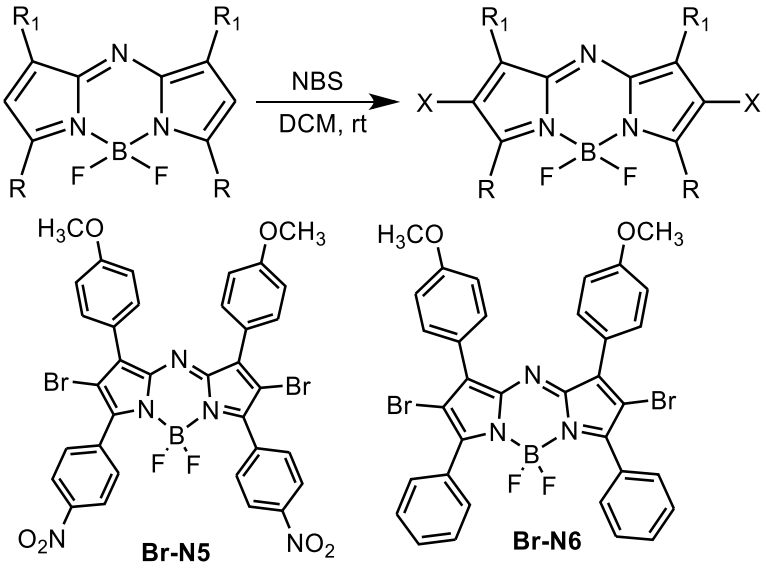

Scheme 2.3: Synthesis of brominated azaBODIPYs.

The relevant azaBODIPY was added to a solvent system of 3:1 chloroform and glacial acetic acid and 2.5 mol equiv. of NBS were added under an inert atmosphere at 30°C, **Scheme 2.3**. 0.506 g (0.063 mmol) was used for **N5-BDY**, and 0.56 g (0.078 mmol) was used for **N6-BDY**. The completion of the reaction was monitored by TLC and UV-Vis spectroscopy. In addition to washing with DCM or chloroform or ethyl acetate, distilled water, and brine solution, a sodium thiosulfate solution was used for the removal of excess NBS. Thereafter, sodium sulfate was used to dry the solution and the solvent removed. After drying, the resultant product was purified by silica column chromatography using chloroform as the eluent.

Br-N5

2,6-Dibromo-1,7-(4-methoxyphenyl)-3,5-(4-nitrophenyl)-borondifluoride azadipyrromethene, yield: 256 mg. ^{1}H NMR (600 MHz, $CDCl_3$) δ 7.84 (d, *J* = 9.0 Hz, 4H), 7.79 (d, *J* = 8.4 Hz, 4H), 7.53 (d, *J* = 8.4Hz, 4H), 7.11−7.14 (m, 4H), 3.88 (s, 6H) ppm. MALDI TOF-MS calc. 805.19 amu; Found 804.04 m/z.

Br-N6

2,6-Dibromo-1,7-(4-methoxyphenyl)-3,5-phenyl-borondifluoride azadipyrromethene, yield: 273 mg. ^{1}H NMR (600 MHz, $CDCl_3$) δ 8.07 (d, *J* = 7.2 Hz, 4H), 7.78 (d, *J* = 7.2 Hz, 4H), 7.47−7.50 (m, 6H), 7.03 (d, *J* = 9.0 Hz, 4H), 3.89 (s, 6H) ppm. MALDI TOF-MS calc. 715.20 amu; Found 714.80 m/z.

2.6 Synthesis of homoleptic azadipyrromethenes

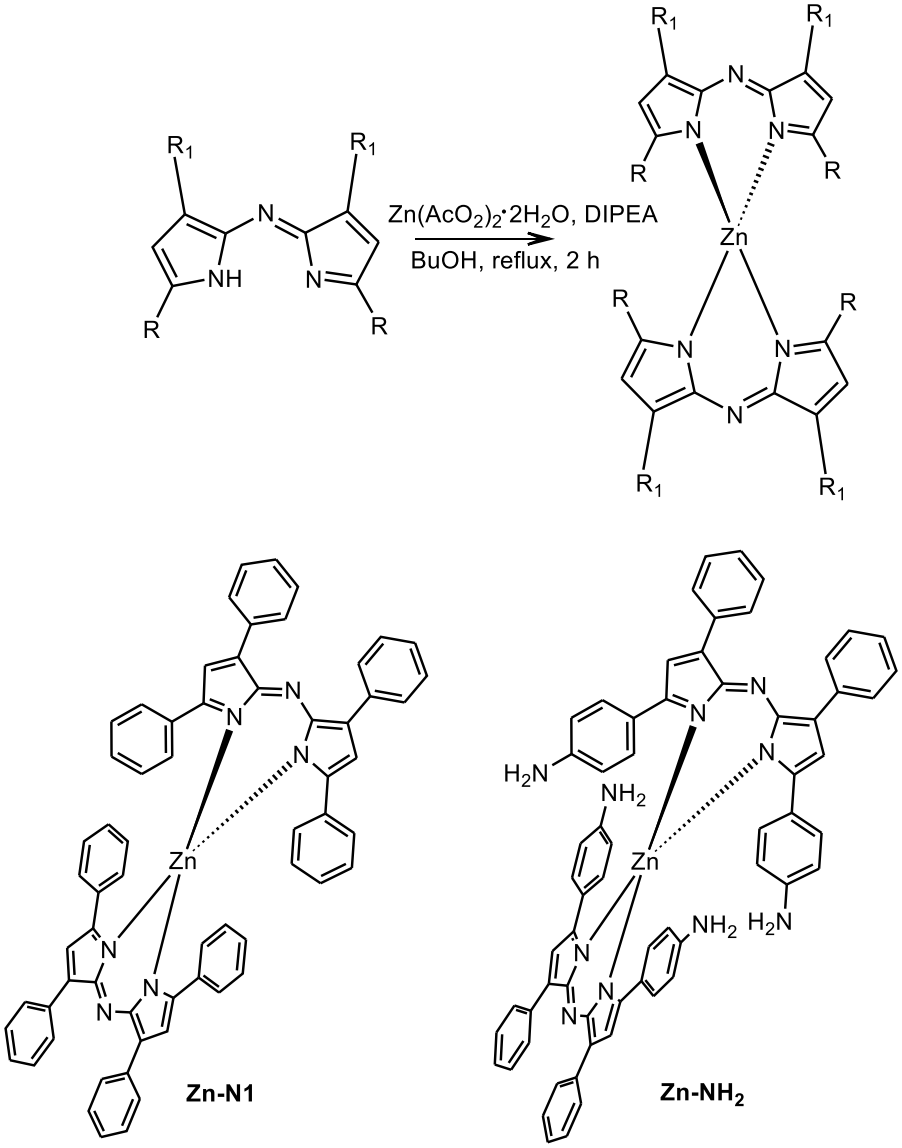

Scheme 2.4: Synthesis of homoleptic Zn-azadipyrromethenes.

To prepare the homoleptic zinc complexes, **Scheme 2.4**, azadipyrromethenes were dissolved in BuOH, 2 mol equiv. of base was added and left to stir for a few hours. Thereafter, 2 mol

equiv. of $Zn(AcO_2)2H_2O$ was introduced into the reaction mixture. TLC and UV-Vis absorption were used to track the reaction to completion. Silica gel column chromatography was used to purify the resultant product with chloroform used as the eluent.

Zn-NH_2

{[(5-(4-aminophenyl)-3-phenyl-1*H*-pyrrol-2-yl)-(5-(4-aminophenyl)-3-phenyl-pyrrol-2-ylidene)]amine} zinc(II), yield: 932 mg. MALDI TOF-MS calc. 1020.34 amu; Found 1020.82 m/z. Solubility issues made ^{1}H NMR measurements impossible.

Zn-N1

{[(3-phenyl-5-phenyl-1*H*-pyrrol-2-yl)-(3-phenyl-5-phenyl-pyrrol-2-ylidene)]amine} zinc(II), yield: 782 mg. ^{1}H NMR (600 MHz, $CDCl_3$) δ 8.22 (d, *J* = 7.8 Hz, 8H), 7.91 (s, 4H), 7.77 (d, *J* = 7.2 Hz, 4H), 7.32−7.56 (m, 28H) ppm. MALDI TOF-MS calc. 962.48 amu; Found 962.70 m/z.

2.7 PACT studies

Staphylococcus aureus (*S. aureus*) was the microorganism selected for the PACT studies. *Staphylococcus aureus* was grown on agar plates, following the manufacturer's specifications, to obtain a colony of bacteria.[42] The colony was introduced to nutrient broth and thereafter placed on a rotary shaker at 200 rpm in an incubator at 37°C overnight to allow bacteria growth. Aliquots of the bacteria culture were transferred into fresh broth (4 mL) then incubated at 37°C until a mid-logarithmic phase (OD at 620 nm ≈ 0.6) was achieved. The cultured broth was removed through centrifugation for 15 min at 3000 rpm to obtain the bacteria. The bacteria extract was washed three times with PBS, removing the nutrient broth then diluted to 1:1000 (v/v) *Staphylococcus aureus*/PBS to achieve the working stock solution of *Staphylococcus aureus*.

PACT studies were conducted following a previously reported procedure.[42] For all experiments, *Staphylococcus aureus* suspensions were incubated for 30 min in an oven fitted

with a shaker at 37°C. 3 mL of the incubated *Staphylococcus aureus* suspension was irradiated at the absorption maxima of the main spectral band of the azaBODIPY in a 24 well plate using the illumination kit of a Modulight® 7710−680 Medical Laser fitted with a Thorlabs M660L3 LED with an irradiance of 280 mW/cm^2 (measured with a Coherent FieldmaxII TOP energy/power meter fitted with a Coherent Powermax PM10 sensor). The other 3 mL of the suspension was kept in a 24 well plate in the dark. The treatment parameters were as follows; dose (1512 J/cm^2) and treatment time (5400 s). After irradiation of 1.5 h in 30 min intervals, 100 µL samples were inoculated onto agar plates and incubated at 37°C for 24 h. A similar procedure was adhered to for the 24 well plate kept in the dark. The colony-forming units values for the bacteria were counted in units of (CFU) / mL using a Scan® 500 automatic colour colony counter.

2.8 PDT studies

2.8.1 *In vitro* dark cytotoxicity

The cell culturing and *in vitro* studies were performed in a manner reported in the literature.[77,78] *In vitro* cytotoxicity studies were carried out in the dark by using human breast adenocarcinoma (MCF–7) cells. The MCF-7 cells were cultured using DMEM containing l-glutamine and phenol red, supplemented with 10% heat-inactivated fetal calf serum (FCS) and 100 unit/mL penicillin-100 µg/mL streptomycin-amphotericin B. The cells were grown in 75 cm^2 vented flasks (Porvair) and incubated at 37°C as well as 5% CO_2 until a cell confluence of 80−100% was reached. The cells were rinsed with DPBS and lifted with trypsin. Viable trypsinised cells were counted with a hemocytometer. 10,000 cells/well were seeded in supplemented DMEM containing phenol red in 96-well tissue culture plates (Porvair®). The cells were incubated at 37°C and 5% CO_2 for 24 h to facilitate cell attachment to the wells. The cells adhered to the wells were washed with 100 µL DPBS twice, followed by the addition

of 100 µL supplemented DMEM for placebo cells. The other cells had **Zn-N1**, **Zn-NH$_2$**, **Br-N5** and **Br-N6** at a range of different concentrations (0.78125, 1.5625, 3.125, 6.25, 12.5, 25 and 50 µg/mL) added. After 24 h treatment, the wells were rinsed with 100 µL DPBS twice, supplemented with fresh media and phenol red was added and the plates were re-incubated for 24 h. The quantification was carried out using a Synergy 2 multi-mode microplate reader (BioTek®) in accordance with the manufacturer's instructions. The percentage cell viability (%cell viability) was determined using Eq. (1):

$$\%\text{cell viability} = \frac{\text{Absorbance sample at 450 nm}}{\text{Absorbance of control at 450 nm}} \times 100 \quad (1)$$

where the Absorbance sample at 450 nm is the absorbance value for the cells containing the photosensitiser dye, while Absorbance of control at 450 nm is the value for the placebo cells containing only supplemented DMEM with phenol red.

2.8.2 *In vitro* photodynamic therapy

The MCF-7 cells treated for PDT were cultured and seeded into 96-well plates with appropriate gradient concentrations of the compounds to be studied. Surviving cells were quantified after re-incubation with supplemented DMEM with Phenol red with the use of MTT assay after 24 h. The cell viability was expressed as a percentage of the absorbance measured for the sample and control by following Eq. 1.

Approximately 10000 cells were seeded on a 96-well plate in 100 µL media per well. Cells were grown for 24 h in a CO_2 incubator and were kept at 37°C incubator in the dark. The plate was then washed with 100 µL of DPBS, and the medium was replaced with supplemented DMEM with no phenol red. The MCF-7 cancer cells were plated in 96 wells and treated with the compounds and were irradiated for 30 min using the illumination kit of a Modulight® 7710−680 Medical Laser fitted with a Thorlabs M625L3 LED for the zinc azadipyrromethene complexes, and a Thorlabs M660L3 LED with an irradiance of 280 mW/cm^2 (measured with a

Coherent FieldmaxII TOP energy/power meter fitted with a Coherent Powermax PM10 sensor) for the brominated azaBODIPYs. After irradiation, the medium was replaced with fresh medium containing phenol red and the cells were left in the dark for 20 h followed by the addition of 20 µL of 5 mg mL^{-1} of MTT to each well and then incubated for 3 h. The culture medium was discarded, and 200 µL of DMSO was added to dissolve the purple formazan crystals. A Synergy 2 multi-mode microplate reader (BioTek®) was used to determine the number of viable cells after treatment at an excitation wavelength of 540 nm. The cytotoxicity of the compounds was measured as the percentage ratio of the absorbance of the treated cells to the untreated controls.

2.8.3 Time-dependent cellular uptake

Approximately 10^4 cells were seeded on 96-well plates and allowed to grow for 24 h. The cells were treated with the azaBODIPY dye (10 µM) in PBS over different time intervals (6, 12 and 24 h). After the incubation, cells were washed twice with PBS to remove any extracellular compounds. Cells were solubilized in 100 µL of 30% Triton X-100 in PBS. The cell accumulated azaBODIPY dye was detected by fluorescence using an ELISA reader with excitation and emission wavelengths of 660 and 680 nm, respectively.

2.9 Attempted syntheses

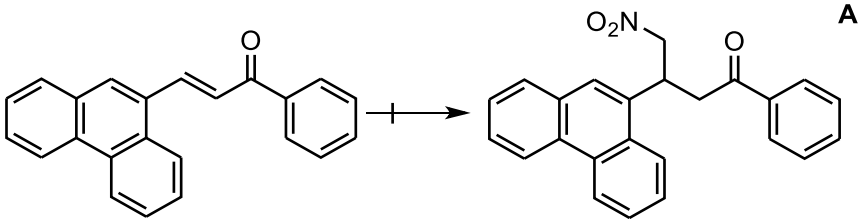

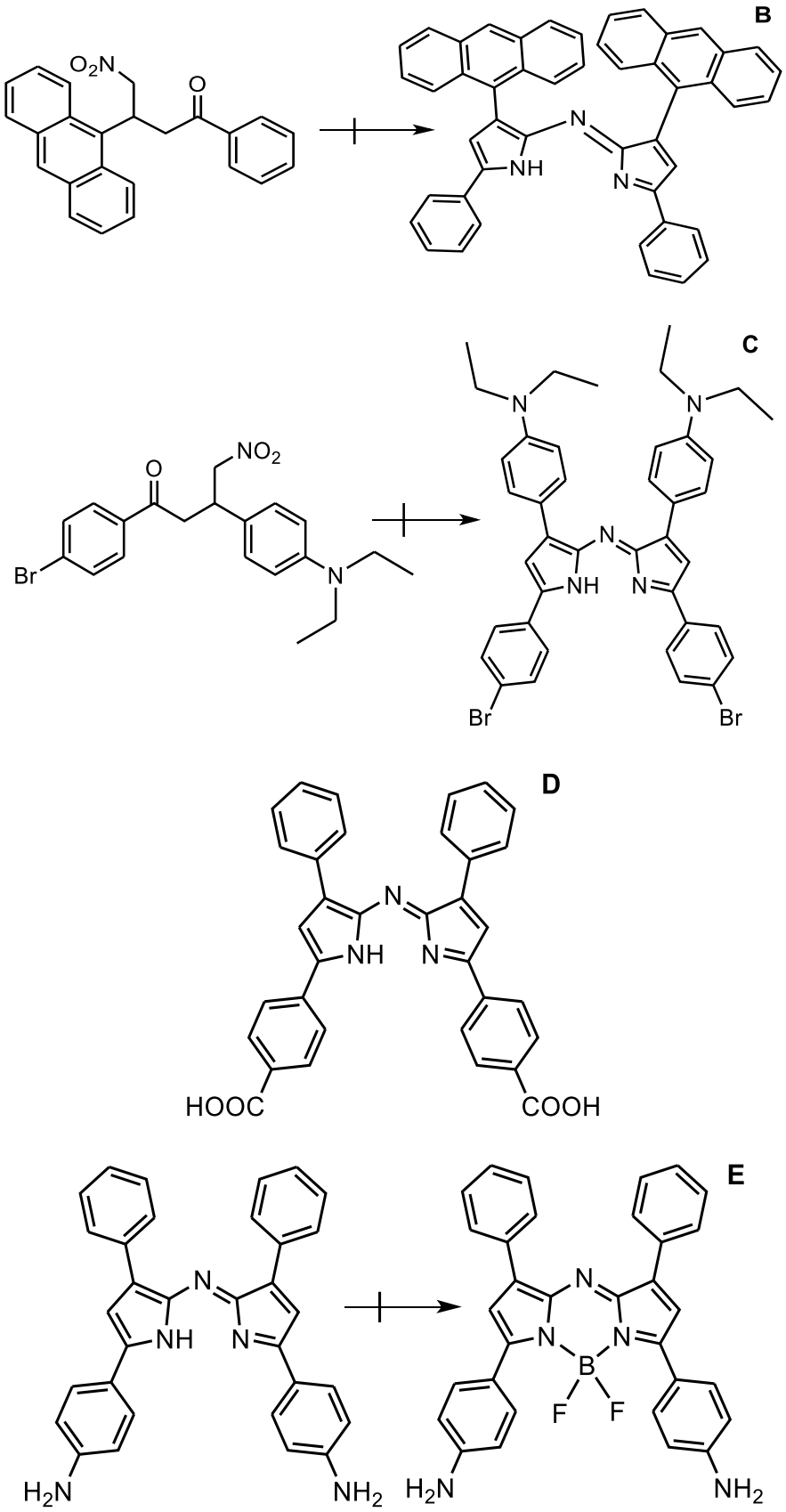

Figure 2.1: Unsuccessful syntheses.

Multiple syntheses were attempted that could not be carried through to completion. Most syntheses required more than one attempt before successful completion. The structures reported in **Figure 2.1A-E** could not be prepared in the time available for the study. Increasing the reaction time, the amount of reactants and the reaction temperature did not result in the formation of the desired product.

The general synthesis procedure described above in the azadipyrromethene section was followed to prepare all of the target compounds shown in **Figure 2.1**. The choice of aldehyde and ketone were as follows **A**: 9-phenanthrenecarboxaldehyde (3 g, 14.5 mmol) and acetophenone (1.74 mL, 14.5 mmol), **B**: 9-anthracenecarboxaldehyde (2 g, 9.69 mmol) and acetophenone (1.13 mL, 9.69 mmol), **C**: 4-diethylaminobenzaldehyde (3 g, 16.9 mmol) and 4-bromoacetophenone (3.36 g, 16.9 mmol) and **D**: benzaldehyde (2 g, 18.8 mmol) and 4-carboxyacetophenone (3.09 g, 18.8 mmol). A 1:1 ratio of the aldehyde and ketone was dissolved in ethanol, followed by 14 mol equiv. of base (KOH or NaOH) for 24 h. The chalcone was crystallised by pouring it over ice and neutralised with HCl. Thereafter, recrystallisation was achieved using MeOH or EtOH depending on the solubility of the chalcone. The recrystallised product was vacuum filtered and allowed to dry. To synthesise the nitromethane adduct, the chalcone was dissolved in degassed MeOH or EtOH. 2-4 pellets of base and 5 mol equiv. of nitromethane were added under an inert atmosphere, and the mixture was heated at reflux for 24 h. Although the synthesis of the nitromethane adduct was generally successful, unfortunately **A** was an exception to this. The challenge of poor solubility of the chalcone in both ethanol and methanol contributed to the unsuccessful conversion to a nitro adduct, in this context. TLC was used to track the completion of the reaction. The reaction mixture pH was adjusted to pH ≈ 4, washed with DCM and distilled water, brine solution and dried with sodium sulfate. Finally, a solution of the nitromethane adduct in

butanol/glacial acetic acid (3:2) was purged with nitrogen or argon gas. 30 mol equiv. of ammonium acetate or urea were used for the conversion to the azadipyrromethene. Challenges with the conversion of the nitromethane adduct to the azadipyrromethene were usually encountered, as observed in the case of **B** and **C**. Failure of the azadipyrromethene syntheses can be attributed to poor stability of the target molecules under the applied conditions. It has been reported that microwave-assisted synthesis offers increased purity, better reaction times and higher reaction yields.[79] This should be considered as an alternative approach in future.

TLC was used to monitor whether all the starting material was consumed, the residue was washed with DCM and distilled water, and rotavapped. The azadipyrromethene **D** was synthesised, but poor solubility prevented further analysis of the dye. The chelation reaction to form **E** has previously been reported as unsuccessful, which was presumed to be due to an unstable cyclic intermediate. A different approach was followed by protecting the -NH_2 group with tert-butyloxycarbonyl (Boc) before proceeding with the chelation, **Scheme 2.5**.[80]

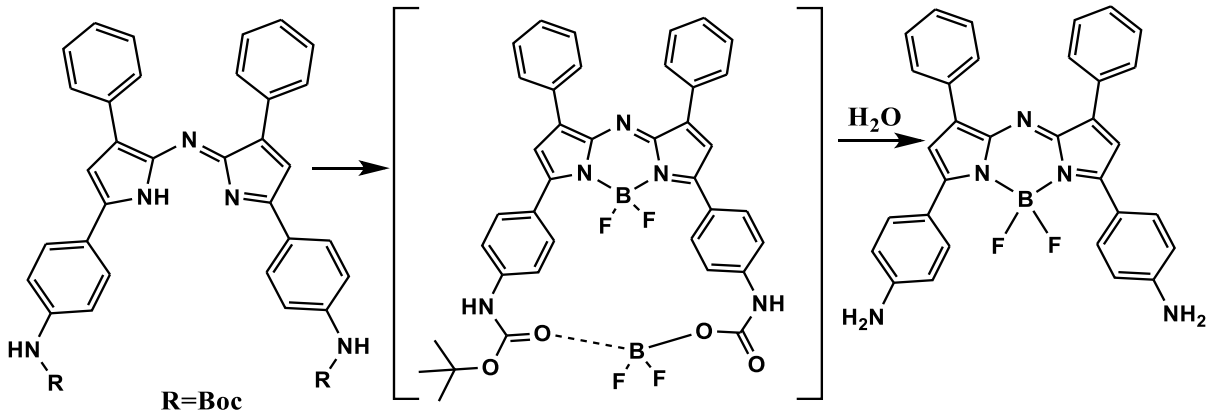

Scheme 2.5: Alternative synthesis method for the amino-substituted azaBODIPY.[80]

3: Characterisation

This chapter reports on the synthesis and characterisation of the azadipyrromethenes and Zn(II) and BF_2 complexes that were prepared for the various applications investigated in the study. The substitution patterns for the dyes typically involved introducing aryl groups at the 1,3,5,7-positions (**Scheme 3.1**). The characterisation techniques used include ^{1}H NMR and UV-Vis absorption spectroscopy and MALDI-TOF MS.

The synthesis of azadipyrromethene ligands was carried out using the procedure shown in **Scheme 3.1**. This was typically followed by the addition of boron trifluoride (**Scheme 3.2**), and electrophilic substitution with heavy atoms (**Scheme 3.3**). The formation of homoleptic complexes (**Scheme 3.4**), complexing with zinc is also described. **N1-BDY** has been synthesised in numerous occasions, generally as a comparative compound. The first synthesis of tetraphenylazadipyrromethene dates back to the 1940s.[9] The synthesis of **N3-BDY**, although it was not the target compound, has been previously reported,[81] while **Br-N6** has also previously been prepared for use as a photosensitizing agent in photodynamic therapy.[13]

3.1 Synthesis of azadipyrromethenes

The synthesis of azadipyrromethenes was achieved via the commonly-used three-step synthesis route, **Scheme 3.1**. Synthesizing a symmetrical azadipyrromethene depends on the initial selection of an aldehyde and ketone to yield a diaryl-α,β-unsaturated ketone **3**, which is prepared in ethanol in the presence of a base. In an attempt to red-shift the absorption band, electron-withdrawing and electron-donating groups were incorporated at the proximal and/or distal positions. Michael addition of nitromethane to the chalcone results in 1,3-diaryl-4-nitrobutan-1-one **4** in the presence of KOH as the base, and this intermediate is used in the following step. Condensation with ammonium acetate in refluxing butanol renders the azadipyrromethene.

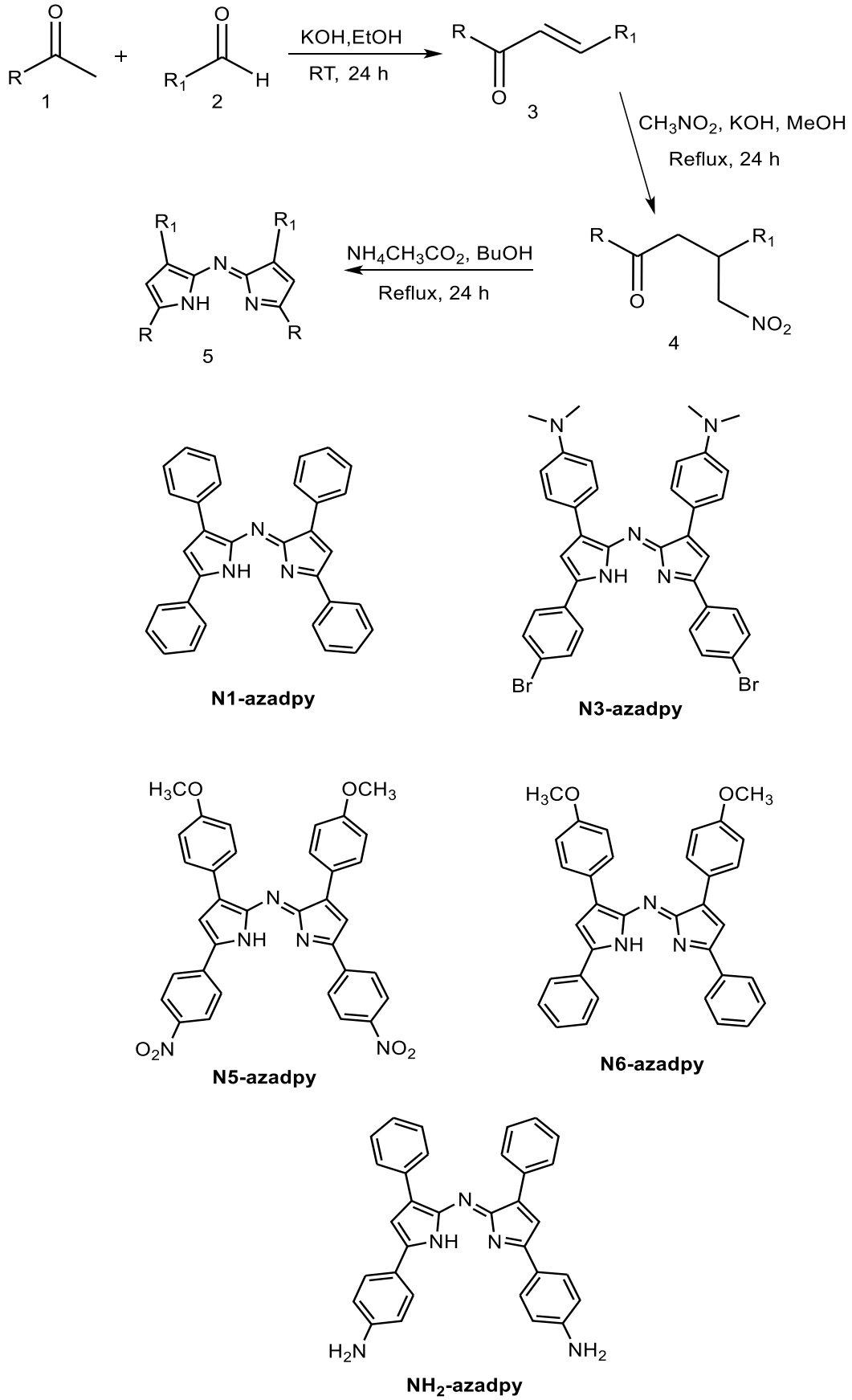

Scheme 3.1: Synthetic pathway followed for azadipyrromethenes synthesis.

3.1.1 Structural analysis

The signals from the twenty-two protons of **N1-azadpy** can be readily identified in the ^{1}H NMR spectrum. Two multiplets that lie in the 7.47−7.57 and 7.36−7.45 ppm region, which integrate to a total of twelve protons, and doublet signals at 7.96 and 8.07 ppm, which each integrate to four protons can be assigned to the phenyl ring protons. A singlet peak at 7.22 ppm integrates to two protons and can be assigned to the 2,6-position protons of the dye.

The ^{1}H NMR spectrum of **N3-azadpy** has the anticipated thirty protons. Four doublets at 8.02, 7.76, 7.63 and 6.77 ppm, which each integrate to four protons, can be assigned to the four phenyl rings. A singlet peak at 7.01 ppm can be attributed to the 2,6-position protons. A twelve proton singlet at 3.05 ppm can be assigned to the dimethylamino protons.

The twenty-four protons of **N5-azadpy** can be readily identified from the ^{1}H NMR spectrum signals, **Figure 3.1**. The three multiplets that lie at 7.62−7.66, 7.57−7.61 and 7.51−7.55 ppm integrate to twelve protons, a singlet at 7.43 ppm integrates to two protons, and the doublet at 6.81 ppm integrates to four protons. These peaks can be assigned to 1,3,5,7-position phenyl rings and the 2,6-position pyrrole protons. The singlet peak at 3.88 ppm can be assigned to the six protons of the 1,7-position methoxy groups.

In a similar manner, the twenty-six proton signals of **N6-azadpy** can be readily identified in the ^{1}H NMR spectrum. The twenty protons of the aromatic region lie in the 7.43−8.20 ppm region. The singlet peak at 3.90 ppm integrates to six protons and can be attributed to the methoxy groups on the distal rings.

The twenty-four protons of **NH_2-azadpy** can also be readily identified in the ^{1}H NMR spectrum. The twenty protons of the aromatic region lie from 6.80−8.07 ppm. The singlet peak that lies at 4.03 ppm integrates to four protons and can be assigned to the amino protons at the 3,5-positions.

MALDI-TOF-MS further confirmed the characterisation of the compounds: **N1-azadpy** calc. 449.56 amu, found 450.08 m/z; and **N3-azadpy** calc. 693.49 amu, found 694.60 m/z.

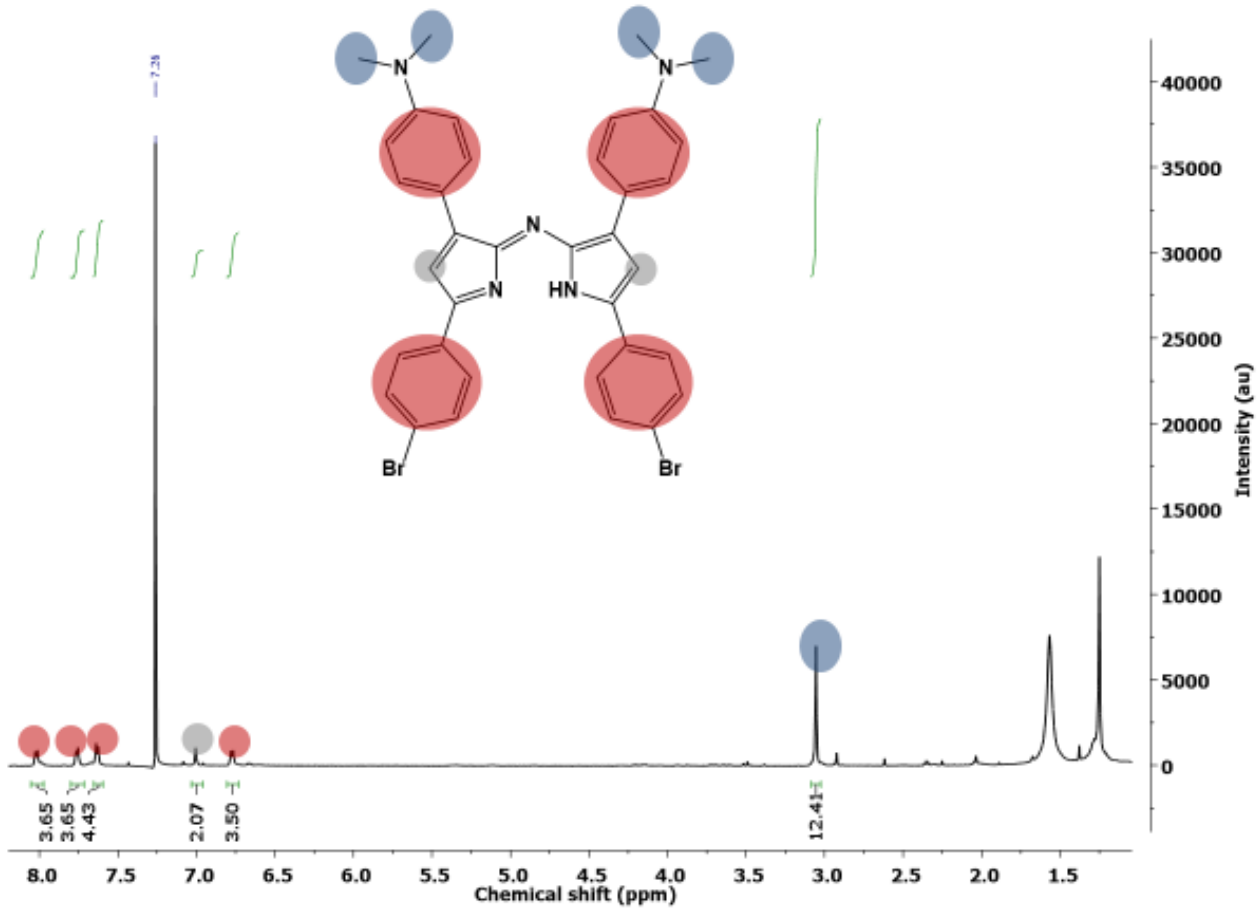

Figure 3.1: The ^{1}H NMR spectrum of **N3-azadpy**, a typical proton ^{1}H NMR spectrum.

To yield azaBODIPY dyes suitable for use as photosensitiser dyes for PACT and PDT, further structural modifications, such as bromination, are required for the azaBODIPY dyes that are formed. **N3-azadpy** was synthesised to prepare a non-brominated azaBODIPY dye intended for use in optical limiting applications.

3.2 Synthesis of azaBODIPYs

Azadipyrromethenes were complexed with excess boron trifluoride in DCM in the presence of a base at room temperature to yield azaBODIPYs, **Scheme 3.2**.

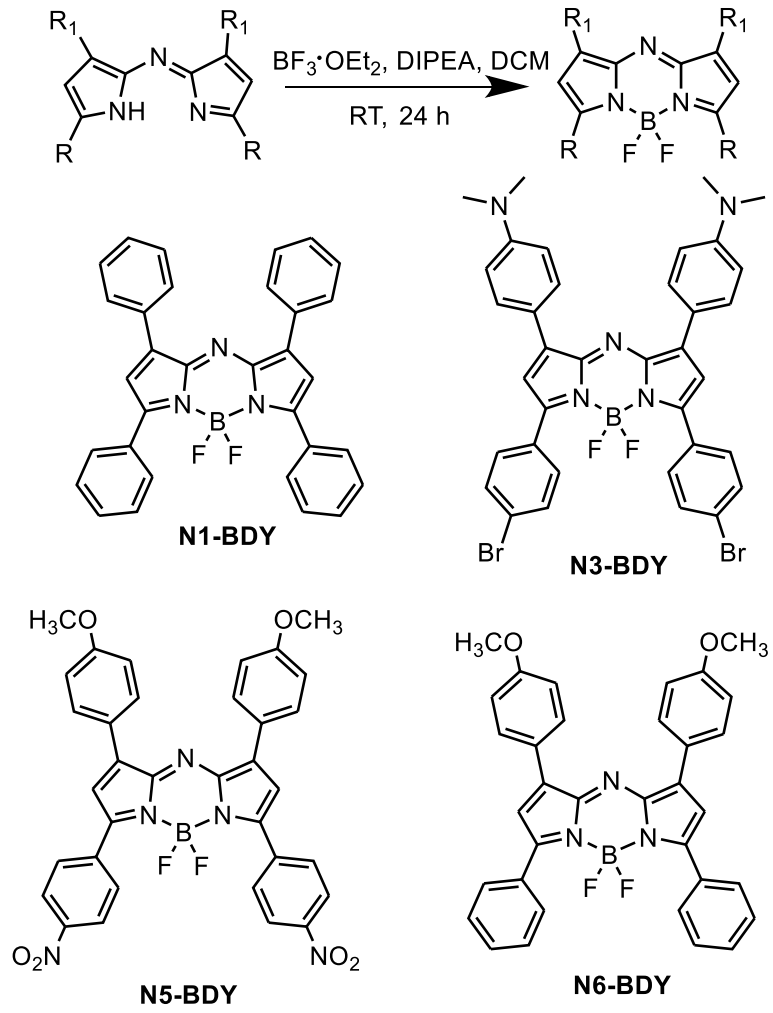

Scheme 3.2: Synthesis of azaBODIPYs.

3.2.1 Structural analysis

In the ^{1}H NMR spectrum of **N1-BDY**, the twenty distal and proximal ring protons form a doublet at 8.21 ppm that integrates to four protons, multiplets at 8.03−8.09 and 7.43−7.58 ppm with a total of fourteen protons, and a doublet at 7.76 ppm that integrates to two protons. A singlet peak at 7.79 ppm can be assigned to the 2,6-position protons. The number of protons present in the ^{1}H NMR spectra of the azaBODIPY dyes and their azadipyrromethene precursors is the same, as the proton that is present at the pyrrole nitrogen atom of the azadipyrromethene is usually not detected. This is believed to be due to resonance effects.[13,16,82,83]

The signals for all thirty protons of **N3-BDY** can be readily identified in the ^{1}H NMR spectrum. The doublets at 6.91, 7.70, 8.02 and 8.22 ppm each integrate to four protons and can be assigned to the four phenyl rings. The singlet peak at 7.17 ppm can be assigned to the pyrrolic 2,6-position protons. A singlet peak at 3.13 ppm integrates to twelve protons and can be assigned to the methyl groups on the dimethylamino groups that are introduced at the 1,7-positions.

All twenty-six protons of **N6-BDY** can be readily identified in the ^{1}H NMR spectrum. In the aromatic region, doublets at 8.20 and 8.06 ppm each integrate to four protons, and multiplets at 7.70−7.73 and 7.49−7.54 ppm integrate to two and six protons, respectively. A singlet integrating to six protons can be readily assigned to the methoxy groups at the 1,7-positions.

To confirm the molecular weights of the synthesised dyes, MALDI-TOF-MS was used and the following data were obtained: **N1-BDY** calc. 497.36 amu, found 497.39 m/z; **N3-BDY** calc. 741.29 amu, found 741.86 m/z, **Figure 3.2**; and **N6-BDY** calc. 557.41 amu, found 557.66 m/z.

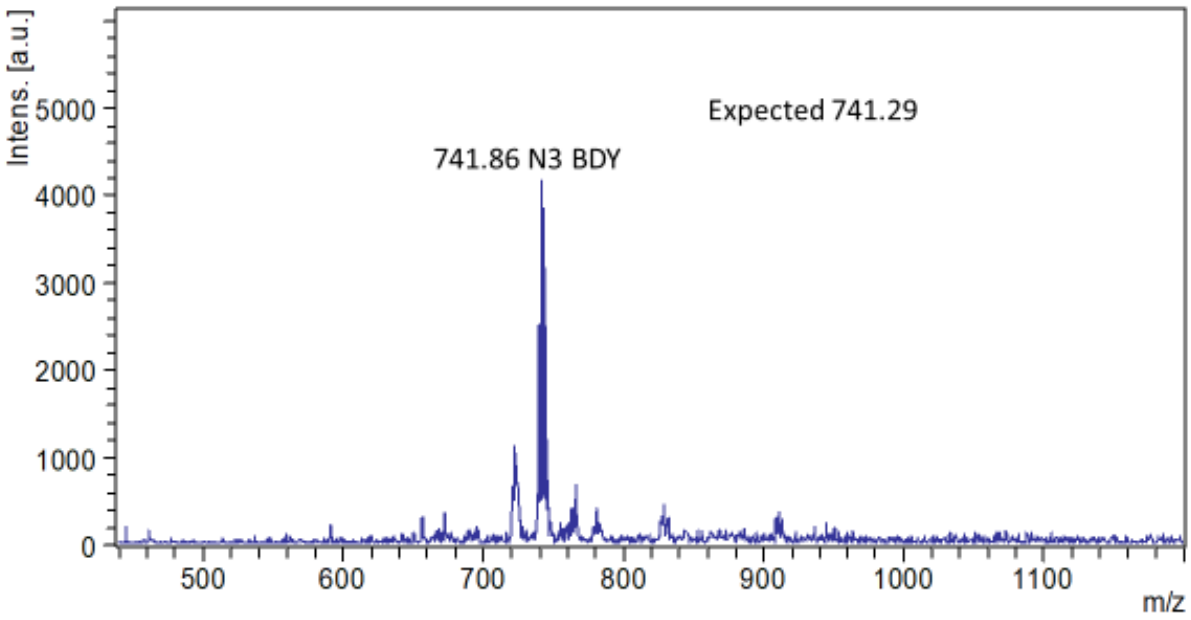

Figure 3.2: MALDI-TOF MS data for **N3-BDY** indicating the calculated and obtained molecular weight.

3.3 Synthesis of 2,6-dibrominated compounds

To facilitate intersystem crossing for singlet oxygen applications, dyes were functionalised with bromine atoms at the 2,6-positions, **Scheme 3.3**. This was achieved at room temperature with NBS in DCM.

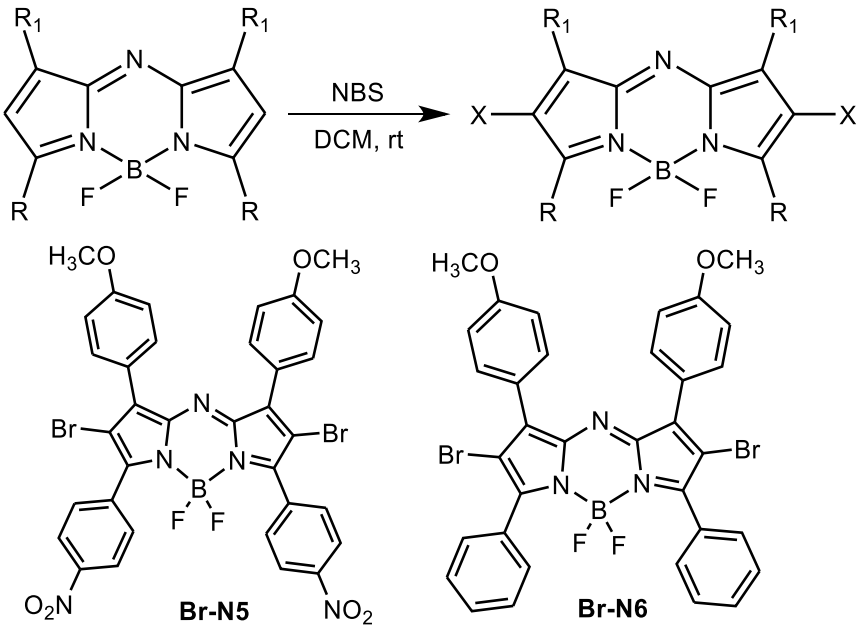

Scheme 3.3: Electrophilic halogenation reactions at the 2,6-positions.

3.3.1 Structural analysis

The key differences in the ^{1}H NMR spectra between the azaBODIPY and the brominated azaBODIPY are associated with the absence of a peak for the protons at the 2,6-positions.

The twenty-two protons of **Br-N5** were readily identified by ^{1}H NMR spectroscopy. The doublets at 7.53, 7.79 and 7.84 ppm and the multiplet at 7.11−7.14 ppm integrate to four protons each and can be assigned to the phenyl rings. A singlet peak at 3.88 ppm integrates to six protons and can be assigned to the methoxy groups.

All twenty-four protons were readily identified in the ^{1}H NMR spectrum of **Br-N6**. Doublet peaks at 7.03, 7.76 and 8.07 ppm integrate to four protons and a multiplet at 7.47−7.50 ppm

which accounts for six protons, can be assigned to the phenyl rings. A singlet peak at 3.89 ppm integrates to six protons arising from the methoxy groups.

The molecular weights of the synthesised dyes were assessed by MALDI-TOF-MS: **Br-N5** calc. 805.19 amu, found 804.04 m/z; and **Br-N6** calc. 715.20 amu, found 714.80 m/z.

3.4 Synthesis of zinc azadipyrromethene complexes

The addition of a Zn(II) ion to provide a heavy atom was also attempted as a strategy to enhance singlet oxygen formation. Azadipyrromethenes were reacted with zinc acetate dihydrate in the presence of a base at reflux in butanol to synthesize the zinc azadipyrromethene complexes, **Scheme 3.4**.

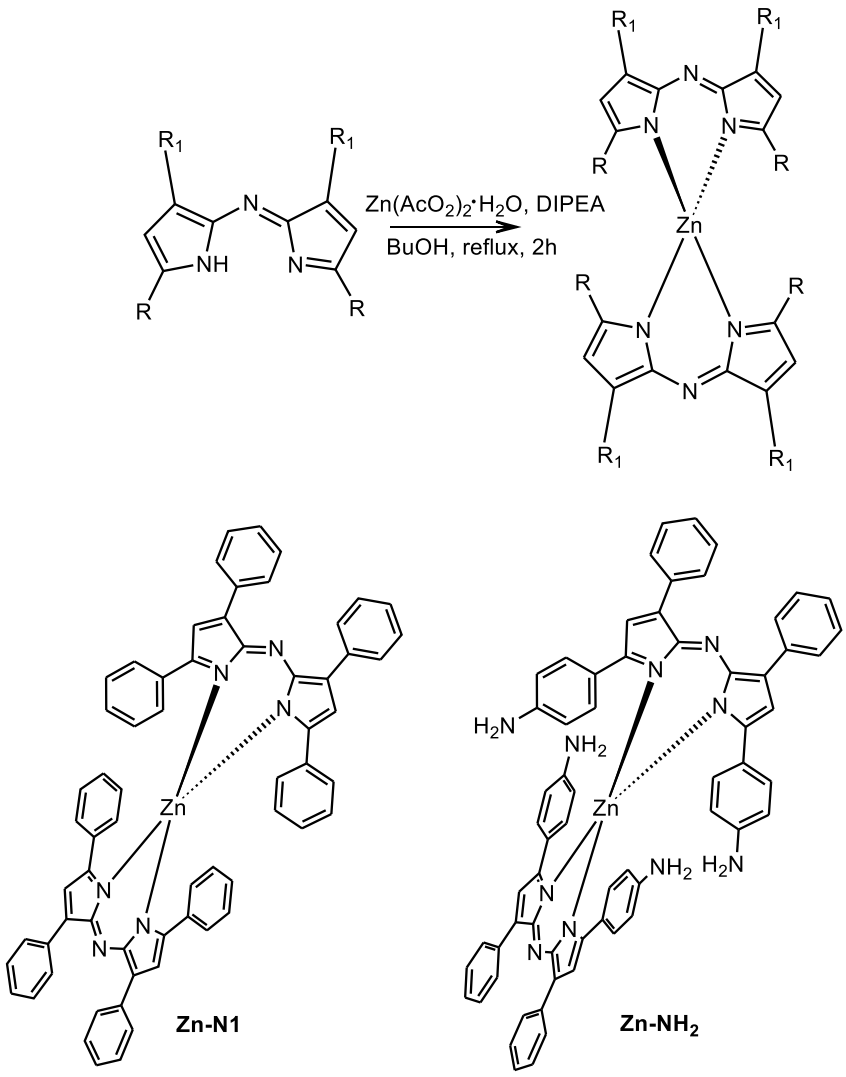

Scheme 3.4: Synthesis of homoleptic zinc azadipyrromethene complexes.

3.4.1 Structural analysis

The ^{1}H NMR spectrum confirmed the presence of all forty-four protons of **Zn-N1**. Two doublets at 7.77 and 8.22 ppm integrate to eight and four protons, respectively, and a multiplet from 7.32−7.56 ppm integrates to 28 protons fully accounting for the phenyl ring protons. A singlet at 7.91 ppm can be assigned to the pyrrolic position protons.

The MALDI-TOF-MS was used to confirm the molecular weights of the synthesised zinc azadipyrromethene complexes: **Zn-N1** calc. 962.48 amu, found 962.70 m/z; and **Zn-NH$_2$** calc. 1020.34 amu, found 1020.82 m/z. Thin-layer chromatography was used to assist in assessing the fractions of dye available when preparing for a column. Subsequently, more fractions appeared after running the column. This resulted in an inability to obtain a ^{1}H NMR spectrum for **Zn-NH$_2$** since the final yield of the purified dye was insufficient to provide a spectrum that could be integrated due to solubility issues.

3.5 Spectroscopic properties

The ground state absorption spectra of all of the dyes were recorded in DCM. The main absorption band for all the azadipyrromethenes originates from the $S_0 \rightarrow S_1$ transition. This also applies to most synthesised compounds, excluding the zinc complexes, which indicates additional transitions discussed further in the molecular modelling chapter. The **N1-azadpy** was synthesised to determine the magnitude of the red-shift of the main spectral band provided by the additional *para*-substituents. It has been shown that introducing an electron-donating group and extending the π-conjugation system can be used to shift the main spectral band to the red.[84] Additionally, the presence of electron-accepting units can also result in a red-shift.[85] The introduction of both electron-withdrawing and electron-donating groups on the azadipyrromethene would result in an increased effect. All substituted azadipyrromethenes exhibited a bathochromic shift of the main spectral band when

compared to the **N1-azadpy** with the largest shift of 57 nm observed in the case of **NH_2-azadpy**, **Table 3.1**. The trends involved will be examined in greater detail in Chapter 7 as part of a molecular modelling study.

Upon chelation with the electron-deficient boron difluoride at the co-ordination pocket, the absorption bands shift closer to the NIR region. This can be observed in **Figure 3.3**. After introducing bromines as heavy atoms at the 2,6-positions, a slight blue-shift was observed (**Figure 3.3**). This was also the case after complexation with zinc, **Figure 3.4**. No evidence of aggregation was observed in various solvents in Beer-Lambert plots. The absorption and emission properties of the target molecules were studied in DCM, DMSO and Toluene for **N3-azadpy**, **N3-BDY**, **Zn-N1** and **Zn-NH_2**. The results are summarised in **Table 3.1**.

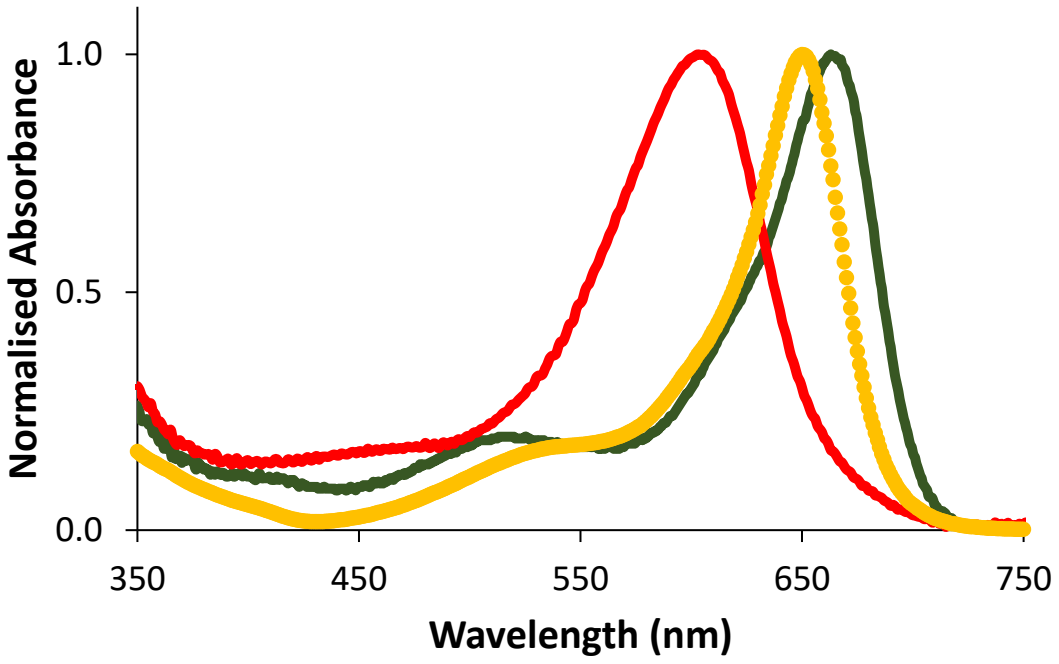

Figure 3.3: The red shift of the main spectral band of **N6-azadpy** (red) when **N6-BDY** (green) and **Br-N6** (yellow) are formed.

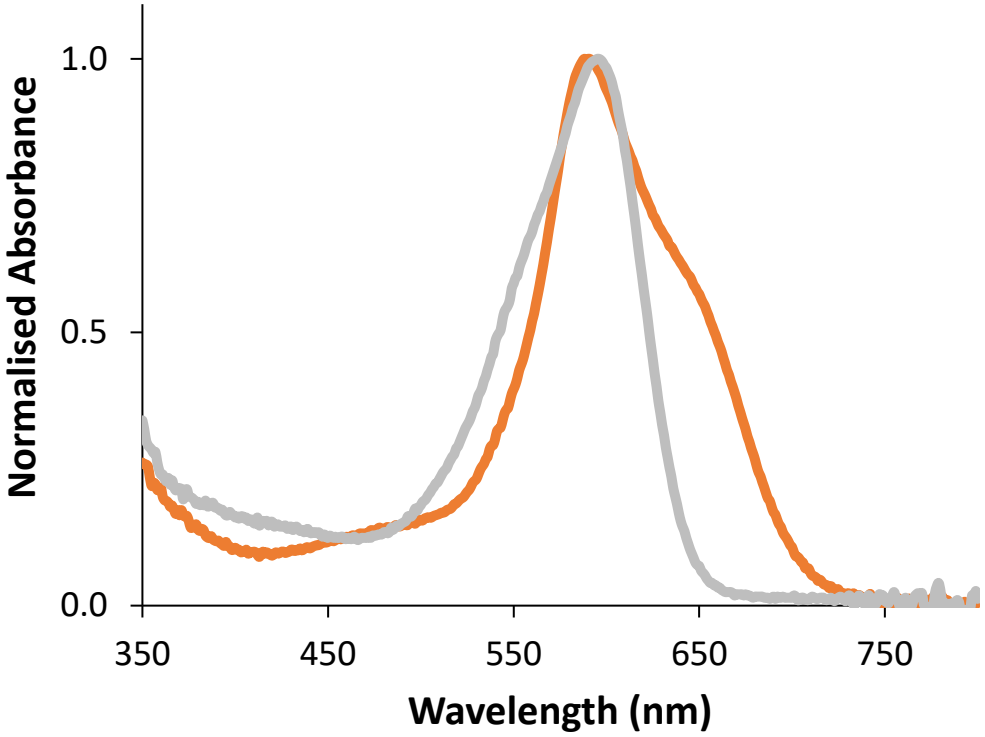

Figure 3.4: The normalised visible region spectra of **N1-azadpy** (grey) and the **Zn-N1** complex (orange).

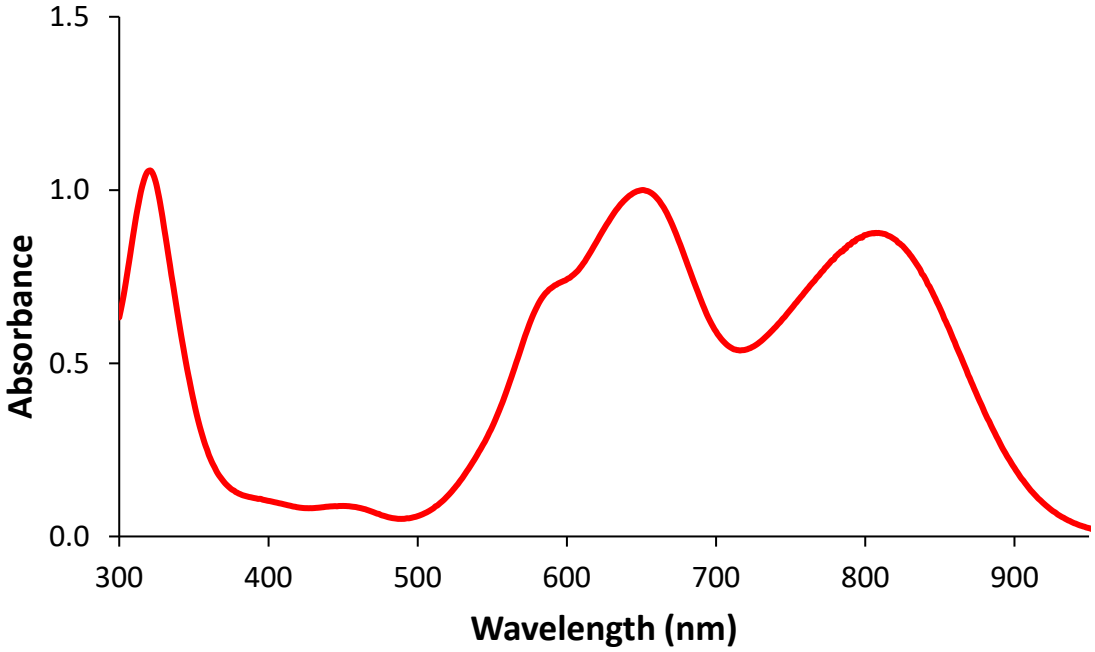

Figure 3.5: The UV-visible-NIR absorption spectrum of **N3-BDY** in DCM.

The morphology of the main spectral bands in the electronic absorption spectrum is influenced by the presence of the dimethylaminophenyl groups at the 1,7-positions, **Figure 3.5**. The introduction of a BF_2 moiety results in a bathochromic shift of the absorption band. The **N3-BDY** selected for study for optical limiting showed no sign of aggregation in Beer-Lambert plots and absorbance maximum at 653 and 810 nm in DCM.

3.6 Photophysical and photochemical studies

Dilute solutions of the dyes and standards were used for the measurement of the fluorescence properties, so that the optical density is around 0.05. The fluorescence quantum yields were determined using a comparative method, making use of zinc phthalocyanine as the standard. The azadipyrromethenes and the zinc complexes in this study were found to be almost completely non-emissive with ϕ_F values > 0.01. The d^{10} metal complexes of azadipyrromethenes have previously been reported to fluoresce with quantum yields > 0.015 at room temperature.[86] In contrast, azaBODIPY structures are known to exhibit high fluorescence quantum yields.[87] This was not the case for **N3-BDY**, however, which was also found to have an ϕ_F value > 0.01. The presence of intramolecular charge transfer (ICT), due to the presence of the dimethylamino groups at the 1,7-positions, quenches fluorescence as it enhances the rate of non-radiative decay.[88]

Table 3.1: Photophysical data of **N3-azadpy**, **N3-BDY**, **Zn-N1** and **Zn-NH_2** in DCM, toluene and DMSO.

Solvent	Compound	λ_{abs} (nm)	Log ε	Solvent	Compound	λ_{abs} (nm)	Log ε
DCM	**N1-azadpy**	598	N.S.	Toluene	**N3-azadpy**	633	N.S.
	N5-azadpy	607	N.S.		**N3-BDY**	637, 787	N.S.
	N6-azadpy	600	N.S.		**Zn-N1**	594	N.S.
	NH_2-azadpy	655	N.S.		**Zn-NH_2**	627	N.S.
	N1-BDY	650	N.S.	DMSO	**N3-BDY**	684, 857	N.S.
	N6-BDY	663	N.S.		**Zn-NH_2**	648	N.S.
	N3-azadpy	631	4.41				
	N3-BDY	653, 810	4.40				
	Zn-N1	590	3.94				
	Zn-NH_2	623	4.12				

N.S.= not studied

The absorption band maxima of **Br-N5** and **Br-N6** in DCM and ethanol and other photophysical and photochemical data are summarised in **Table 3.2**. For **Br-N5** and **Br-N6**, the incorporation of heavy atoms led to low fluorescence quantum yield values, so fluorescence is not the main radiative deactivation pathway to the ground state. This signifies that the triplet state population may be significant.[89] The singlet oxygen quantum yields obtained are consistent with this, **Table 3.2**. AzaBODIPY dyes functionalised with heavy atoms such as bromine and iodine, especially at the 2,6-positions can be used as photosensitiser dyes to generate singlet oxygen, **Figure 3.6**. The singlet oxygen quantum yields can be used to assess the potential for use as photosensitisers. While tracking the spectral change of DPBF absorbance with irradiation time, no spectral changes were noted in the main spectral band for both dyes demonstrating that they exhibit high photostability and resistance to photobleaching. Based on the singlet oxygen quantum yields, it would be anticipated that **Br-N6** would provide better performance as a photosensitiser.

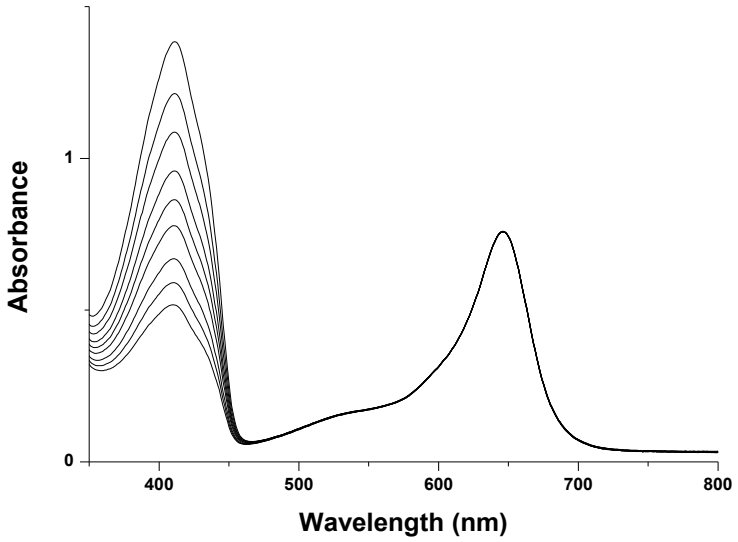

Figure 3.6: Singlet oxygen determination for **Br-N6** in ethanol using DPBF as a singlet oxygen scavenger.

Table 3.2: Photophysical and photochemical data for **Br-N5** and **Br-N6** in DCM and ethanol.

Solvent	AzaBODIPY	λ_{abs} (nm)	λ_{em} (nm)	ϕ_F	ϕ_Δ	τ_T (μs)	Log ε
DCM	**Br-N5**	664	728	0.026	0.64	13.2	4.56
	Br-N6	650	711	0.001	0.68	12.1	4.80
Ethanol	**Br-N5**	662	726	0.011	0.70	N.S.	N.S.
	Br-N6	646	706	0.002	0.78	N.S.	N.S.

N.S.= not studied

The triplet state lifetimes and transient absorption spectra were recorded in DCM using an Edinburgh Instruments LP980 spectrometer, **Figures 3.7** and **3.8**. Singlet depletion is observed in the region that corresponds with the main ground state absorption band. The transient intermediates formed from **Br-N5** and **Br-N6** decayed by a first-order process with τ_T values of 13.2 and 12.1 μs in DCM indicating that there is no formation of any permanent products and/or degradation of the dye, **Table 3.2**. The singlet oxygen quantum yields for **Zn-N1** and **Zn-NH_2** were much lower than anticipated, **Table 3.3**. Singlet oxygen was the only type of ROS whose generation was quantified in this context, but since it is not the only type of ROS that can be formed, it was concluded that the molecules could still hold potential as photosensitisers in certain contexts and that PDT activity experiments should still be carried out.

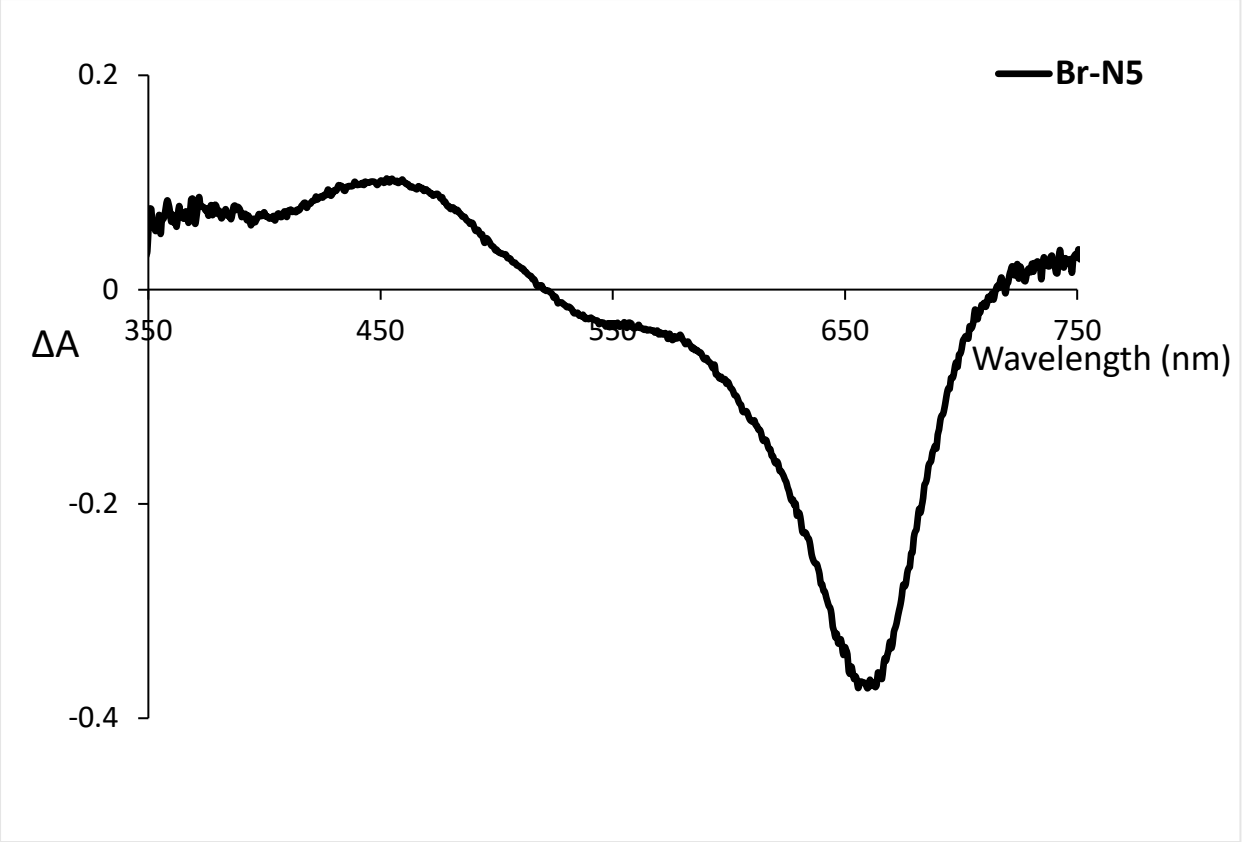

Figure 3.7: Transient absorption spectrum for **Br-N5** in DCM.

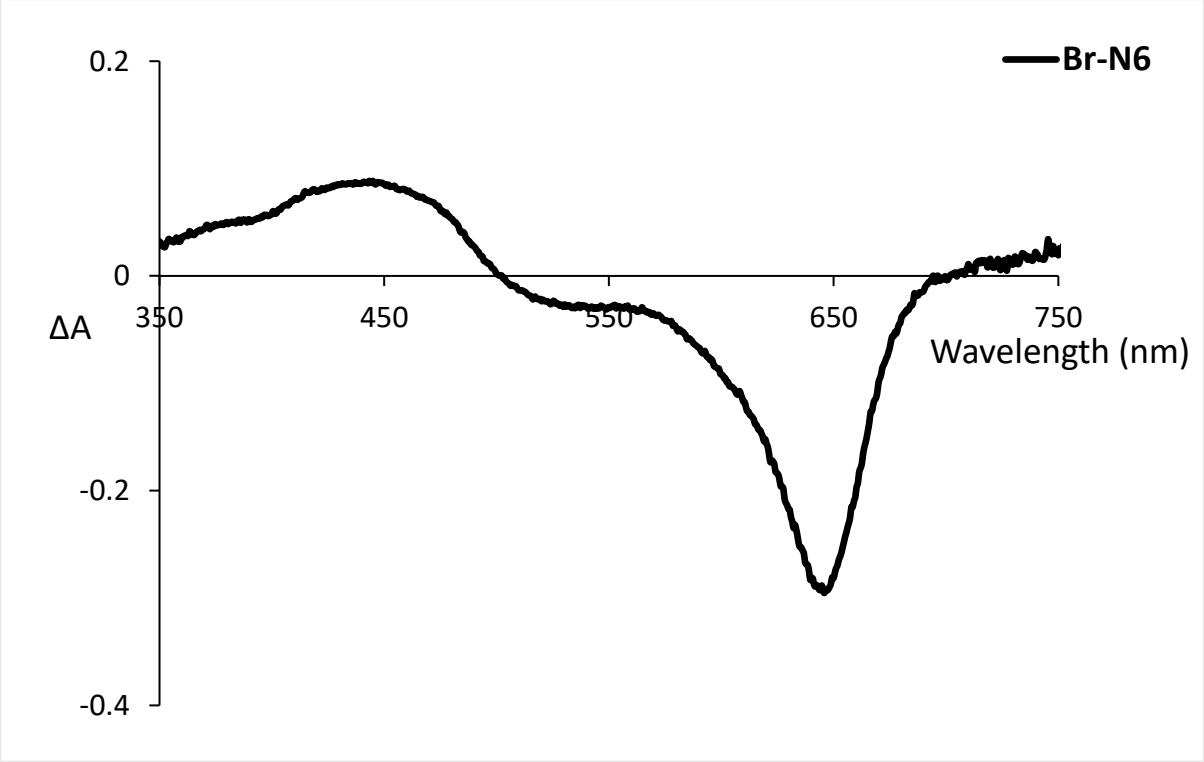

Figure 3.8: Transient absorption spectrum for **Br-N6** in DCM.

Table 3.3: Photophysical and photochemical properties for **Zn-N1** and **Zn-NH$_2$** in DMSO.

Solvent	Zinc azadipyrromethene	λ_{abs} (nm)	λ_{em} (nm)	ϕ_F	ϕ_Δ
DMSO	**Zn-N1**	598	N.D.	N.D.	0.05
	Zn-NH$_2$	648	N.D.	N.D.	N.D.

*__Zn-NH$_2$__ was unable to degrade DPBF.

3.7 Concluding remarks

AzaBODIPY and zinc azadipyrromethene complexes were synthesised and characterised. The introduction of bromine atoms onto the azaBODIPY structure as heavy atoms enhances the generation of singlet oxygen. The ability of the brominated azaBODIPY dyes to generate singlet oxygen and their photostability makes the dyes potentially suitable for use as PS dyes in PDT and PACT. Chelation with zinc atoms as heavy atoms did not provide the anticipated enhancement of singlet oxygen generation, however.

4: Photodynamic antimicrobial chemotherapy

This chapter reports the results obtained for PACT studies using brominated azaBODIPYs **Br-N5** and **Br-N6** as photosensitiser dyes on *S. aureus*. These compounds were selected as they exhibited absorbance maxima in the ideal UV-visible to NIR region, a reasonably high singlet oxygen quantum yield and a neutral charge.[39,42,43] A compound with these characteristics can be expected to be effective against gram (+) microbes. A Thorlabs 660 nm LED was used with an irradiance value of 280 mW/cm^2. *S. aureus* is a gram (+) bacteria with relatively porous cell walls due to the peptidoglycan layer having pore sizes of 15−80 nm, and the absence of an extra polysaccharide layer above the peptidoglycan layer. For this reason, *S. aureus* has the ability to be photoinactivated by charged (positive or negative) as well as neutral photosensitisers.[90] Both investigated photosensitiser dyes are neutral, but the presence of the NO_2 groups on **Br-N5** potentially allows the compound to faster penetrate the bacteria as compared to **Br-N6**. In Chapter 3, **Br-N5** was found to have a slightly lower singlet oxygen quantum yield than **Br-N6**, however.

4.1 PACT studies of *Staphylococcus aureus* in solution

PACT studies were performed in aqueous solutions with 0.2% DMSO for both compounds due to the compounds being insoluble in water. A comparative study between azaBODIPYs **Br-N5** and **Br-N6** was conducted. The activity of the azaBODIPYs was assessed against *S. aureus*. The effect of 0.2% DMSO in PBS on *S. aureus* has previously been shown to be negligible.[91] Following optimisation, a constant concentration of 1 µg/mL of each azaBODIPY was studied. 100% bacterial colony survival values are based on the values derived for zero irradiation time. Brominated azaBODIPYs dyes, **Br-N5** and **Br-N6**, were found to be effective when used as photosensitiser dyes in the inactivation of *S. aureus* (**Figures 4.1** and **4.2** and **Table 4.1**). **Br-N5** proved to be more effective than **Br-N6**. **Br-N5** showed minimal dark toxicity after 60 min;

thereafter, greater toxicity is observed even in the absence of light activation. In contrast, **Br-N6** showed a steadier decrease in the population survival. After 90 min, 67% had survived.

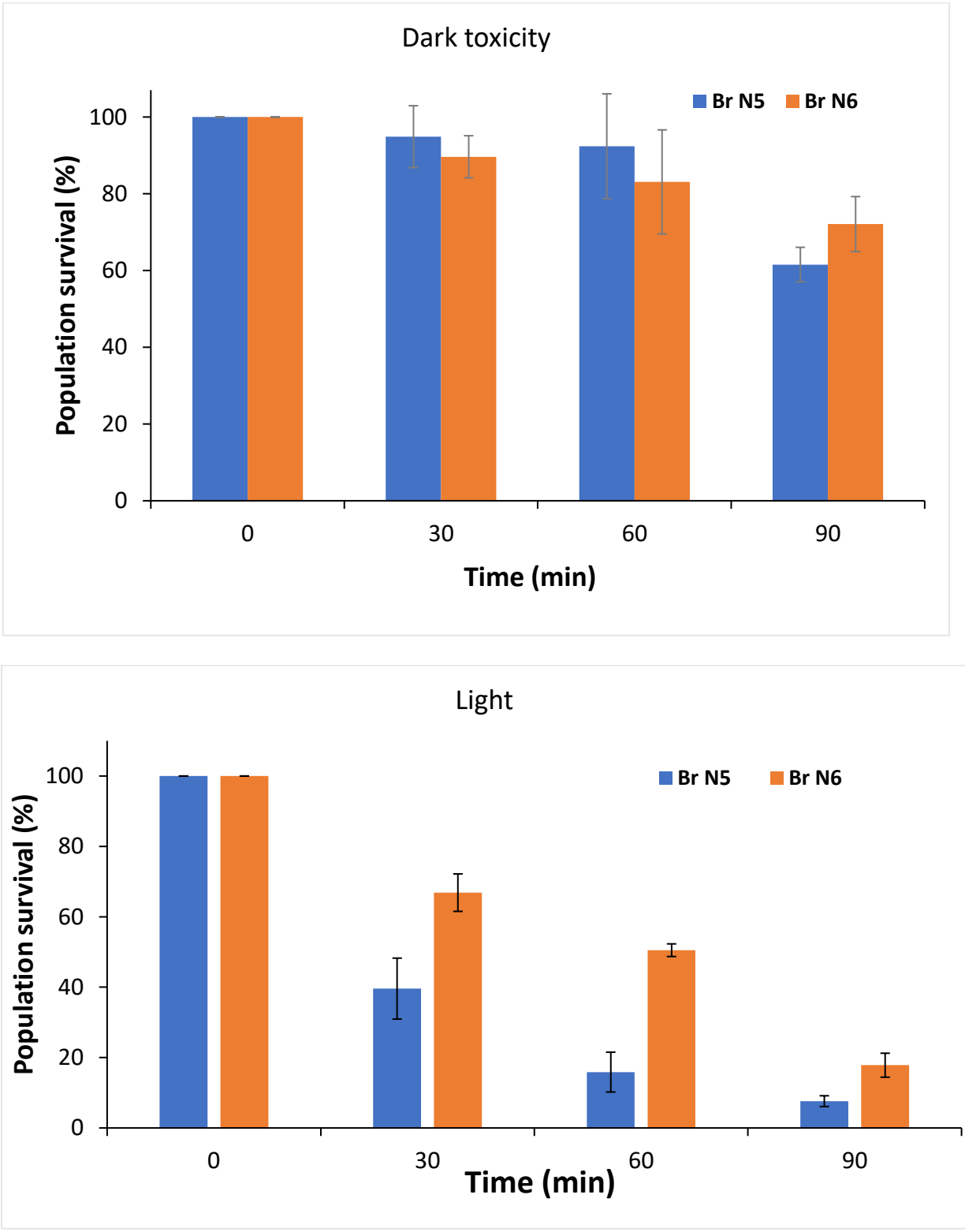

Figure 4.1: The dark toxicity (TOP) and photoirradiation (BOTTOM) studies conducted for **Br-N5** and **Br-N6** against *S. aureus* colonies.

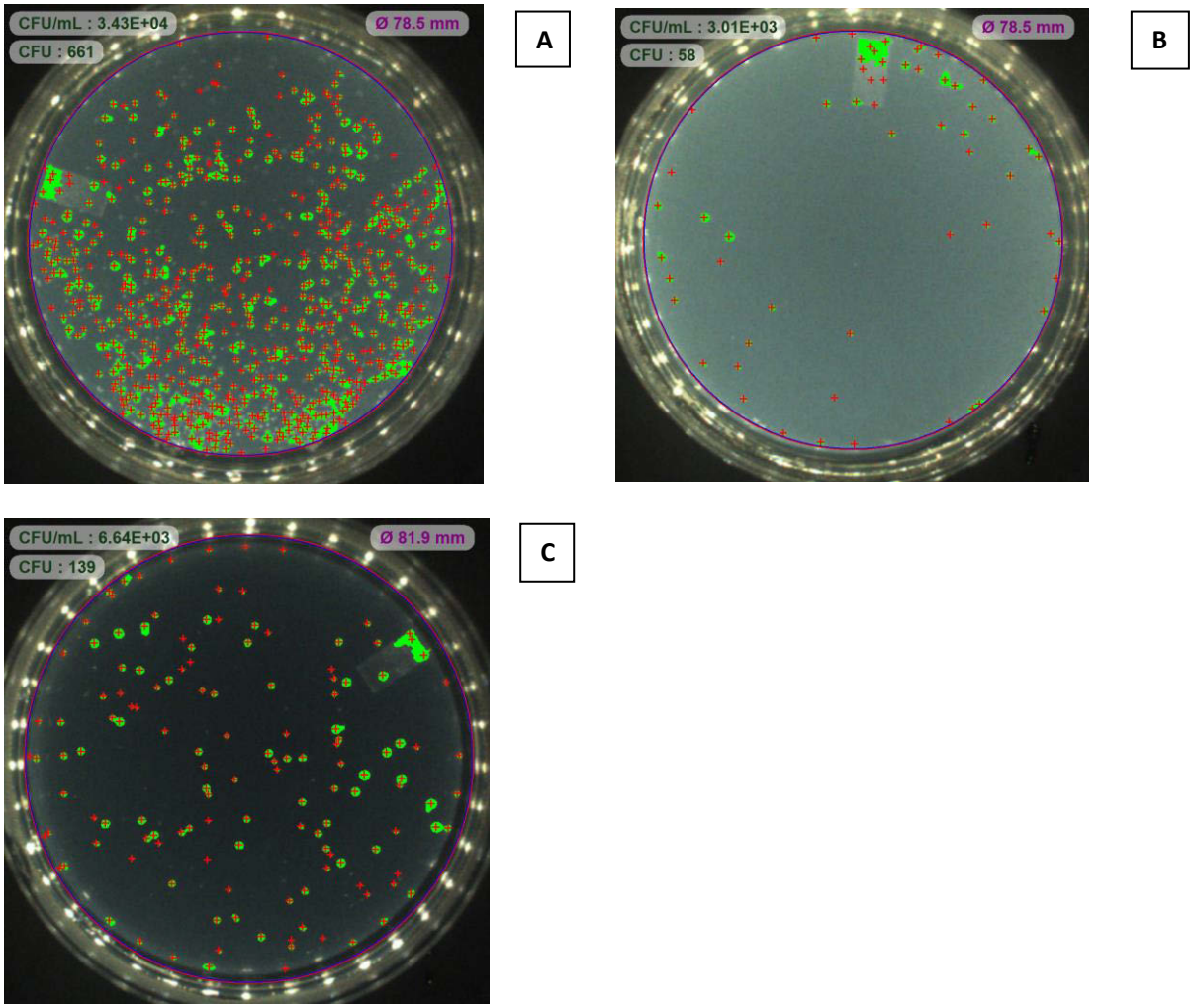

Figure 4.2: Images of the progression with PACT studies, A: at zero irradiation time, whereas B and C display impact of **Br-N5** and **Br-N6** on *S. aureus* colonies, respectively at 90 min irradiation.

Table 4.1: Summarised PACT results.

AzaBODIPYs	Overall % population inactivation
Br-N5	92
Br-N6	82

4.2 Concluding remarks

The PACT activities of two brominated azaBODIPYs dyes were investigated against *S. aureus*. With the aid of DMSO, aqueous solubility of the azaBODIPYs dyes was achieved. The dyes exhibited relatively weak activity compared to 2,6-dibrominated distyrylBODIPY dyes that have been studied recently using a similar approach that achieved log reduction values of

over 9.[92] This suggests that azaBODIPY dyes may be less suitable for study than conventional BODIPY dyes in this context. Nitro-substituted **Br-N5** had better activity after 90 min than **Br-N6**, and the antibacterial effect in the dark toxicity experiments was also more pronounced.

5: Photodynamic Therapy

Preliminary photodynamic activity experiments against MCF-7 human breast adenocarcinoma cells were evaluated for the homoleptic zinc azadipyrromethene complexes and two brominated azaBODIPY dyes **Br-N5** and **Br-N6**. All studies were conducted *in vitro*. The percentage of viable cells was determined using the MTT assay.[93] The investigation included *in vitro* dark toxicity & photodynamic activity tests. Previous studies concerning azaBODIPYs have been conducted examining their use in PDT. A variety of cancerous cells were investigated such as HeLa cervical carcinoma cells, fibroblast cancer cells and human breast cancer cells.[12,13,94] A recent study probing azaBODIPYs against MCF-7 breast cancer cells was conducted *in vivo* and *in vitro*, which included the use of nanomicelles whose IC_{50} results are comparable to the best results discussed in this chapter.[94]

5.1 PDT activity of homoleptic zinc azadipyrromethene dyes

The photodynamic activity properties of the homoleptic zinc azadipyrromethene dyes and the corresponding azadipyrromethene dyes were determined using the MTT assay on MCF-7 cells following a methodology previously reported in the literature.[93] The effect was explored over a 0.8−50 $\mu g.mL^{-1}$ concentration range. The zinc complexes were illuminated for 30 min in a 96 well plate using a Modulight® 7710-680 Medical Laser fitted with a Thorlabs M625L3 light-emitting diode with an irradiance of 240 $mW.cm^{-2}$. Stock solutions for **N1-azadpy**, **NH_2-azadpy**, **Zn-N1** and **Zn-NH_2** were prepared in DMSO and were diluted to < 1% once appropriate aliquots were added to the wells. Three separate wells were filled at each concentration for all of the compounds to enable statistical analysis. Placebo cells were incubated with supplemented DMEM only and with 1% DMSO (v/v), the maximum percentage of DMSO that is present. No significant cytotoxic effect was observed on the MCF-7 cells in the absence of dyes. Minimal dark toxicity was observed for the Zn complexes at low concentrations, **Figure 5.1**. A gradual increase was observed with increasing concentration.

The precursors (azadipyrromethenes) exhibit more significant dark toxicity than the homoleptic zinc azadipyrromethene complexes.

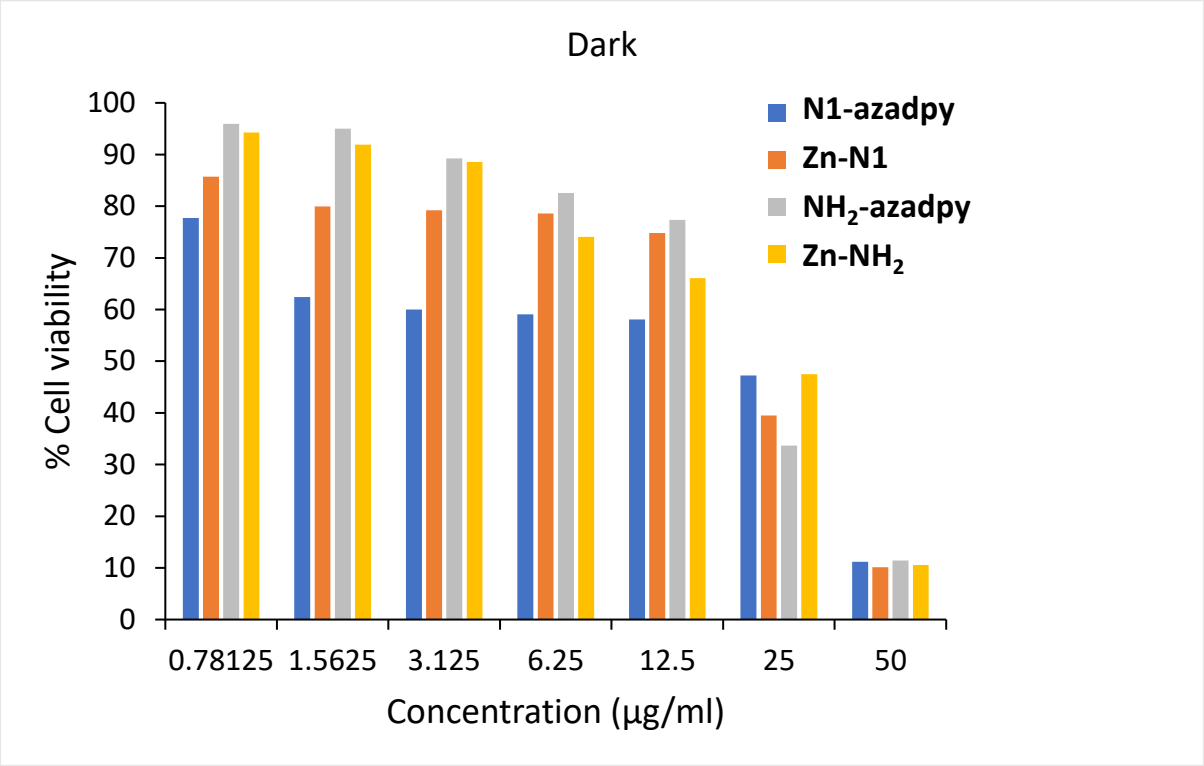

Figure 5.1: Dark toxicity exhibited *in vitro* by zinc complexes and their precursors.

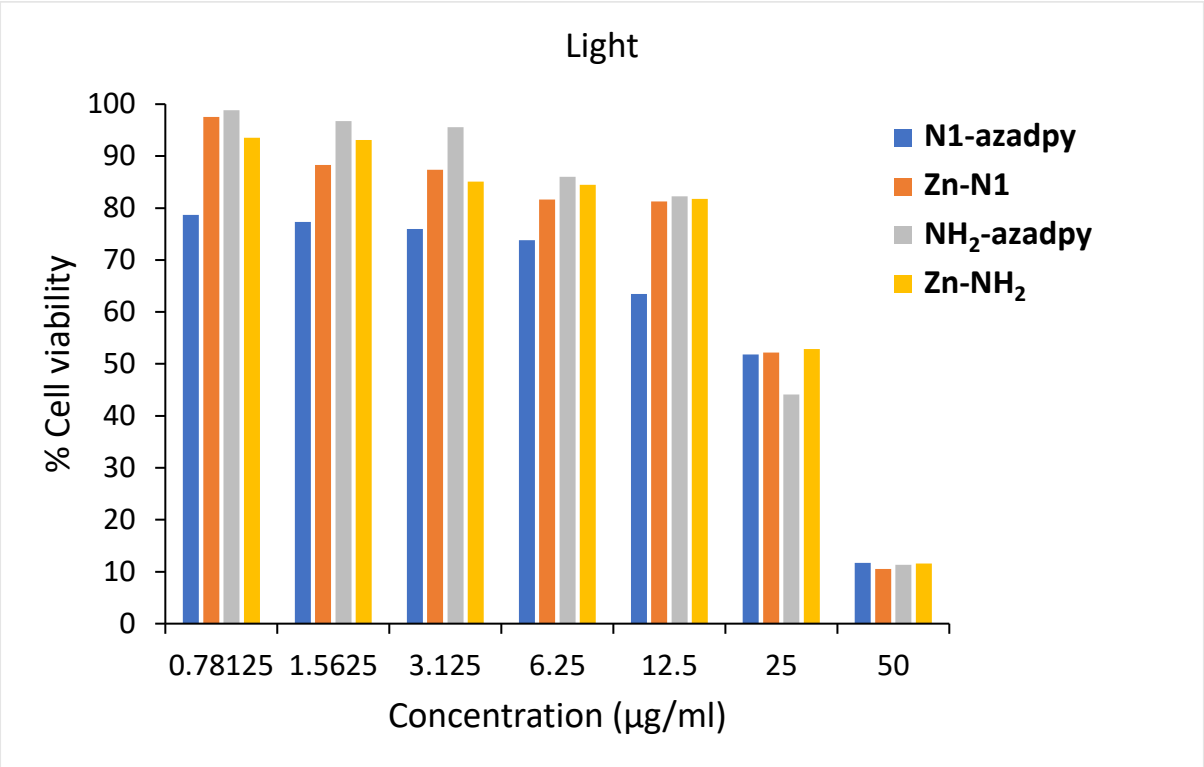

Figure 5.2: PDT activity displayed *in vitro* by zinc complexes and their precursors.

Upon illumination, the PDT results indicate that the zinc complexes were not effective against the destruction of cancerous cells, **Figure 5.2**. In fact, the compounds proved to provide better activity in the dark than when the PS were irradiated with light. For the lower concentrations investigated, **N1-azadpy** showed the most activity when compared to the other molecules. In Chapter 3, the absence of singlet oxygen generation, one of the two types of photosensitisation available, was discussed. The availability of Type I photosensitisation involving ROS formed through electron transfer, still held the potential for the zinc complexes to be successful candidates for PDT, but the results clearly demonstrate that this was not the case.

5.2 PDT activity of brominated azaBODIPY dyes

5.2.1 Cellular uptake

The cellular uptake of the azaBODIPY dyes was investigated by incubating the MCF-7 cells with **Br-N5** and **Br-N6** dyes for periods of 6, 12 and 24 h, **Figure 5.3**. To quantify the incorporated azaBODIPYs, the fluorescence intensity was measured. Cellular uptake peaked at 6 h for **Br-N6** and 12 h for **Br-N5**.

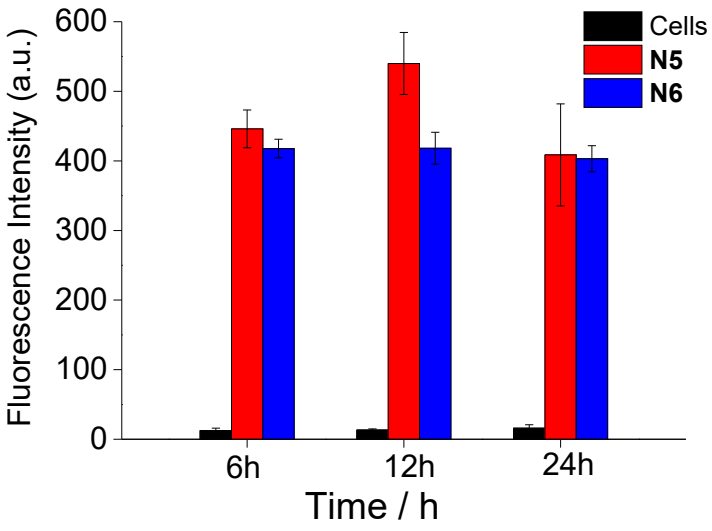

Figure 5.3: Time-dependent cellular uptake of **Br-N5** and **Br-N6** in MCF-7 cells. [Concentration, 10 µM]

5.2.2 Cytotoxicity

The photodynamic activity of **Br-N5** and **Br-N6** was determined using the MTT assay on MCF-7 cells following a methodology previously reported in the literature.[95] The activity was explored over a 0.8–50 $\mu g.ml^{-1}$ concentration range. The azaBODIPYs were illuminated for 30 min in a 96 well plate using a Modulight® 7710-680 Medical Laser fitted with a Thorlabs M660L3 light-emitting diode with an irradiance of 280 $mW.cm^{-2}$. Stock solutions for **Br-N5** and **Br-N6** were prepared in DMSO and were diluted to < 1% when appropriate aliquots were added to the wells. Three separate wells were filled at each concentration for both dyes to enable statistical analysis. The dark toxicity of the dyes was determined, and **Br-N6** was found to be less toxic than **Br-N5** in the absence of light. Placebo cells were incubated with supplemented DMEM only and with 1% DMSO (v/v), the maximum percentage of DMSO that is present. No significant cytotoxic effect was observed on the MCF-7 cells in the absence of **Br-N5** or **Br-N6**.

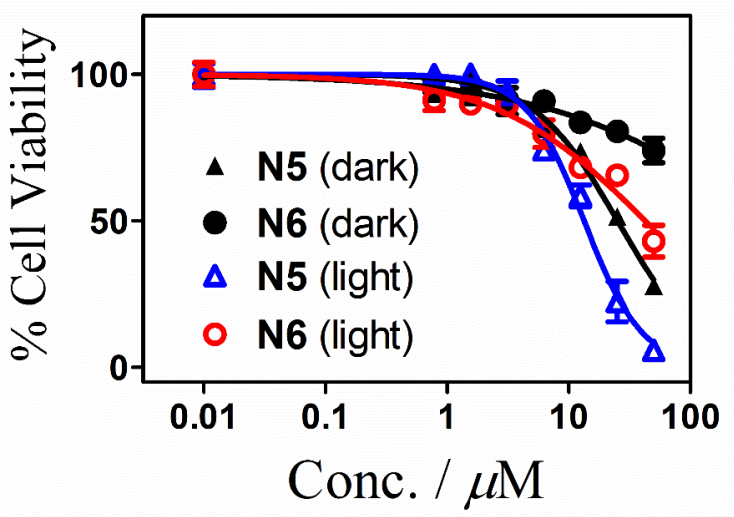

Figure 5.4: Percentage cell viability plots showing the cytotoxicity effects imposed on MCF-7 cells by **Br-N5** and **Br-N6** in the dark (black symbols) and after irradiation (blue and red symbols).

Upon illumination, the PDT activity of both azaBODIPYs increased at higher concentrations, and **Br-N5** showed a greater reduction of the percentage of viable cells compared to **Br-N6**, **Figure 5.4**. PDT activity and dark toxicity both significantly increased in the 10−100 μM range. **Br-N5** had an IC_{50} value of 13.4 ± 1.1 μM, while **Br-N6** had a value of 42.5 ± 1.8 μM, **Table 5.1**. This demonstrates that **Br-N5** has higher PDT activity. These results are consistent with the higher cellular uptake recorded for **Br-N5** after 12 h.

Table 5.1: Cytotoxicity data recorded for **Br-N5** and **Br-N6** against MCF-7 cells in the dark and under irradiation with a 660 nm Thorlabs LED.

	IC_{50} (μM) Dark[a]	**IC_{50} (μM) Light[b]**
Br-N5	25.2 (± 1.0)	13.4 (± 1.1)
Br-N6	> 50	42.5 (± 1.8)

[a] For 12 h incubation in the dark; [b] For 12 h incubation in the dark followed by exposure to 660 nm LED laser light (504 J cm^{-2}) for 30 min

5.3 Closing remarks

Studies to assess the PDT activity of azadipyrromethene complexes and brominated azaBODIPY complexes against human breast adenocarcinoma MCF-7 cells were carried out. All synthesised homoleptic complexes were inferior as PDT photosensitisers compared with their ligands. A possible solution for the enhancement of the production of singlet oxygen might be to incorporate heavy atoms to the pyrrolic positions of the ligands during future investigations of these complexes. The brominated azaBODIPY dyes were also examined for their potential as PDT photosensitisers, since they have relatively high singlet oxygen quantum yields. Their cellular uptake was investigated, and **Br-N5** was found to have peaked at 12 h. The inclusion of the nitro group to the proximal rings may have led to greater cellular uptake. Although **Br-N6** has a higher singlet oxygen quantum yield of 0.78 compared to 0.70

for **Br-N5** in ethanol (**Table 3.2**), the PDT activity displayed by **Br-N6** was lower than that of **Br-N5**. The PDT activity of **Br-N5** showed an enhanced effect when compared to **Br-N6** with an IC_{50} value of 13.4 ± 1.1 μM, which was consistent with the trends observed in the cellular uptake data.

6: Nonlinear optical limiting parameters

6.1 Introduction

The goal of this chapter is to investigate OL properties of **N3-azadpy** and **N3-BDY**, and the **Zn-N1** and **Zn-NH_2** azadipyrromethene complexes, so a comparison can be made between these three types of structurally related 1,3,5,7-tetraphenylazadipyrromethene compounds. **N3-azadpy** and **N3-BDY** have electron-withdrawing and -donating groups introduced at the *para*-positions of the phenyl rings at the 3,5- and 1,7-positions, respectively, so that a donor-π-acceptor (D-π-A) π-system is formed. According to the literature, molecules possessing systems with donor and acceptor substituents, separated by a π-conjugated system tend to display large third-order susceptibility, increasing the rate of OL response of the material.[68,96,97] Molecular dyes with an extended π-conjugated system also characteristically possess large electronic polarisability. This contributes to hyperpolarisability, and in particular to second-order hyperpolarisability. Following complexation with BF_2, the **N3-BDY** dye has a red-shifted main band absorption leading to minimal absorbance across most of the visible region in a manner that makes the molecule potentially suitable for optical limiting. The Zn(II) ion of the zinc azadipyrromethene complexes have a heavy atom effect that promotes intersystem crossing to the triplet manifold, and this could enhance OL in a similar manner to what has been reported for phthalocyanines.[69]

All z-scan measurements were conducted in the linear range of Beer-Lambert plots. To ensure no aggregation took place, the UV-vis absorption spectra were also carefully checked before and after each measurement. Aggregation of the solution could lead to significant NLS and interfere with the NLA results. As mentioned in Chapter 1, the Z-scan setup uses nanosecond laser pulses. The RSA responses observed at the focal point are therefore not expected to be strictly due to TPA and are likely to be due primarily to ESA from the S_1 and/or T_1 states.

As described in Chapter 1, the efficiency of an optical limiter is described by several parameters, including the effective nonlinear absorption coefficient (β_{eff}), the imaginary third-order susceptibility ($Im[\chi^{(3)}]$), the second-order hyperpolarisability (γ) and the limiting threshold intensity (I_{lim}). These parameters are described in this chapter and summarised for the dyes studied. The β_{eff} value describes the degree of nonlinear absorptivity of measurements on the nanosecond timescale. A positive nonlinear absorption coefficient is indicative of a material which has an RSA response. RSA is characterised by high transmittance under ambient light conditions, but markedly decreased transmittance at high light intensities.[98] The rate of response of an OL material to the perturbation induced by an incident laser pulse is given by $Im[\chi^{(3)}]$, while γ measures the interaction of an incident photon with the permanent dipole moments of an OL. The I_{lim} value defines the threshold input energy at which 50% transmittance is achieved.[98,99] The optimal range for γ values is 10^{-34}–10^{-29} esu, $Im[\chi^{(3)}]$ within 10^{-15}–10^{-8} esu and ideally, I_{lim} should be below 0.95 J.cm^{-2} at 532 nm.[70,100–102]

6.2 Results

6.2.1 Azadipyrromethene

N3-azadpy could only be studied in DCM due to aggregation effects in other solvents, **Figure 6.1**. The effect of using a higher concentration was explored. The β_{eff}, $Im[\chi^{(3)}]$ and γ values all lie in the optimal range that has been reported for these parameters, **Table 6.1**. A trend was observed where the values decrease with an increase in laser pulse energy. The I_{lim} values, on the other hand, were quite high, but as would normally be anticipated improved at a higher concentration.

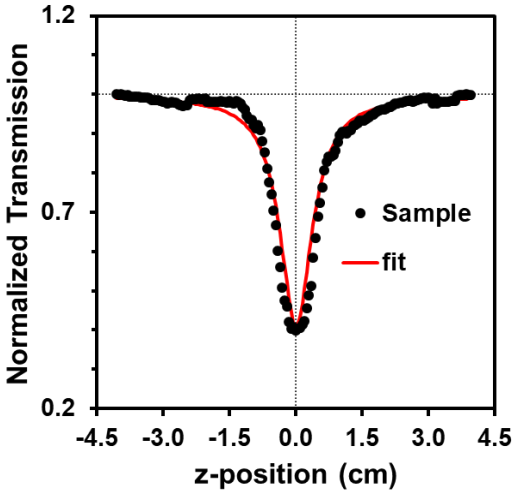

Figure 6.1: The RSA response of **N3-azadpy** (5×10^{-4} M in DCM) at 50 µJ.

Table 6.1: OL parameters for **N3-azadpy** in DCM.

Concentration (M)	Energy (µJ)	α (cm^{-1})	β_{eff} ($cm.GW^{-1}$)	$Im[\chi^{(3)}]$ (esu)	γ (esu)	I_{lim} ($J.cm^{-2}$)
2.5×10^{-4}	ca. 20	7.19	129.7	2.78×10^{-10}	5.94×10^{-31}	–
	ca. 30		97.24	2.08×10^{-10}	4.46×10^{-31}	–
	ca. 40		105.5	2.26×10^{-10}	4.83×10^{-31}	3.78
	ca. 50		72.8	1.56×10^{-10}	3.34×10^{-31}	3.57
5.0×10^{-4}	ca. 20	14.4	294	6.30×10^{-10}	6.69×10^{-31}	–
	ca. 30		300	6.41×10^{-10}	6.82×10^{-31}	1.72
	ca. 40		271	5.80×10^{-10}	6.17×10^{-31}	1.77
	ca. 50		191	4.05×10^{-10}	4.35×10^{-31}	2.20

6.2.2 D-π-A azaBODIPY dye

The optical limiting ability of **N3-BDY** was studied in DCM, toluene and chloroform + 1% TEA. There is minimal absorbance at a wavelength of 532 nm, **Figure 6.2**. Different concentrations were studied to assess the NLO responses. The observed responses were characteristic of RSA, **Figure 6.3**. Z-scan profiles exhibit positive nonlinear absorption with a decrease in transmittance along the z-axis approaching the zero position. The compound was investigated at four different laser pulse energies. A comparison between lower and higher concentrations was carried out in DCM, whereas toluene and chloroform + 1% TEA solution were only studied at the lower concentration, due to issues with solubility.

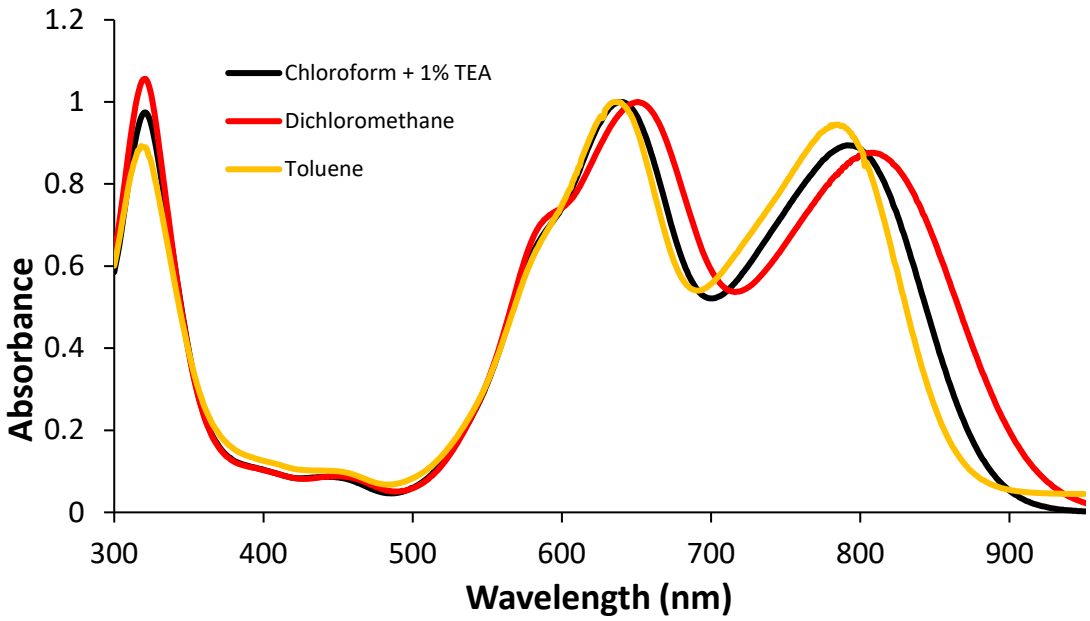

Figure 6.2: Normalised absorption spectra of **N3-BDY** in various solvents.

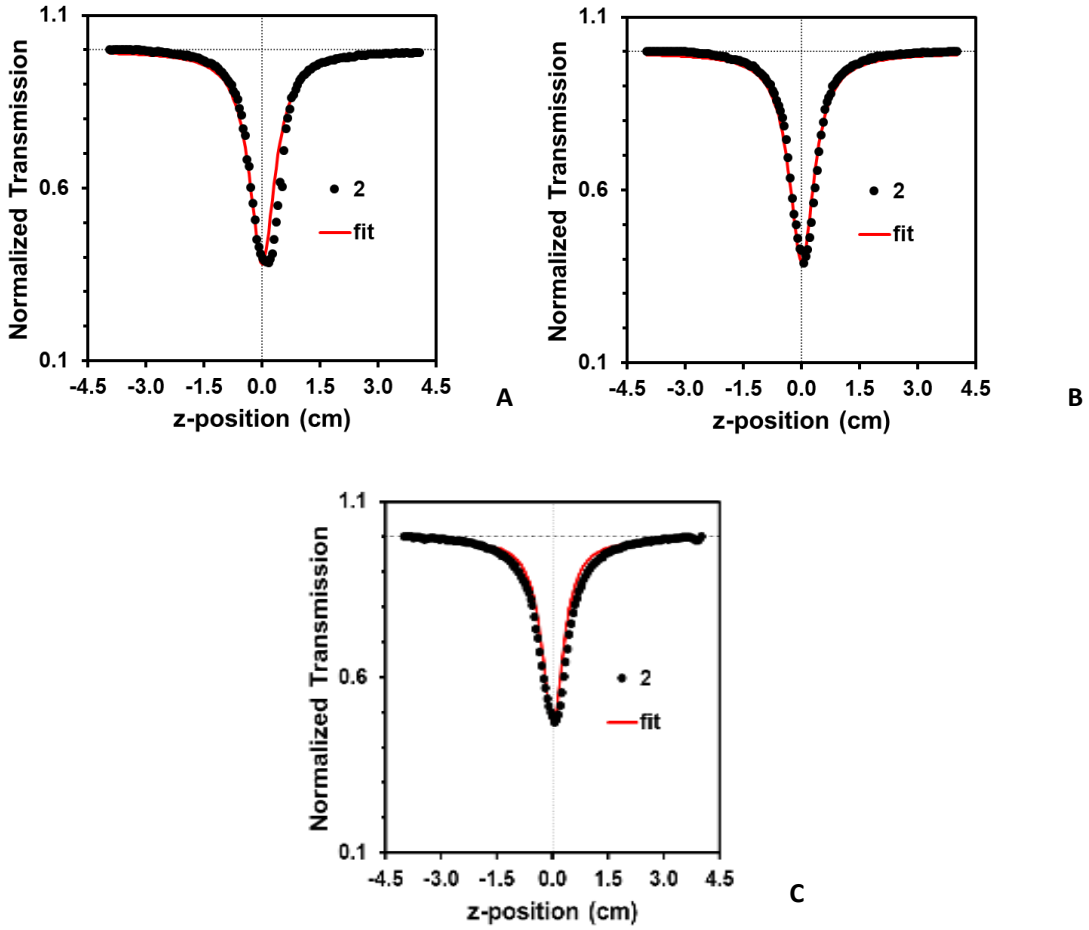

Figure 6.3: Characteristic open aperture z-scan profiles **N3-BDY** RSA: (A) 5×10^{-4} M at 20 µJ in DCM, (B) 2.5×10^{-4} M at 20 µJ in Toluene and (C) 2.5×10^{-4} M at 30 µJ in chloroform + 1% TEA.

Table 6.2: Spectral properties of **N3-BDY** solution in different solutions.

Solvent	λ_{max} (nm)	Abs at λ_{max}	Abs at 532 nm
Chloroform + 1% TEA	639	1.219	0.224
DCM	651	1.279 (2.667)	0.232 (0.490)
Toluene	637	1.183	0.209

*Figures in brackets indicate the value of the red-shifted second peak.

Table 6.3: OL parameters for **N3-BDY** in DCM.

Concentration (M)	Energy (μJ)	α (cm^{-1})	β_{eff} ($cm.GW^{-1}$)	$Im[\chi^{(3)}]$ (esu)	γ (esu)	I_{lim} ($J.cm^{-2}$)
2.5×10^{-4}	ca. 20	2.68	146	3.13×10^{-10}	6.54×10^{-31}	–
	ca. 30		97	2.08×10^{-10}	4.35×10^{-31}	2.20
	ca. 40		80	1.71×10^{-10}	3.58×10^{-31}	2.81
	ca. 50		67	1.43×10^{-10}	2.99×10^{-31}	3.28
5.0×10^{-4}	ca. 20	5.65	241.6	5.17×10^{-10}	5.91×10^{-31}	0.94
	ca. 30		198.3	4.24×10^{-10}	4.26×10^{-31}	1.16
	ca. 40		170	3.64×10^{-10}	3.65×10^{-31}	0.98
	ca. 50		161.1	3.54×10^{-10}	3.46×10^{-31}	–

Table 6.4: OL parameters for **N3-BDY** in Toluene.

Concentration (M)	Energy (μJ)	α (cm^{-1})	β_{eff} ($cm.GW^{-1}$)	$Im[\chi^{(3)}]$ (esu)	γ (esu)	I_{lim} ($J.cm^{-2}$)
2.75×10^{-5}	ca. 20	2.41	188	4.02×10^{-10}	9.10×10^{-31}	1.37
	ca. 30		160	3.42×10^{-10}	7.75×10^{-31}	1.30
	ca. 40		129	2.75×10^{-10}	6.23×10^{-31}	1.36
	ca. 50		99	2.12×10^{-10}	4.81×10^{-31}	1.83

Table 6.5: OL parameters for **N3-BDY** in Chloroform + 1% TEA.

Concentration (M)	Energy (μJ)	α (cm^{-1})	β_{eff} ($cm.GW^{-1}$)	$Im[\chi^{(3)}]$ (esu)	γ (esu)	I_{lim} ($J.cm^{-2}$)
2.75×10^{-5}	ca. 20	2.59	142	3.04×10^{-10}	6.67×10^{-31}	–
	ca. 30		127	2.72×10^{-10}	5.98×10^{-31}	1.73
	ca. 40		89.5	1.91×10^{-10}	4.21×10^{-31}	–
	ca. 50		76	1.63×10^{-10}	3.57×10^{-31}	2.36

N3-BDY exhibited an ability to reduce transmittance below 50% as observed in the OA z-scan profiles, **Figure 6.3**. As anticipated, an increase in dye concentration and higher laser pulse energies led to a greater reduction in transmittance. To provide some insight on the results obtained, the spectral properties of **N3-BDY** in different solvents are summarised in **Table 6.2**. Since the main azaBODIPY spectral band is shifted to the red relative to conventional BODIPY

core dyes, there is minimal absorbance around 532 nm. The dye was evaluated at a relatively low concentration of 2.5×10^{-4} M. The OL results are summarised in **Tables 6.3–6.5**.

The $\mathrm{Im}[\chi^{(3)}]$ and γ values in all solvents studied and at all concentrations fall within the reported optimal ranges of 10^{-15}–10^{-8} and 10^{-34}–10^{-29} esu, respectively.[70,102] A trend is immediately observed in the β_{eff}, $\mathrm{Im}[\chi^{(3)}]$ and γ values since the values decrease with an increase in laser pulse energy. The I_{lim} values obtained for all but one set of the experimental data for **N3-BDY** in solution were unable to reach the threshold limit and did not display any trend. The one exception was found at the higher concentration of the dye at the 20 µJ laser pulse. Higher concentrations could be readily achieved in the polymer thin films that would be used in practical applications, however, so the dyes could still function effectively in that context.[70]

6.2.3 Zinc azadipyrromethene complexes

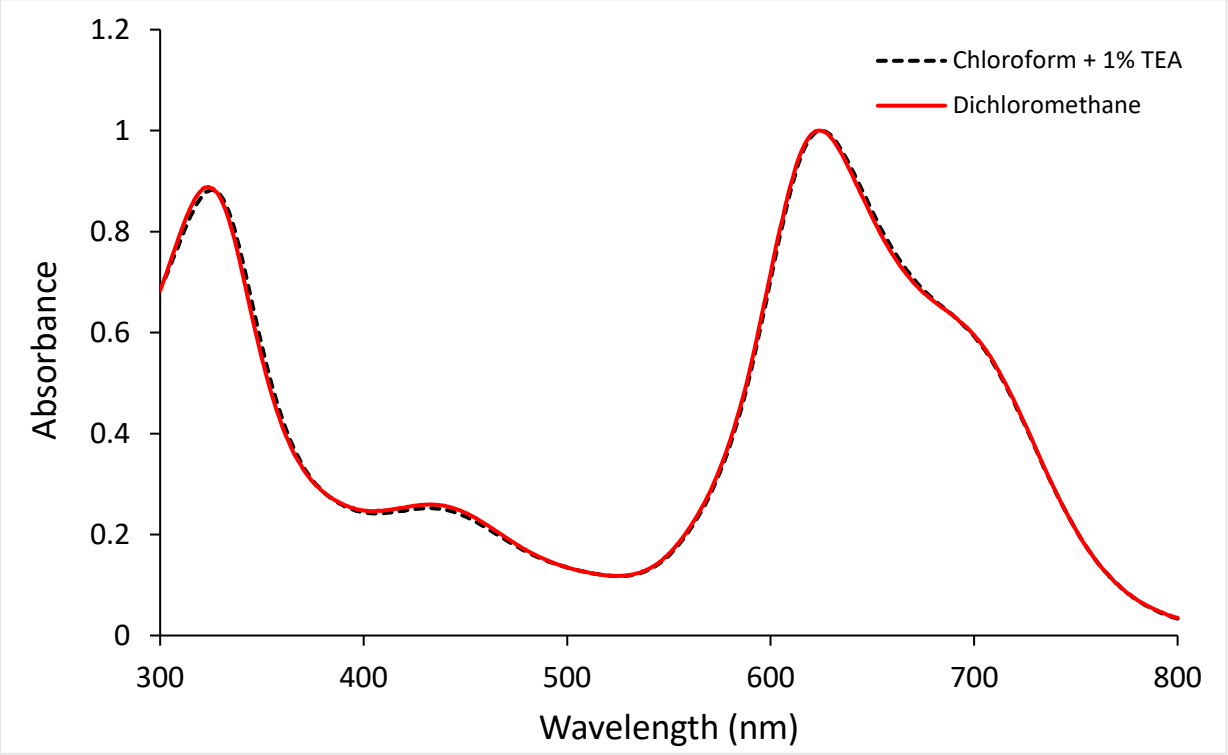

Figure 6.4: UV-vis absorption spectra of **Zn-NH_2** in chloroform + 1% TEA and DCM.

A comparative study for the zinc azadipyrromethene complexes was carried out, **Tables 6.6-6.8**. **Zn-NH_2** was studied at a low concentration in DCM and chloroform + 1% TEA, and a higher concentration in DCM. The UV-visible absorption spectra are very similar in both solvents, **Figure 6.4**. **Zn-N1** was incapable of decreasing transmittance to below 50%, prompting a limited study. Solubility challenges were encountered in different solvents. A decrease in $Im[\chi^{(3)}]$ and γ values was noted, while the I_{lim} values showed no apparent trend. Similar results were obtained at low concentration in DCM and chloroform + 1% TEA of **Zn-NH_2**, and a lower I_{lim} value was observed at higher concentration.

Table 6.6: OL parameters for **Zn-NH_2** in Chloroform + 1% TEA.

Concentration (M)	Energy (μJ)	α (cm^{-1})	β_{eff} ($cm.GW^{-1}$)	$Im[\chi^{(3)}]$ (esu)	γ (esu)	I_{lim} ($J.cm^{-2}$)
2.75×10^{-5}	ca. 20	2.08	67	1.43×10^{-10}	3.05×10^{-31}	–
	ca. 30		61	1.30×10^{-10}	2.78×10^{-31}	–
	ca. 40		51	1.09×10^{-10}	2.32×10^{-31}	–
	ca. 50		49	1.04×10^{-10}	2.23×10^{-31}	3.57

Table 6.7: OL parameters for **Zn-NH_2** in DCM.

Concentration (M)	Energy (μJ)	α (cm^{-1})	β_{eff} ($cm.GW^{-1}$)	$Im[\chi^{(3)}]$ (esu)	γ (esu)	I_{lim} ($J.cm^{-2}$)
2.75×10^{-5}	ca. 20	2.10	75	1.59×10^{-10}	3.41×10^{-31}	–
	ca. 30		62	1.33×10^{-10}	2.85×10^{-31}	–
	ca. 40		63	1.35×10^{-10}	2.88×10^{-31}	2.69
	ca. 50		57	1.23×10^{-10}	2.63×10^{-31}	3.61
5.0×10^{-5}	ca. 20	4.21	130	2.79×10^{-10}	2.97×10^{-31}	–
	ca. 30		97	2.07×10^{-10}	2.21×10^{-31}	1.81
	ca. 40		88	1.88×10^{-10}	2.00×10^{-31}	–
	ca. 50		81	1.73×10^{-10}	1.85×10^{-31}	1.64

Table 6.8: OL parameters for **Zn-N1** in DCM.

Concentration (M)	Energy (μJ)	α (cm^{-1})	β_{eff} ($cm.GW^{-1}$)	$Im[\chi^{(3)}]$ (esu)	γ (esu)	I_{Lim} ($J.cm^{-2}$)
2.75×10^{-5}	ca. 20	2.67	40	8.57×10^{-11}	8.93×10^{-32}	–
	ca. 50		19	4.05×10^{-11}	4.22×10^{-32}	–

Zn-N1 was investigated at high energy laser pulses with the Im[$\chi^{(3)}$] and γ values falling within the reported optimal range, however, as a result of their inability to decrease transmittance by at least 50%, I_{lim} values could not be determined.

6.3 Concluding remarks

The OL properties of a series of different dyes were successfully studied at 532 nm using 10 ns pulses from an Nd/YAG laser. All dyes studied exhibited Im[$\chi^{(3)}$] and γ values that lie in the reported optimal range, with the **N3-BDY** displaying a better set of results, especially in toluene. With the red-shift in the main spectral band following substitution at the 1,3,5,7-positions, minimal absorbance at 532 nm was achieved. To gauge the influence of the solvent, the OL properties of chloroform + 1% TEA, DCM and toluene solutions were studied for **N3-BDY**. When a comparison is made with the OL parameters that have recently been reported for 3,5-distyrylBODIPY dyes by Mack and coworkers,[103] however, it becomes clear that the γ values obtained for **N3-BDY** are up to two order of magnitude lower than those that have been reported for D-π-A type 3,5-distyrylBODIPYs. Similar results were reported previously for benzo-fused BODIPY dyes by Kubheka *et al*.[70] This suggests that 1,3,5,7-tetraarylBODIPY and benzo-fused BODIPY dyes are probably not the best candidates for further in depth study for optical limiting applications.

7: Molecular modelling

7.1 Geometry optimisations and TD-DFT calculations

Molecular modelling calculations were conducted to identify trends in the electronic structures and predicted spectra of a set of synthesised azadipyrromethenes and their difluoroboron and zinc(II) complexes, **Figure 7.1**, using a previously described approach.[1,7] The Gaussian 09 programme package was employed for the calculations. Density functional theory (DFT) calculations were used to conduct geometry optimisations with the Becke-3-Parameter, Lee Yang and Parr (B3LYP) functional with the default SDD basis sets of the Gaussian programme.[75] The SDD basis set offers reasonable approximations for all atoms, including bromine and iodine used in this study. The B3LYP functional has a tendency to underestimate the energies of transitions with long-range charge transfer character that frequently arise with π-extended BODIPY dyes.[104] Time-dependant DFT (TD-DFT) calculations with the Coulomb-attenuated B3LYP (CAM-B3LYP) functional were carried out to predict the electronic absorption properties. The CAM-B3LYP functional better handles transitions with charge transfer character through a combination of the hybrid B3LYP functional with increasing fractions of the Hartree-Fock (HF) exchange parameters, resulting in a functional with improved long-range correction capabilities.[104,105]

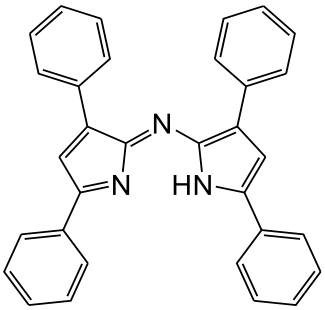

1a, 6a (N1-azadpy)

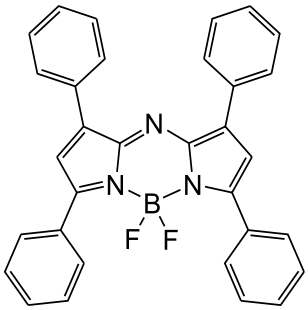

1b (N1-BDY)

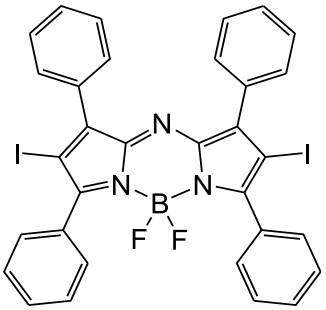

1c (I-N1)

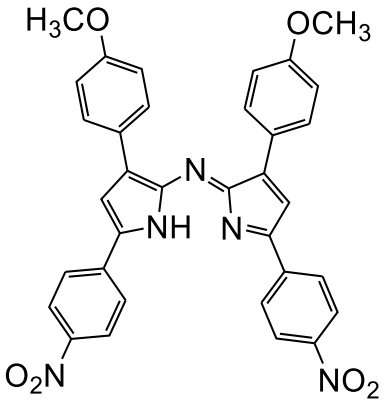

2a (N5-azadpy)

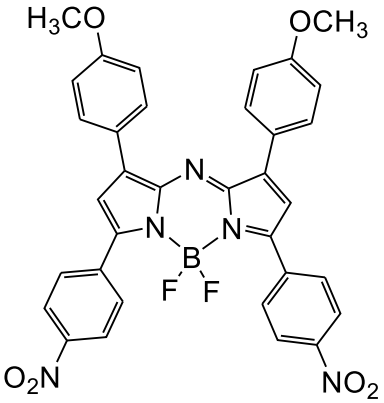

2b (N5-BDY)

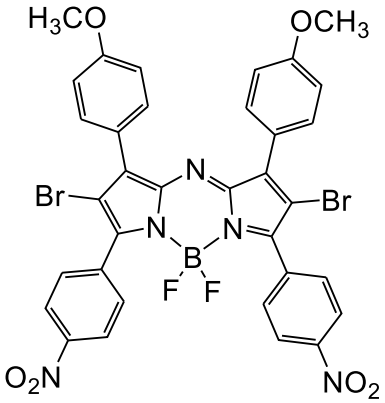

2c (Br-N5)

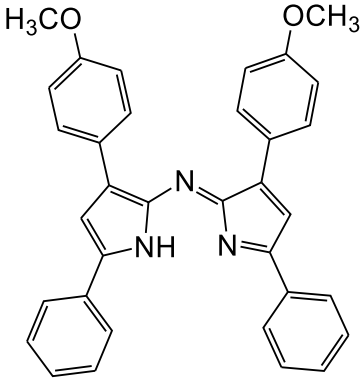

3a (N6-azadpy)

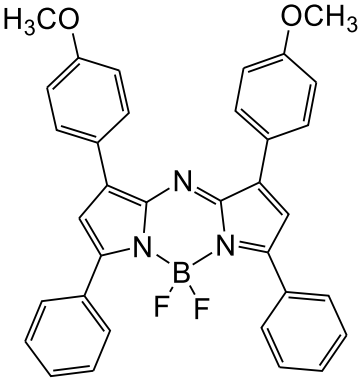

3b (N6-BDY)

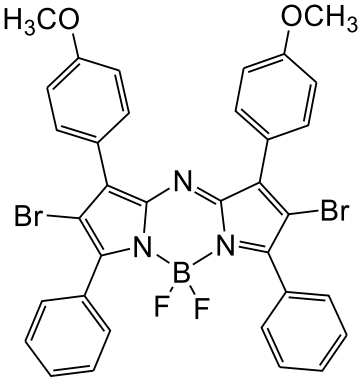

3c (Br-N6)

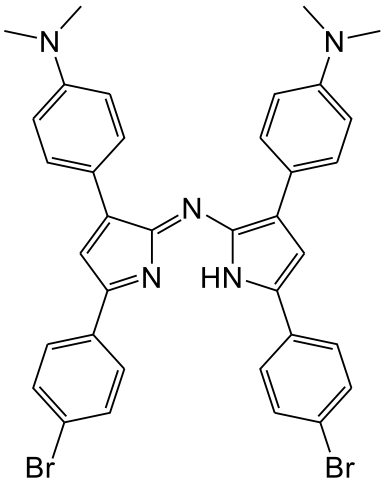

4a (N3-azadpy)

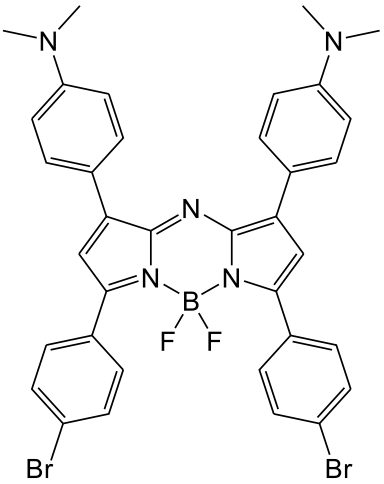

4b (N3-BDY)

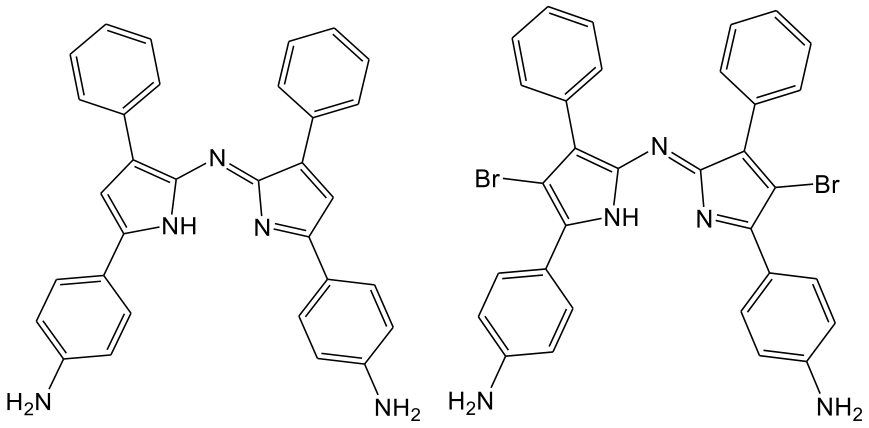

5a (NH_2-azadpy) **5b (Br-NH_2)**

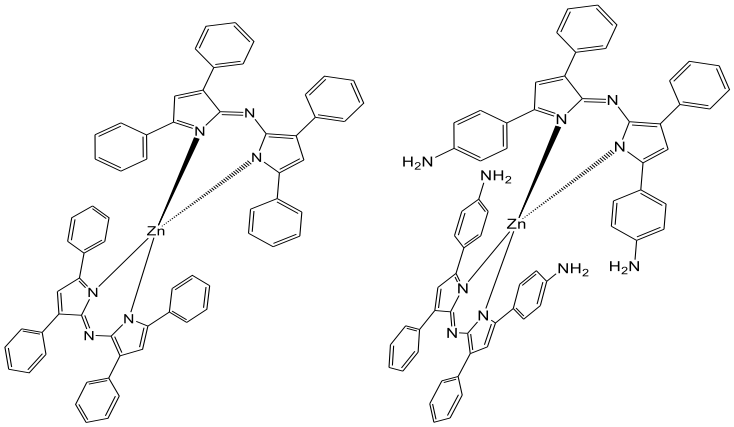

6b (Zn-N1) **7 (Zn-NH_2)**

Figure 7.1: The azadipyrromethene and complexes discussed in this chapter.

7.2 Molecular modelling of azadipyrromethenes and their complexes

The TD-DFT calculations (**Table 7.1**) for the compounds in this study (**Figure 7.1**) predict that the lowest-lying $S_0 \rightarrow S_1$ transition can be mainly attributed to the HOMO → LUMO one-electron transition. **I-N1** and **Br-NH_2** are included in this chapter as model complexes, but were formed in insufficient yield upon halogenation of **N1** and **NH_2-azadpy** at the 2,6-positions to form part of the experimental studies. **N1-azadpy** was studied to provide a comparison of the electron-withdrawing and electron-donating effects that *para*-substituents on the phenyl rings at the 1,3,5,7-positions, **Figure 7.1**, have on the wavelengths of the absorption band as was discussed in Chapter 3. Studies have previously been conducted to establish the extent of red-shifts by placing electron-donating and electron-withdrawing (-

OCH_3 and $-NO_2$) groups at the distal or proximal rings with proximal substitution displaying greater red-shifting of the main spectral band.[13,79] All modifications made in this study resulted in lower HOMO−LUMO band gap energies, promoting a bathochromic shift with the greatest shift predicted for the **N3-azadpy** dye, which has both electron-withdrawing and electron-donating substituents leading to a "push-pull" effect, **Table 7.1**.

Upon complexation with boron trifluoride, the HOMO and LUMO are energetically well-separated from the other MOs, **Figures 7.2** and **7.3**. The observed red-shift after chelation originates from the stabilisation effect of the energy levels, especially of the LUMO.[106] This corresponds with the larger LUMO coefficient at the nitrogen atoms. This effect manifests between the azadipyrromethene and its corresponding azaBODIPY, where the HOMO−LUMO gap for the boron complexes is smaller than that of the ligands, **Figure 7.2** and **7.3**. The effect that the structural changes have on the optical properties have a large influence on the HOMO and LUMO energies, and this is of primary interest since the other MOs are generally not involved in the one-electron transitions associated with the main spectral band. The structural changes and associated effects are the basis of a bathochromic shift to the azaBODIPY main spectral band as a result of the narrowing of the HOMO−LUMO energy band gap. The extent of the red-shifting is governed by the different substituents present on the azadipyrromethene ligand. The addition of electron-donating groups to distal rings introduces a mesomeric effect where the electron distribution extends from the proximal to distal rings when compared to reference compound **1a**, **Figure 7.1**.

The angular nodal patterns for the frontier orbitals of the dyes, **Figures 7.4-7.6**, show a general distribution at the core and proximal rings for both the HOMO and LUMO. They are differently distributed on the N-bridge and on the N atoms on the pyrrole ring for the HOMO and LUMO, where a large MO coefficient with a strong contribution on the N atoms,

particularly at the aza-methene bridge exists on the LUMO narrows the band gap.[5,107] The HOMO has small MO coefficients at the pyrrole nitrogen atoms and nodal planes at the aza-methene bridge N atom. The introduction of *para*-substituents on the distal rings such as dimethylamino and methoxy groups affects the HOMO energies to a more significant extent, **Figures 7.2** and **7.3**. It has previously been demonstrated that the electron distribution is more substantially affected at the 3,5-position than at the 1,7-positions, since there are larger MO coefficients at the points of attachment of the phenyl rings.[108] In a similar manner, chelating with BF_2 strongly influences LUMO energy which has the largest coefficients localised on the pyrrole nitrogen atoms on the azaBODIPY core.

The zinc complexes exhibit an energetic situation that is different to the other azadipyrromethene complexes due to the presence of two ligands which lead to several allowed optical transitions with absorption energies very close to each other observed in the main spectral band region. In **Figure 7.6**, the angular nodal patterns of the frontier π-MOs are shown. The HOMO and HOMO−1 are localised on one of the ligands of the complex. In a similar manner, the LUMO and LUMO+1 of **Zn-N1** are localised on a single ligand, while in contrast with **Zn-NH_2** only the HOMO and HOMO−1 are localised, and the LUMO and LUMO+1 are distributed over both ligands. The optical transitions for both zinc complexes in the main spectral band region were found to have a partial inter-ligand charge-transfer character (**Table 7.1**).

7.3 Applications

The large energy gaps between the S_1 and S_2 excited states that are predicted for most of the dyes in **Table 7.1** results in relatively weak absorbance across the visible region in a manner that makes the dyes suitable for OL applications in this spectral region. Similar trends have recently also been reported in the context of 3,5-distyrylBODIPYs by Mack and coworkers,

and it is this property of BODIPYs and their analogues that have inspired Z-scan studies on these compounds.[103]

Table 7.1: TD-DFT calculated transitions for the azadipyrromethene, azaBODIPY and Zn azadipyrromethene compounds.

	#[a]	E[b] (eV)	f[c]	λ_{calc}[d] (nm)	λ_{exp}[e] (nm)	ν[f] (cm^{-1})	Wavefunction [g]
N1-azadpy	1	2.42	0.76	512	598	19.5	97% H→L; …
	2	2.94	0.06	417		24.0	91% H−1→L; …
	3	3.50	0.14	354		28.3	92% H−2→L; …
N3-azadpy	1	2.16	0.64	573	632	17.5	91% H→L; …
	2	2.59	0.34	479		20.9	76% H−1→L; …
	3	3.01	0.25	412		24.3	83% H−2→L; …
N5-azadpy	1	2.22	0.69	558	607	17.9	92% H→L; …
	2	2.62	0.22	474		21.1	79% H−1→L; …
	3	3.13	0.21	397		25.2	85% H−2→L; …
N6-azadpy	1	2.35	0.71	527	600	19.0	95% H→L; …
	2	2.81	0.16	441		22.7	82% H−1→L; …
	3	3.32	0.17	372		26.8	89% H−2→L; …
NH_2-azadpy	1	2.31	0.80	538	655	18.6	97% H→L; …
	2	3.04	0.03	408		24.5	63% H−2→L; 29% H−1→L; …
	3	3.56	0.21	348		28.7	54% H−3→L; 20% H−1→L; 14% H−2→L; …
N1-BDY	1	2.26	0.78	548	650	18.2	99% H→L; …
	2	2.98	0.01	416		24.0	89% H−1→L; …
	3	3.18	0.29	390		25.6	87% H−2→L; …
N3-BDY	1	2.03	0.73	612	810	16.3	98% H→L; …
	2	2.61	0.54	476	653	21.0	87% H−1→L; …
	3	2.66	0.16	467		21.4	83% H−2→L; …

N5-BDY	1	2.13	0.75	581	687	17.2	98% H→L; …
	2	2.71	0.08	457		21.9	74% H−2→L; 16% H−1→L; …
	3	2.79	0.42	445		22.5	76% H−1→L; 16% H−2→L; …
N6-BDY	1	2.19	0.78	566	663	17.7	99% H→L; …
	2	2.85	0.03	435		23.0	67% H−2→L; 23% H−1→L; …
	3	2.95	0.39	420		23.8	69% H−1→L; 23% H−2→L; …
Br-NH_2	1	2.36	0.82	525	625	19.1	97% H→L; …
	2	2.92	0.02	425		23.6	57% H−2→L; 35% H−1→L; …
I-N1	1	2.35	0.82	527	660	19.0	98% H→L; …
	2	2.80	0.04	443		22.6	94% H−1→L; …
	3	2.96	0.24	418		23.9	92% H−2→L; …
Br-N5	1	2.19	0.75	565	664	17.7	98% H→L; …
	2	2.55	0.06	486		20.6	92% H−2→L; …
	3	2.64	0.36	469		21.3	94% H−1→L; …
Br-N6	1	2.24	0.81	555	651	18.0	99% H→L; …
	2	2.69	0.02	461		21.7	92% H−2→L; …
	3	2.79	0.33	444		22.7	94% H−1→L; …
Zn-N1	1	2.27	0.23	545	591	18.3	36% H−1→L; 29% H→L+1; 24% H→L; …
	2	2.39	0.57	518		19.3	46% H−1→L; 37% H→L+1; 7% H→L; …
	3	2.58	0.04	481		20.8	54% H→L; 24% H→L+1; 12% H−3→L; …
Zn-NH_2	1	1.86	0.06	668	623	15.0	51% H→L; 32% H−1→L+1; …
	2	2.19	1.13	567		17.6	60% H→L+1; 28% H−1→L; …
	3	2.37	0.02	522		19.1	50% H−1→L+1; 38% H−1→L; …

[a] – Number of the excitation state in ascending energy. [b] – Calculated band energies. [c] – Theoretically calculated oscillator strengths. [d] – Theoretically calculated wavelengths. [e] – Experimental wavelengths for the main spectral ba*nds* in DCM. [f] – Calculated band energies (10^3 cm^{-1}). [g] – MO wavefunctions based on eigenvectors predicted by TD-DFT calculation for the B3LYP geometries optimised using 6-31G(d) basis set. H and L = HOMO and LUMO, respectively.

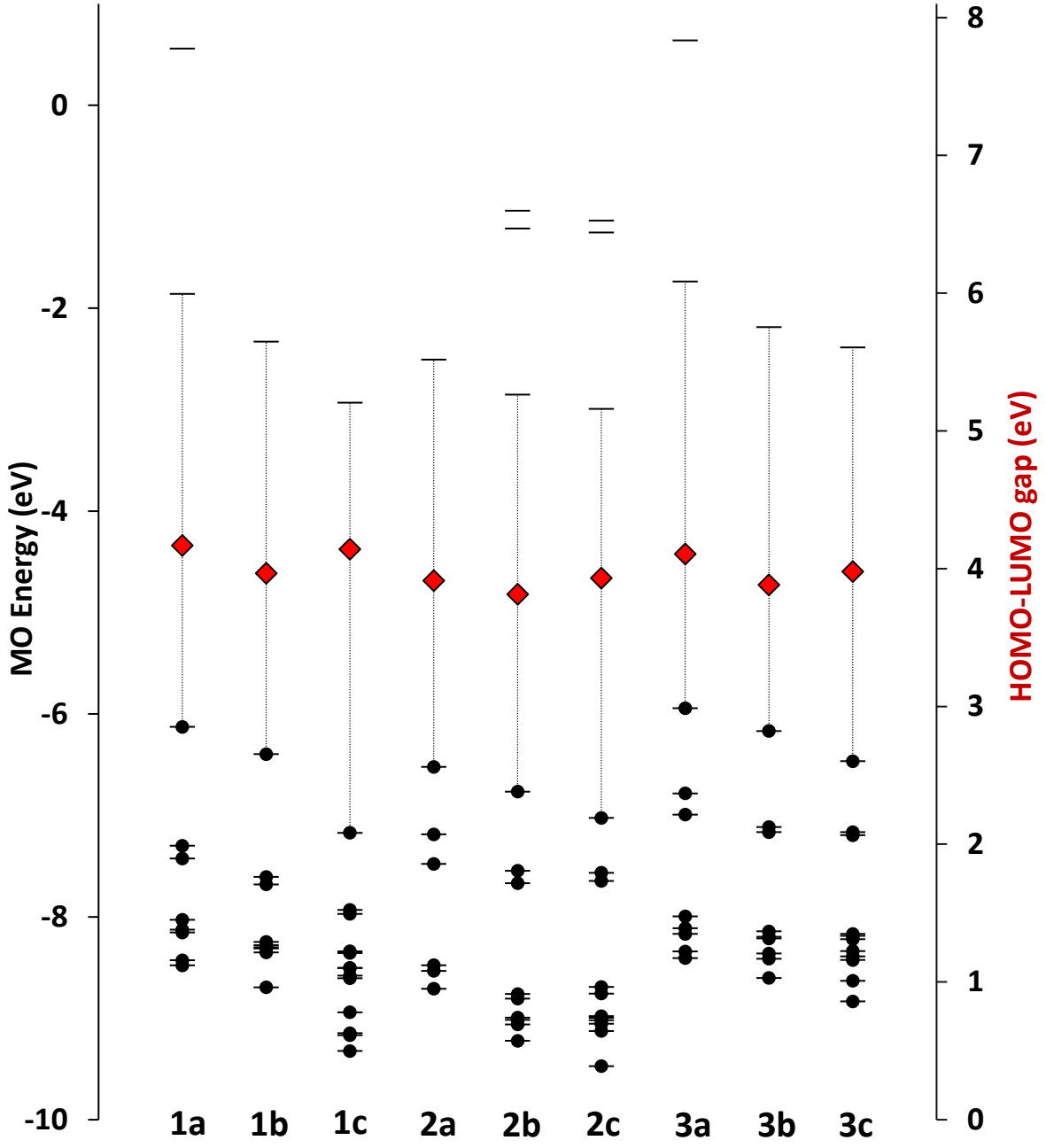

Figure 7.2: Frontier MO energies and HOMO−LUMO gaps of **1a-3c** (**Figure 7.1**) at the CAM-B3LYP/6-31G(d) level of theory. The HOMO−LUMO gaps are plotted against a secondary axis and are denoted by red diamonds. The occupied MOs are highlighted with black circles.

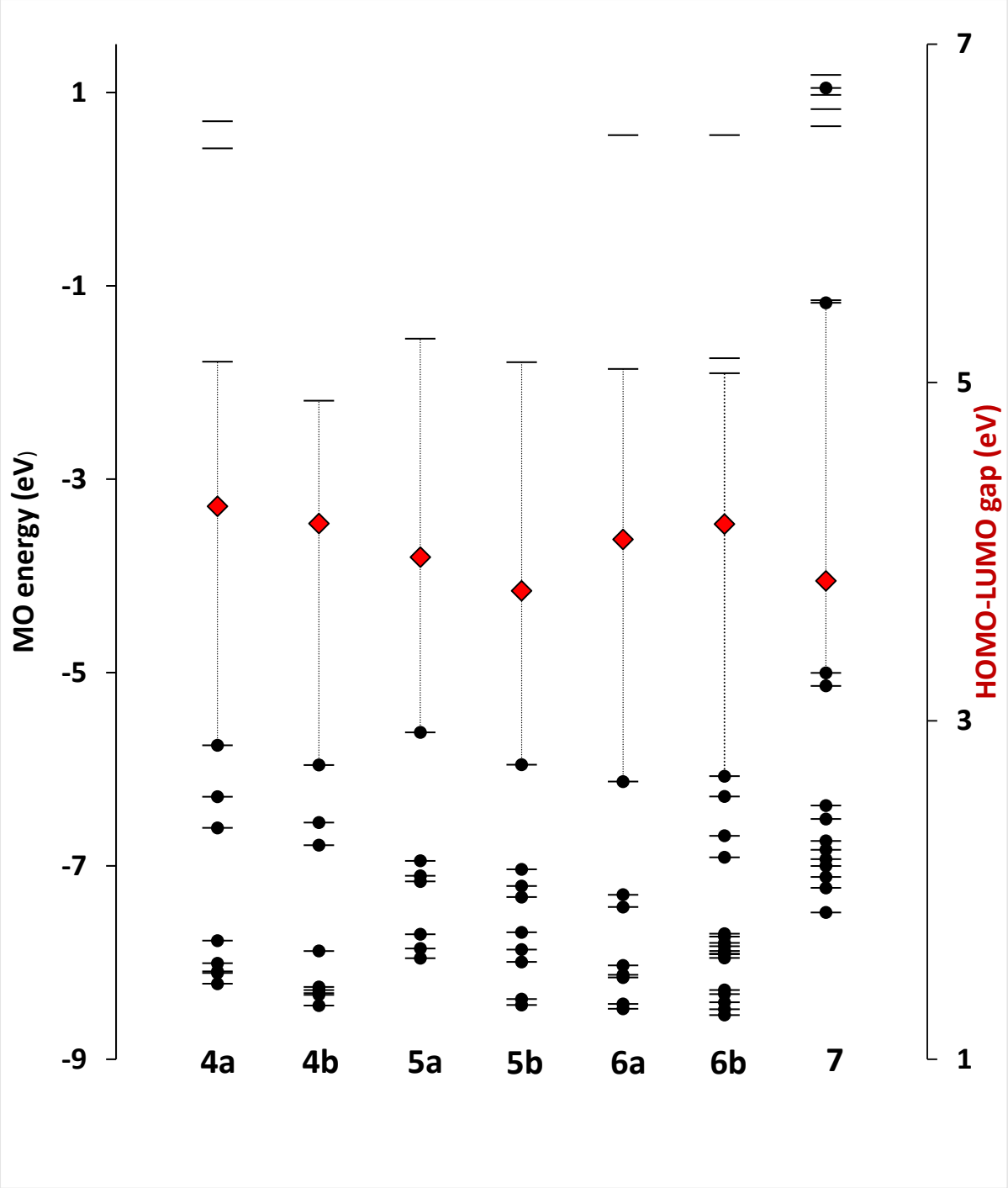

Figure 7.3: Frontier MO energies and HOMO−LUMO gaps of **4a-7** (**Figure 7.1**) at the CAM-B3LYP/6-31G(d) level of theory. The red diamonds denote the HOMO−LUMO band gaps and are plotted against a secondary axis. The occupied MOs are highlighted with black circles.

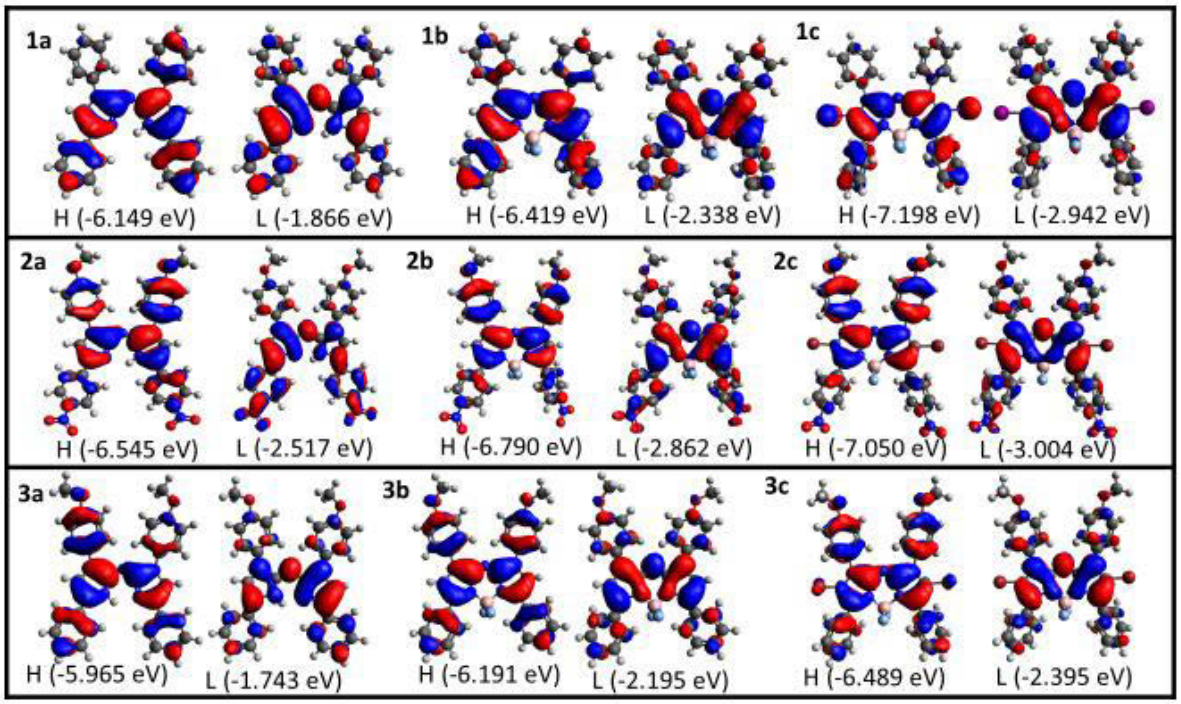

Figure 7.4: Angular nodal patterns and MO energies of HOMO and LUMO **1a-c**, **2a-c** and **3a-c**. H and L refer to the HOMO and LUMO, respectively.

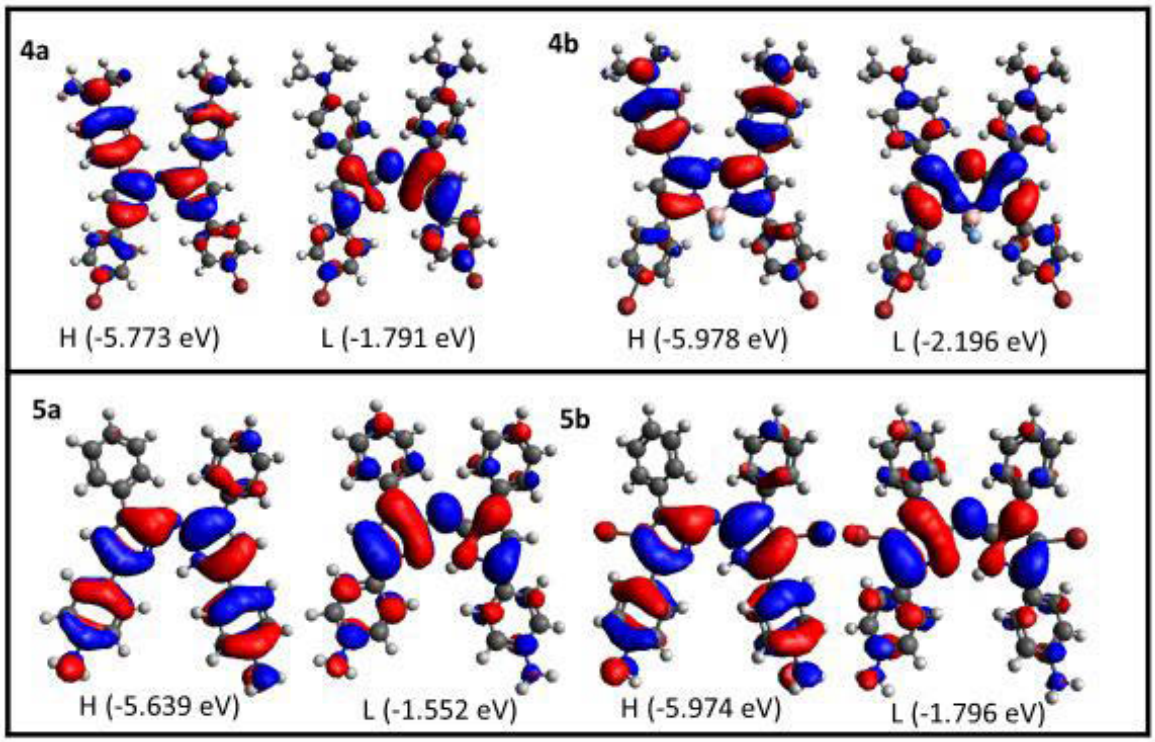

Figure 7.5: Angular nodal patterns and MO energies of the HOMOs and LUMOs of **4a**, **4b**, **5a** and **5b**. H and L refer to the HOMO and LUMO, respectively.

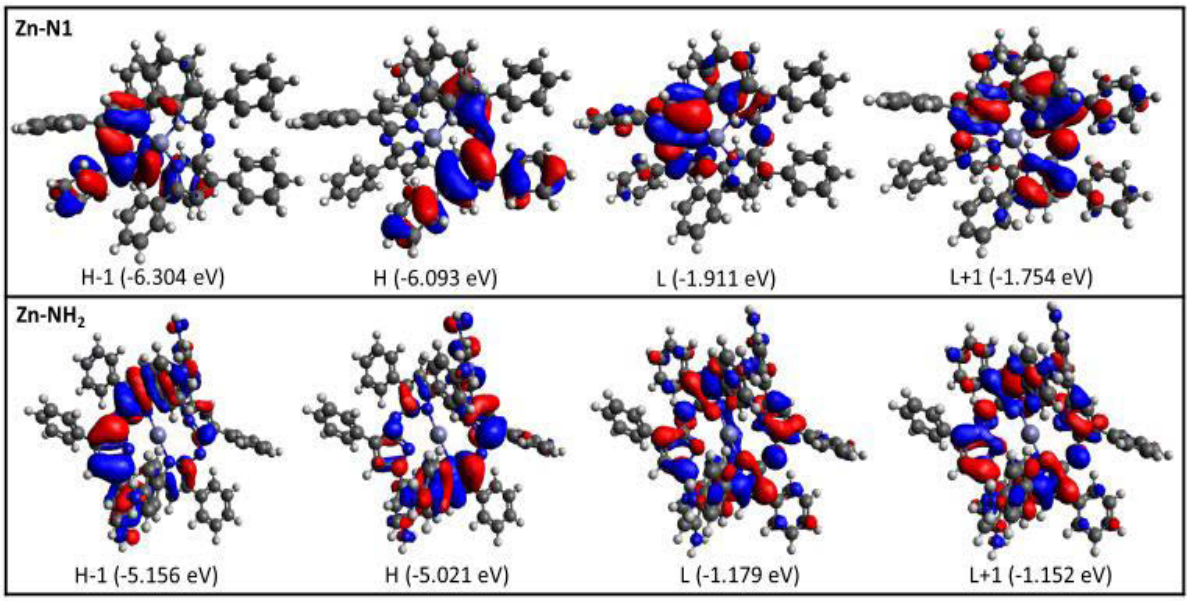

Figure 7.6: Angular nodal patterns and MO energies associated with zinc complexes and their azadipyrromethene precursors. H and L refer to the HOMO and LUMO, respectively.

The trends observed in the TD-DFT spectra, **Figures 7.7 and 7.8**, for the energies of the main spectral band upon complexation and functionalisation with heavy atoms at the 2,6-positions follow the trends observed during experimental work, **Table 7.1**. There is a consistent over-estimation of the transition energies in the calculations relative to the experimental spectra. It is particularly noteworthy that the presence of two intense bands in the visible and NIR regions of the **N3-BDY** spectrum is predicted, **Figure 7.8** and **Table 7.1**. The introduction of the dimethylaminophenyl rings of **N3-azadpy** and **N3-BDY** results in the presence of occupied MOs that lie closer in energy to the HOMO than is the case with the other dyes studied, **Figures 7.2** and **7.3**.

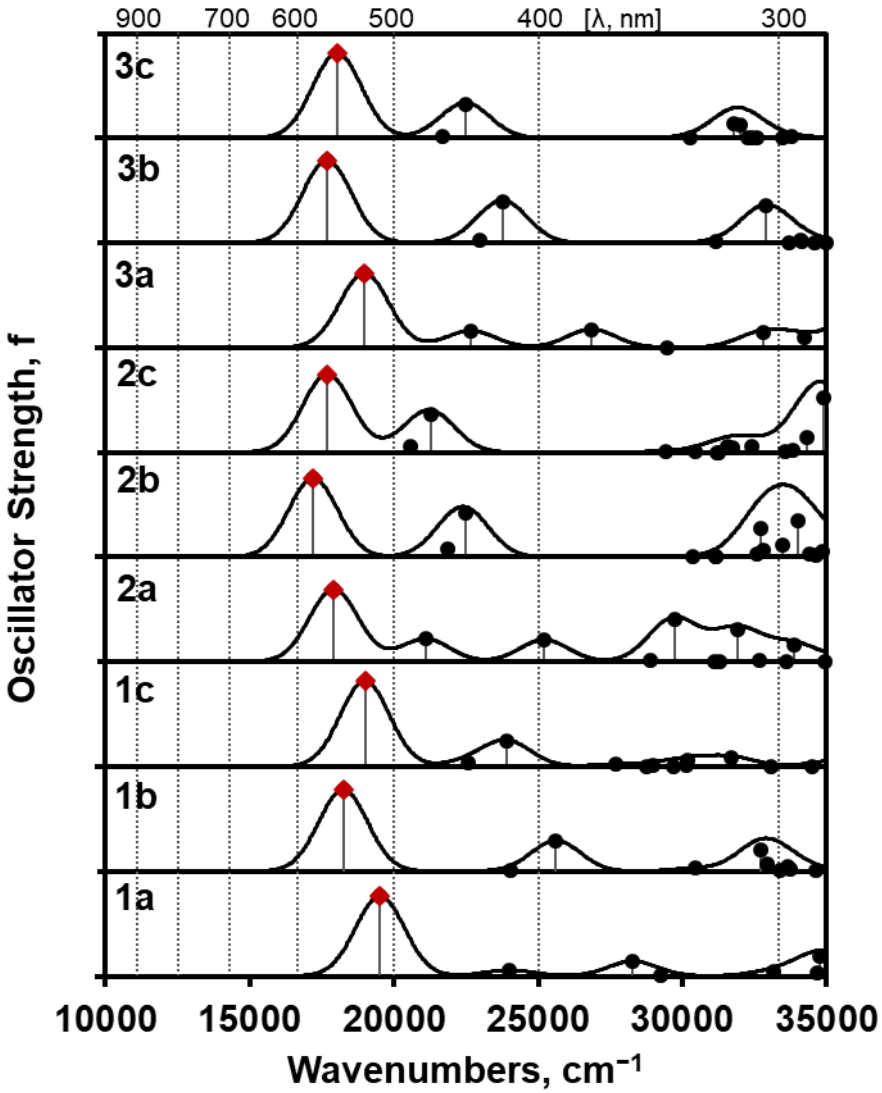

Figure 7.7: Calculated TD-DFT spectra for the optimised geometries of **1a**-**3c (Figure 7.1)** at the CAM-B3LYP/6-31G(d) level of theory. The main spectral bands associated with the HOMO−LUMO transition are found between 500−600 nm and are highlighted with red diamonds. Simulated spectra were obtained using the Chemcraft program with a fixed bandwidth of 2000 cm^{-1}.[109]

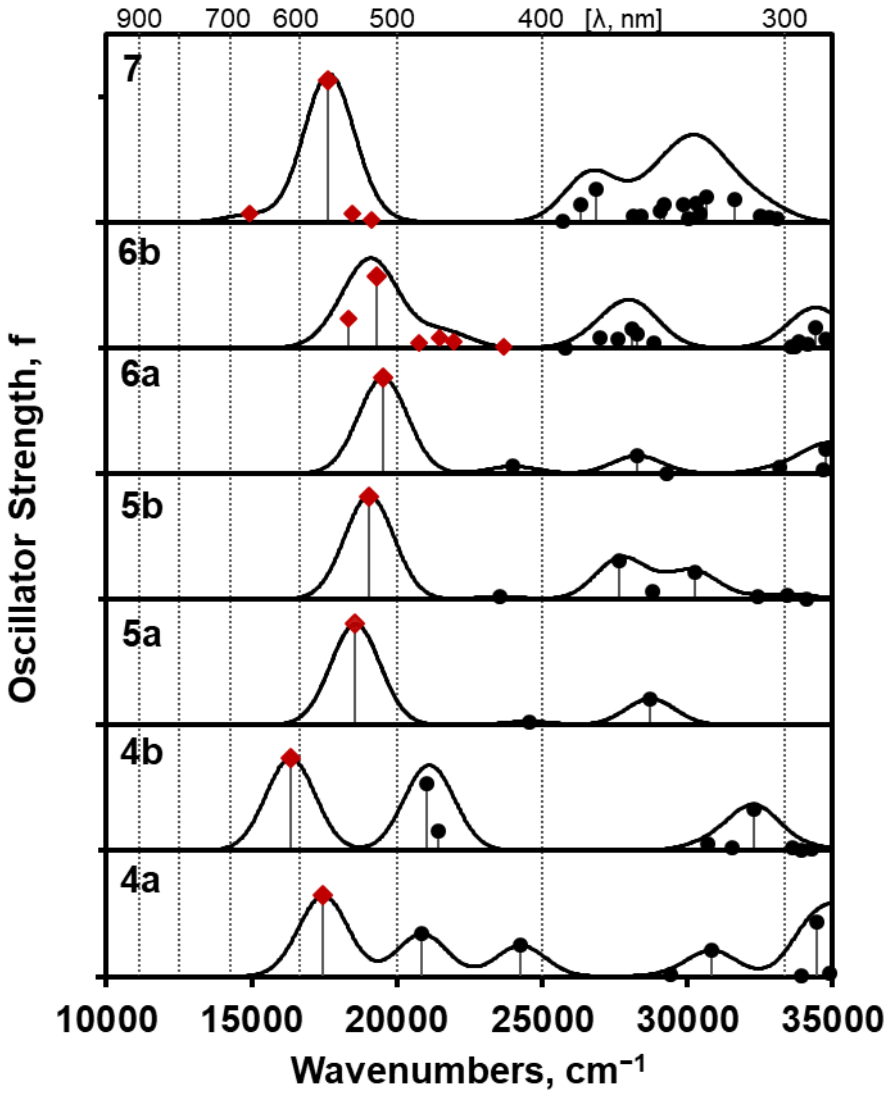

Figure 7.8: Calculated TD-DFT spectra for the optimised geometries of **4a-7 (Figure 7.1)** at the CAM-B3LYP/6-31G(d) level of theory. The main spectral bands associated with the HOMO−LUMO transitions are found in the 400−700 nm region and are highlighted with red diamonds. Multiple bands of this type are anticipated for the Zn(II) azadipyrromethene complexes. Simulated spectra were obtained using the Chemcraft program by using a fixed bandwidth of 2000 cm^{-1}.[109]

7.4 Concluding remarks

TD-DFT calculations are a useful tool in the design of azaBODIPY and azadipyrromethene complexes for various applications as it provides insight on structure-property relationships through predicting trends in the frontier MOs energies and spectroscopic properties associated with structural modifications. The large MO coefficient on the LUMO of azaBODIPY dyes, **Figures 7.4** and **7.5**, results in a narrowing of the HOMO−LUMO gap relative to BODIPY dyes, since there is a stabilisation of the LUMO. This means that the main spectral band of azaBODIPYs lies in the therapeutic window (620−1000 nm) making brominated azaBODIPY dyes such as **Br-N5** and **Br-N6** potentially suitable for use as photosensitiser dyes in PDT. To achieve a more highly red-shifted main spectral band and minimise absorbance across most of the visible region in the context of the **N3-BDY** complex used for the optical limiting, it was necessary to introduce *para*-substituents on the phenyl rings at both the 3,5- and 1,7-positions to form a "push-pull" system. The trends observed in the predicted electronic absorption spectra, **Figure 7.7** and **7.8**, consistently followed the experimental data obtained, **Table 7.1**, demonstrating that calculations of this type could be used to predict the properties of similar dyes that have yet to be synthesised and could be used to guide the rational design of novel azadipyrromethene ligands.

8: Conclusions and future prospects

8.1 General conclusions

Series of azadipyrromethenes, azaBODIPYs and homoleptic Zn(II) azadipyrromethenes were rationally selected to study their potential utility for specific applications. The preparation of these bidentate ligands proved to be highly challenging and was only successfully achieved following several attempts. The sensitivity of some of the intermediates to moisture led to failed conversions in some cases, and steric hindrance may have been a significant issue in others. A desirable feature of azaBODIPY dyes compared to conventional BODIPYs is the presence of the highly electronegative aza-nitrogen atom that stabilises the LUMO due to a large MO coefficient at this position resulting in a narrowing of the HOMO−LUMO gap and a red-shift of the absorbance maxima of the main spectral band towards the red end of the visible and the NIR region. The zinc complexes were studied, since a heavy atom effect was anticipated due to the Zn(II) ion. Surprisingly, these complexes generate very little or no singlet oxygen upon photoexcitation at the λ_{max} of the main absorption band. In contrast, when bromine atoms were incorporated added at the 2,6-positions azaBODIPY dyes in **Br-N5** and **Br-N6**, ϕ_{Δ} values of 0.70 and 0.78 were obtained in ethanol making these dyes potentially suitable for use as photosensitiser dyes in PACT and PDT. PACT activity against *S. aureus* was found to be relatively poor compared to BODIPY dyes previously reported on. Nevertheless, the 3,5-*p*-nitrophenyl-substituted **Br-N5** dye had the better activity of the two. The PDT activity displayed by **Br-N5** against MCF-7 human breast cancer cells was also greater than that of **Br-N6**. **Br-N5** exhibited higher cellular uptake and better phototoxicity against MCF-7 cells with an IC_{50} value of 13.4 ± 1.1 μM. The azadipyrromethene, azaBODIPY and homoleptic Zn(II) azadipyrromethene compounds investigated for NLO did not yield the anticipated results since the γ values were up to two orders of magnitude lower than those reported using a similar approach with 3,5-distyrylBODIPY dyes.[92]

8.2 Future prospects

I. To improve singlet oxygen production by the zinc complexes, heavy atoms could be incorporated at the 2,6-positions of the azadipyrromethene ligands.

II. With the most promising results being recorded for the PDT work carried out with **Br-N5** and **Br-N6** as photosensitisers, other approaches could be attempted to enhance the activity of the dyes. This could be achieved, for example, by encapsulating the complexes with modified nanocarriers.

III. For PACT, newly designed azaBODIPYs with functional groups that improve water solubility through the addition of a cationic charge could be used to test the effectiveness of dyes of this type against both gram (+) and gram (-) bacterial strains.

IV. Finally, in addition to azaBODIPY dyes that have close to zero absorbance at 532 nm, working with complexes with either a longer fluorescence or triplet lifetime could potentially improve OL ability. For practical application, thin film fabrication with embedded dyes would also be necessary.

References

[1] H. Lu, J. Mack, Y. Yang, Z. Shen, Structural modification strategies for the rational design of red/NIR region BODIPYs, Chemical Society Reviews, 43 (2014) 4778–4823.

[2] L. Jiao, W. Pang, J. Zhou, Y. Wei, X. Mu, G. Bai, E. Hao, Regioselective stepwise bromination of boron dipyrromethene (BODIPY) dyes, Journal of Organic Chemistry, 76 (2011) 9988–9996.

[3] A. Kamkaew, S.H. Lim, H.B. Lee, L.V. Kiew, L.Y. Chung, K. Burgess, BODIPY dyes in photodynamic therapy, Chemical Society Reviews, 42 (2013) 77–88.

[4] A. Burghart, H. Kim, M.B. Welch, L.H. Thoresen, J. Reibenspies, K. Burgess, F. Bergström, L.B. Johansson, 3,5-diaryl-4,4-difluoro-4-bora-3a,4a-diaza-s-indacene (BODIPY) dyes: Synthesis, spectroscopic, electrochemical, and structural properties, Journal of Organic Chemistry, 64 (1999) 7813–7819.

[5] J. Mack, M. Wildervanck, T. Nyokong, TD-DFT calculations and MCD spectroscopy of porphyrin and phthalocyanine analogues: Rational design of photosensitizers for PDT and NIR region sensor applications, Turkish Journal of Chemistry, 38 (2014) 1013–1026.

[6] Y.W. Wang, A.B. Descalzo, Z. Shen, X.Z. You, K. Rurack, Dihydronaphthalene-fused boron-dipyrromethene (BODIPY) dyes: Insight into the electronic and conformational tuning modes of BODIPY fluorophores, Chemistry - A European Journal, 16 (2010) 2887–2903.

[7] L. Gai, J. Mack, H. Lu, H. Yamada, D. Kuzuhara, G. Lai, Z. Li, Z. Shen, New 2,6-distyryl-substituted BODIPY isomers: Synthesis, photophysical properties, and theoretical calculations, Chemistry - A European Journal, 20 (2014) 1091–1102.

[8] J. Michl, Magnetic Circular Dichroism of Cyclic π-Electron Systems. 1. Algebraic Solution of the Perimeter Model for the A and B Terms of High-Symmetry Systems with a (4N +

2)-Electron [n]Annulene Perimeter, Journal of the American Chemical Society, 100 (1978) 6801–6811.

[9] M.A.T. Rogers, 2 : 4-Diarylpyrroles. Part I. Synthesis of 2 : 4-Diarylpyrroles and 2 : 2’ : 4 : 4’-Tetra-arylaxadipyrrornethines, Journal of the Chemical Society (Resumed), 53 (1943) 590–596.

[10] A.W. Ingersoll, J.H. Brown, C.K. Kim, W.D. Beauchamp, G. Jennings, Extensions of the Leuckart Synthesis of Amines, Journal of the American Chemical Society, 58 (1936) 1808–1811.

[11] W. Zhao, E.M. Carreira, Conformationally restricted aza-BODIPY: Highly fluorescent, stable near-infrared absorbing dyes, Chemistry - A European Journal, 12 (2006) 7254–7263.

[12] Y. Ge, D.F. O’Shea, Azadipyrromethenes: From traditional dye chemistry to leading edge applications, Chemical Society Reviews, 51 (2015) 10664–10667.

[13] A. Gorman, J. Killoran, C. O’Shea, T. Kenna, W.M. Gallagher, D.F. O’Shea, In vitro demonstration of the heavy-atom effect for photodynamic therapy, Journal of the American Chemical Society, 126 (2004) 10619–10631.

[14] M.J. Hall, S.O. McDonnell, J. Killoran, D.F. O’Shea, A modular synthesis of unsymmetrical tetraarylazadipyrromethenes, Journal of Organic Chemistry, 70 (2005) 5571–5578.

[15] M. Sheik-Bahae, A.A. Said, T.H. Wei, D.J. Hagan, E.W. Van Stryland, Sensitive Measurement of Optical Nonlinearities Using a Single Beam, IEEE Journal of Quantum Electronics, 26 (1990) 760–769.

[16] Y. V. Zatsikha, L.I. Shamova, T.S. Blesener, I.A. Kuzmin, Y. V. Germanov, D.E. Herbert, V.N. Nemykin, Development of a Class of Easily Scalable, Electron-Deficient, Core-

Extended Benzo-Fused Azadipyrromethene Derivatives (“MB-DIPY”), Journal of Organic Chemistry, 84 (2019) 14540–14557.

[17] R. Gresser, H. Hartmann, M. Wrackmeyer, K. Leo, M. Riede, Synthesis of thiophene-substituted aza-BODIPYs and their optical and electrochemical properties, Tetrahedron, 67 (2011) 7148–7155.

[18] A. Loudet, K. Burgess, BODIPY dyes and their derivatives: Syntheses and spectroscopic properties, Chemical Reviews, 107 (2007) 4891–4932.

[19] X.D. Jiang, J. Zhao, D. Xi, H. Yu, J. Guan, S. Li, C.L. Sun, L.J. Xiao, A New Water-Soluble Phosphorus-Dipyrromethene and Phosphorus-Azadipyrromethene Dye: PODIPY/aza-PODIPY, Chemistry - A European Journal, 21 (2015) 6079–6082.

[20] L. Jiao, C. Yu, J. Li, Z. Wang, M. Wu, E. Hao, β-formyl-BODIPYs from the Vilsmeier-Haack reaction, Journal of Organic Chemistry, 74 (2009) 7525–7528.

[21] A. Kamkaew, K. Burgess, Aza-BODIPY Dyes With Enhanced Hydrophilicity, Chemical Communications, 51 (2015) 10664–10667.

[22] L. Gao, W. Senevirathna, G. Sauvé, Azadipyrromethene-based conjugated oligomers with Near-IR absorption and high electron affinity, Organic Letters, 13 (2011) 5354–5357.

[23] A.B. Nepomnyashchii, M. Bröring, J. Ahrens, A.J. Bard, Synthesis, photophysical, electrochemical, and electrogenerated chemiluminescence studies. Multiple sequential electron transfers in BODIPY monomers, dimers, trimers, and polymer, Journal of the American Chemical Society, 133 (2011) 8633–8645.

[24] T.S. Teets, D. V. Partyka, J.B. Updegraff, T.G. Gray, Homoleptic, four-coordinate azadipyrromethene complexes of d10 zinc and mercury, Inorganic Chemistry, 47 (2008) 2338–2346.

[25] A. Palma, J.F. Gallagher, H. Müller-Bunz, J. Wolowska, E.J.L. McInnes, D.F. O'Shea, Co(ii), Ni(ii), Cu(ii) and Zn(ii) complexes of tetraphenylazadipyrromethene, Dalton Transactions, (2009) 273–279.

[26] S. Liu, Z. Shi, W. Xu, H. Yang, N. Xi, X. Liu, Q. Zhao, W. Huang, A class of wavelength-tunable near-infrared aza-BODIPY dyes and their application for sensing mercury ion, Dyes and Pigments, 103 (2014) 145–153.

[27] R. Fernando, S. Pejić, A. Thomsen, C. Wang, G. Sauvé, Azadipyrromethene-based near-IR dyes with styryl substituents at the pyrrolic positions for organic photovoltaic applications, Dyes and Pigments, 168 (2019) 257–263.

[28] W. Sheng, J. Cui, Z. Ruan, L. Yan, Q. Wu, C. Yu, Y. Wei, E. Hao, L. Jiao, [a]-Phenanthrene-fused BF 2 azadipyrromethene (AzaBODIPY) dyes as bright near-infrared fluorophores, Journal of Organic Chemistry, 82 (2017) 10341–10349.

[29] R. Gresser, A. Hoyer, M. Hummert, H. Hartmann, K. Leo, M. Riede, Homoleptic Co(II), Ni(II), Cu(II), Zn(II) and Hg(II) complexes of bis-(phenyl)-diisoindol-aza-methene, Dalton Transactions, 40 (2011) 3476–3483.

[30] F.S. Etheridge, R.J. Fernando, S. Pejić, M. Zeller, G. Sauvé, Synthesis and characterization of fluorinated azadipyrromethene complexes as acceptors for organic photovoltaics, Beilstein Journal of Organic Chemistry, 12 (2016) 1925–1938.

[31] R.T. Kuznetsova, Y. V. Aksenova, D.E. Bashkirtsev, A.A. Prokopenko, E.N. Tel'Minov, G. V. Mayer, N.A. Dudina, E. V. Antina, A.Y. Nikonova, M.B. Berezin, A.S. Semeikin, Photonics of zinc(II) and boron(III) chelates with methyl- And phenyl-substituted dipyrromethenes and azadipyrromethenes, High Energy Chemistry, 49 (2015) 16–23.

[32] P. Batat, M. Cantuel, G. Jonusauskas, L. Scarpantonio, A. Palma, D.F. O'Shea, N.D. McClenaghan, BF 2 -azadipyrromethenes: Probing the excited-state dynamics of a NIR

fluorophore and photodynamic therapy agent, Journal of Physical Chemistry A, 115 (2011) 14034–14039.

[33] K. Gollnick, A. Griesbeck, Singlet oxygen photooxygenation of furans, Tetrahedron, 41 (1985) 2057–2068.

[34] R. Ziessel, G. Ulrich, A. Harriman, The chemistry of Bodipy: A new El Dorado for fluorescence tools, New Journal of Chemistry, 31 (2007) 496–501.

[35] Y.R. Shen, Introduction, in: The Principles of Nonlinear Optics, Wiley, New York, 1984: pp. 1–12.

[36] P.P. Banerjee, Solitons in Optical Fibers, in: Nonlinear Optics : Theory, Numerical Modeling, and Applications, CRC Press, New York, 2004: pp. 155–174.

[37] M. Schneider, G. Kirfel, M. Berthold, M. Frentzen, F. Krause, A. Braun, The impact of antimicrobial photodynamic therapy in an artificial biofilm model, Lasers in Medical Science, 27 (2012) 615–620.

[38] J. Chen, Z. Chen, Y. Zheng, S. Zhou, J. Wang, N. Chen, J. Huang, F. Yan, M. Huang, Substituted zinc phthalocyanine as an antimicrobial photosensitizer for periodontitis treatment, Journal of Porphyrins and Phthalocyanines, 15 (2011) 293–299.

[39] M. Wainwright, Photodynamic Antimicrobial Chemotherapy, Journal of Antimicrobial Chemotherapy, 42 (1998) 13–28.

[40] Y. Ge, D.F. O'Shea, Azadipyrromethenes: From traditional dye chemistry to leading edge applications, Chemical Society Reviews, 45 (2016) 3846–3864.

[41] D.O. Frimannsson, M. Grossi, J. Murtagh, F. Paradisi, D.F. Oshea, Light induced antimicrobial properties of a brominated boron difluoride (BF2) chelated tetraarylazadipyrromethene photosensitizer, Journal of Medicinal Chemistry, 53 (2010) 7337–7343.

[42] A. Sindelo, O.L. Osifeko, T. Nyokong, Synthesis, photophysicochemical and photodynamic antimicrobial chemotherapy studies of indium pyridyl phthalocyanines: Charge versus bridging atom, Inorganica Chimica Acta, 476 (2018) 68–76.

[43] L.M. Giroldo, M.P. Felipe, M.A. De Oliveira, E. Munin, L.P. Alves, M.S. Costa, Photodynamic antimicrobial chemotherapy (PACT) with methylene blue increases membrane permeability in Candida albicans, Lasers in Medical Science, 24 (2009) 109–112.

[44] L. Ryskova, V. Buchta, R. Slezak, Photodynamic antimicrobial therapy, Central European Journal of Biology, 5 (2010) 400–406.

[45] https://www.redbubble.com/people/stanleyillust/works/21341791-gram-positive-vs-gram-negative-bacteria (accessed November 20, 2019).

[46] T.J. Dougherty, Yearly Review Photodynamic Therapy, Photochemistry and Photobiology, 58 (1993) 895–900.

[47] I.J. MacDonald, T.J. Dougherty, Basic principles of photodynamic therapy, Journal of Porphyrins and Phthalocyanines, 5 (2001) 105–129.

[48] J. Tian, J. Zhou, Z. Shen, L. Ding, J.S. Yu, H. Ju, A pH-activatable and aniline-substituted photosensitizer for near-infrared cancer theranostics, Chemical Science, 6 (2015) 5969–5977.

[49] H.J.N. Andreyev, A.R. Norman, J. Oates, D. Cunningham, Why do patients with weight loss have a worse outcome when undergoing chemotherapy for gastrointestinal malignancies?, European Journal of Cancer, 34 (1998) 503–509.

[50] G. Dafnis, L. Påhlman, Y. Raab, U.M. Gustafsson, W. Graf, Transanal endoscopic microsurgery: Clinical and functional results, Colorectal Disease, 6 (2004) 336–342.

[51] L.A. Dawson, M.B. Sharpe, Image-guided radiotherapy: rationale, benefits, and

limitations, Lancet Oncology, 7 (2006) 848–858.

[52] O. Glehen, O. Chapet, M. Adham, J.C. Nemoz, J.P. Gerard, Long-term results of the Lyons R90-01 randomized trial of preoperative radiotherapy with delayed surgery and its effect on sphincter-saving surgery in rectal cancer, British Journal of Surgery, 90 (2003) 996–998.

[53] K.K. Matthay, J.G. Villablanca, R.C. Seeger, D.O. Stram, R.E. Harris, N.K. Ramsay, P. Swift, H. Shimada, C.T. Black, G.M. Brodeur, R.B. Gerbing, C.P. Reynolds, Treatment of high-risk neuroblastoma with intensive chemotherapy, radiotherapy, autologous bone marrow transplantation, and 13-cis-retinoic acid, New England Journal of Medicine, 341 (1999) 1165–1173.

[54] L. Morlet, V. Vonarx-Coinsmann, P. Lenz, M.T. Foultier, L.X. de Brito, C. Stewart, T. Patrice, Correlation between meta(tetrahydroxyphenyl)chlorin (m-THPC) biodistribution and photodynamic effects in mice, Journal of Photochemistry and Photobiology, B: Biology, 28 (1995) 25–32.

[55] H. Barr, N. Krasner, P.B. Boulos, P. Chatlani, S.G. Bown, Photodynamic therapy for colorectal cancer: A quantitative pilot study, British Journal of Surgery, 77 (1990) 93–96.

[56] R. Bonnett, Photosensitizers of the porphyrin and phthalocyanine series for photodynamic therapy, Chemical Society Reviews, 24 (1995) 19–33.

[57] P.G. Calzavara-Pinton, R.M. Szeimies, B. Ortel, C. Zane, Photodynamic therapy with systemic administration of photosensitizers in dermatology, Journal of Photochemistry and Photobiology B: Biology, 36 (1996) 225–231.

[58] A.E. O'Connor, W.M. Gallagher, A.T. Byrne, Porphyrin and nonporphyrin photosensitizers in oncology: Preclinical and clinical advances in photodynamic

therapy, Photochemistry and Photobiology, 85 (2009) 1053–1074.

[59] H.C. Daly, G. Sampedro, C. Bon, D. Wu, G. Ismail, R.A. Cahill, D.F. O'Shea, BF2-azadipyrromethene NIR-emissive fluorophores with research and clinical potential, European Journal of Medicinal Chemistry, 135 (2017) 392–400.

[60] J.R. Riegel, J.C. Godbold Jr, (Eds.), Fundamental Information, in: Laser Therapy in Veterinary Medicine: Photobiomodulation, Wiley, Chichester, 2011: pp. 9–18.

[61] N. Mehraban, H.S. Freeman, Developments in PDT sensitizers for increased selectivity and singlet oxygen production, Materials, 8 (2015) 4421–4456.

[62] N. Adarsh, M. Shanmugasundaram, R.R. Avirah, D. Ramaiah, Aza-BODIPY derivatives: Enhanced quantum yields of triplet excited states and the generation of singlet oxygen and their role as facile sustainable photooxygenation catalysts, Chemistry - A European Journal, 18 (2012) 12655–12662.

[63] W.M. Gallagher, L.T. Allen, C. O'Shea, T. Kenna, M. Hall, A. Gorman, J. Killoran, D.F. O'Shea, A potent nonporphyrin class of photodynamic therapeutic agent: Cellular localisation, cytotoxic potential and influence of hypoxia, British Journal of Cancer, 92 (2005) 1702–1710.

[64] C.W. Spangler, Recent development in the design of organic materials for optical power limiting, Journal of Materials Chemistry, 9 (1999) 2013–2020.

[65] O.M. Bankole, T. Nyokong, Mercaptopyridine-substituted indium, zinc, and metal-free phthalocyanines: Nonlinear optical studies in solution and on polymer matrices, Journal of Coordination Chemistry, 68 (2015) 3727–3740.

[66] G. De La Torre, P. Vázquez, F. Agulló-López, T. Torres, Phthalocyanines and related compounds: Organic targets for Nonlinear Optical applications, Journal of Materials Chemistry, 8 (1998) 1671–1683.

[67] B. Gu, W. Ji, P.S. Patil, S.M. Dharmaprakash, H.T. Wang, Two-photon-induced excited-state absorption: Theory and experiment, Applied Physics Letters, 92 (2008) 091118.

[68] K. Ogawa, T. Zhang, K. Yoshihara, Y. Kobuke, Large third-order optical nonlinearity of self-assembled porphyrin oligomers, Journal of the American Chemical Society, 124 (2002) 22–23.

[69] G. de la Torre, P. Vázquez, F. Agulló-López, T. Torres, Role of structural factors in the nonlinear optical properties of phthalocyanines and related compounds, Chemical Reviews, 104 (2004) 3723–3750.

[70] G. Kubheka, O. Achadu, J. Mack, T. Nyokong, Optical limiting properties of 3,5-diphenyldibenzo-azaBODIPY at 532 nm, New Journal of Chemistry, 41 (2017) 12319–12325.

[71] W. Zhao, P. Palffy-Muhoray, Z-scan technique using top-hat beams, Applied Physics Letters, 63 (1993) 1613–1615.

[72] M. Yin, H.P. Li, S.H. Tang, W. Ji, Determination of nonlinear absorption and refraction by single Z-scan method, Applied Physics B: Lasers and Optics, 70 (2000) 587–591.

[73] E.W. Van Stryland, M. Sheik-Bahae, Z-Scan Measurements of Optical Nonlinearities, in: Characterization Techniques and Tabulations for Organic Nonlinear Materials, M.G. Kuzy, C.W. Dirk (Eds.), Marcel Dekker, Inc, New York, 1998: pp. 655–692.

[74] A. Gnoli, L. Razzari, M. Righini, Z-scan measurements using high repetition rate lasers: how to manage thermal effects, Optics Express, 13 (2005) 7976.

[75] M. Frisch, G. Trucks, H.B. Schlegel, G.E. Scuseria, M.A. Robb, J.R. Cheeseman, G. Scalmani, V. Barone, G.A. Petersson, H. Nakatsuji, X. Li, M. Caricato, A. Marenich, J. Bloino, B.G. Janesko, R. Gomperts, B. Mennucci, H.P. Hratchian, J. V. Ortiz, A.F. Izmaylov, J.L. Sonnenberg, D. Williams-Young, F. Ding, F. Lipparini, F. Egidi, J. Goings, B.

Peng, A. Petrone, T. Henderson, D. Ranasinghe, V.G. Zakrzewski, N.R. J. Gao, G. Zheng, W. Liang, M. Hada, M. Ehara, K. Toyota, R. Fukuda, J. Hasegawa, M. Ishida, T. Nakajima, Y. Honda, O. Kitao, H. Nakai, T. Vreven, K. Throssell, J.A. Montgomery, Jr., J.E. Peralta, F. Ogliaro, M. Bearpark, J.J. Heyd, E. Brothers, K.N. Kudin, V.N. Staroverov, T. Keith, R. Kobayashi, J. Normand, K. Raghavachari, A. Rendell, J.C. Burant, S.S. Iyengar, J. Tomasi, M. Cossi, J.M. Millam, M. Klene, C. Adamo, R. Cammi, J.W. Ochterski, R.L. Martin, K. Morokuma, O. Farkas, J.B. Foresman, and D.J. Fox, Gaussian 09, rev. D. 01, Gaussian Inc., (2016).

[76] M.D. Hanwell, D.E. Curtis, D.C. Lonie, T. Vandermeerschd, E. Zurek, G.R. Hutchison, Avogadro: An advanced semantic chemical editor, visualization, and analysis platform, Journal of Cheminformatics, 4 (2012).

[77] B. Babu, E. Amuhaya, D. Oluwole, E. Prinsloo, J. Mack, T. Nyokong, Preparation of NIR absorbing axial substituted tin(iv) porphyrins and their photocytotoxic properties, Medicinal Chemistry Communications, 10 (2019) 41–48.

[78] D.O. Oluwole, C.M. Tilbury, E. Prinsloo, J. Limson, T. Nyokong, Photophysicochemical properties and in vitro cytotoxicity of zinc tetracarboxyphenoxy phthalocyanine - Quantum dot nanocomposites, Polyhedron, 106 (2016) 92–100.

[79] A. Gut, Ł. Łapok, D. Jamróz, M. Nowakowska, Synthesis of Thermally Robust, Photostable Aza-Dipyrromethene Ligands Substituted with Nitro Groups, Asian Journal of Organic Chemistry, 6 (2017) 207–223.

[80] S.C. Lee, D. Zhai, P. Mukherjee, Y.T. Chang, The development of novel near-infrared (NIR) tetraarylazadipyrromethene fluorescent dyes, Materials, 6 (2013) 1779–1788.

[81] C.A. Swamy P, R.N. Priyanka, S. Mukherjee, P. Thilagar, Panchromatic borane-aza-BODIPY conjugate: Synthesis, intriguing optical properties, and selective fluorescent

sensing of fluoride anions, European Journal of Inorganic Chemistry, 2015 (2015) 2338–2344.

[82] R. Priefer, J. R. Griffiths, J. N. Ludwig, G. Skelhorne-Gross, R. S. Greene, Synthesis of Aza-BODIPY Boron Difluoride PDT Agents to Promote Apoptosis in HeLa Cells, Letters in Organic Chemistry, 8 (2011) 368–373.

[83] A. Loudet, R. Bandichhor, L. Wu, K. Burgess, Functionalized BF2 chelated azadipyrromethene dyes, Tetrahedron, 64 (2008) 3642–3654.

[84] X. Zhang, H. Yu, Y. Xiao, Replacing phenyl ring with thiophene: An approach to longer wavelength aza-dipyrromethene boron difluoride (Aza-BODIPY) dyes, Journal of Organic Chemistry, 77 (2012) 669–673.

[85] Y. Wang, L. Chen, R.M. El-Shishtawy, S.G. Aziz, K. Müllen, Synthesis and optophysical properties of dimeric aza-BODIPY dyes with a push-pull benzodipyrrolidone core, Chemical Communications, 50 (2014) 11540–11542.

[86] D. V. Partyka, N. Deligonul, M.P. Washington, T.G. Gray, Fac-tricarbonyl rhenium(I) azadipyrromethene complexes, Organometallics, 28 (2009) 5837–5840.

[87] S. Tekin, B. Küçüköz, H. Yilmaz, G. Sevinç, M. Hayvali, H. Gul Yaglioglu, A. Elmali, Enhancement of two photon absorption properties by charge transfer in newly synthesized aza-boron-dipyrromethene compounds containing triphenylamine, 4-ethynyl-N,N-dimethylaniline and methoxy moieties, Journal of Photochemistry and Photobiology A: Chemistry, 256 (2013) 23–28.

[88] H. Liu, H. Lu, Z. Zhou, S. Shimizu, Z. Li, N. Kobayashi, Z. Shen, Asymmetric core-expanded aza-BODIPY analogues: Facile synthesis and optical properties, Chemical Communications, 51 (2015) 1713–1716.

[89] A.S. Oliveira, D. Licsandru, R. Boscencu, R. Socoteanu, V. Nacea, L.F. Vieira Ferreira, A

singlet oxygen photogeneration and luminescence study of unsymmetrically substituted mesoporphyrinic compounds, International Journal of Photoenergy, (2009).

[90] Z. Herceg, A.R. Jambrak, V. Lelas, S.M. Thagard, The effect of high intensity ultrasound treatment on the amount of Staphylococcus aureus and Escherichia coli in milk, Food Technology and Biotechnology, 50 (2012) 46–52.

[91] M. Grinholc, B. Szramka, K. Olender, A. Graczyk, Bactericidal effect of photodynamic therapy against methicillin-resistant Staphylococcus aureus strain with the use of various porphyrin photosensitizers, Acta Biochimica Polonica, 54 (2007) 665–670.

[92] K.A. Lebechi, B.P. Ngoy, J. Mack, T. Nyokong, 2,6-Dibrominated 3,5-DistyrylBODIPYs as Photosensitizer Dyes for Photodynamic Antimicrobial Chemotherapy, Macroheterocycles, 12 (2019) 292–299.

[93] M. V. Berridge, P.M. Herst, A.S. Tan, Tetrazolium dyes as tools in cell biology: New insights into their cellular reduction, Biotechnology Annual Review, 11 (2005) 127–152.

[94] N. Adarsh, P.S.S. Babu, R.R. Avirah, M. Viji, S.A. Nair, D. Ramaiah, Aza-BODIPY nanomicelles as versatile agents for the: In vitro and in vivo singlet oxygen-triggered apoptosis of human breast cancer cells, Journal of Materials Chemistry B, 7 (2019) 2372–2377.

[95] B. Babu, E. Prinsloo, J. Mack, T. Nyokong, Synthesis, characterization and photodynamic activity of Sn(iv) triarylcorroles with red-shifted Q bands, New Journal of Chemistry, 43 (2019) 18805–18812.

[96] R.L. Sutherland, D.G. Mclean, S. Kirkpatrick, Characterization of Second Order Nonlinear Optical Materials, in: Handbook of Nonlinear Optics, Dekker, New York, 1973: pp. 241–295.

[97] Y. Chen, M. Hanack, W.J. Blau, D. Dini, Y. Liu, Y. Lin, J. Bai, Soluble axially substituted phthalocyanines: Synthesis and nonlinear optical response, Journal of Materials Science, 41 (2006) 2169–2185.

[98] Y. Chen, M. Hanack, Y. Araki, O. Ito, Axially modified gallium phthalocyanines and naphthalocyanines for optical limiting, Chemical Society Reviews, 34 (2005) 517–529.

[99] M. Hanack, D. Dini, M. Barthel, S. Vagin, Conjugated macrocycles as active materials in nonlinear optical processes: Optical limiting effect with phthalocyanines and related compounds, The Chemical Record, 2 (2002) 129–148.

[100] R.C. Hollins, Materials for optical limiters, Current Opinion in Solid State and Materials Science, 4 (1999) 189–196.

[101] R. Matthes, International Commission on Non-Ionizing Radiation Protection, Revision of guidelines on limits of exposure to laser radiation of wavelengths between 400 nm and 1.4 microm., Health Physics, 79 (2000) 431–440.

[102] C. Mkhize, J. Britton, T. Nyokong, Enhanced nonlinear optical properties of octa-substituted lead and cadmium phthalocyanines when embedded in poly(bisphenol A carbonate) as thin films, Polyhedron, 81 (2014) 607–613.

[103] N. Ndebele, Z. Hlatshwayo, B.P. Ngoy, G. Kubheka, J. Mack, T. Nyokong, Optical limiting properties of BODIPY dyes substituted with styryl or vinylene groups on the nanosecond timescale, Journal of Porphyrins and Phthalocyanines, 23 (2019) 701–717.

[104] T. Yanai, D.P. Tew, N.C. Handy, A new hybrid exchange-correlation functional using the Coulomb-attenuating method (CAM-B3LYP), Chemical Physics Letters, 393 (2004) 51–57.

[105] S. Wang, H. Liu, J. Mack, J. Tian, B. Zou, H. Lu, Z. Li, J. Jiang, Z. Shen, A BODIPY-based ‘turn-on’ fluorescent probe for hypoxic cells imaging, Chemical Communications, 51

(2015) 13389–13392.

[106] R. Gresser, M. Hummert, H. Hartmann, K. Leo, M. Riede, Synthesis and characterization of near-infrared absorbing benzannulated aza-BODIPY dyes, Chemistry - A European Journal, 17 (2011) 2939–2947.

[107] B. Küçüköz, M. Hayvali, H. Yilmaz, B. Uguz, U. Kürüm, H.G. Yaglioglu, A. Elmali, Synthesis, optical properties and ultrafast dynamics of aza-boron-dipyrromethene compounds containing methoxy and hydroxy groups and two-photon absorption cross-section, Journal of Photochemistry and Photobiology A: Chemistry, 247 (2012) 24–29.

[108] J. Fabian, H. Hartmann, Dyes, in: Light Absorption of Organic Colorants: Theoretical Treatment and Empirical Rules, K. Hafner, C.W. Rees, B.M. Trost, J. Lehn, P. von Rague Schleyer, R. Zahnradnik (Eds.), Springer-Verlag, Berlin, 1980: pp. 24–40.

[109] G. Zhurko, D. Zhurko, ChemCraft, Version 16, http://www.chemcraftprog.com, 2009.